Mon. Not. R. Astron. Soc. **000**, 000–000 (0000) Printed 5 February 2008 (MN LATEX style file v2.2)

Dynamical flows through Dark Matter Haloes: Inner perturbative dynamics, secular evolution, and applications

Christophe Pichon [1,2,3⋆], and Dominique Aubert[1,2,3]
[1] *Institut d'Astrophysique de Paris, 98 bis boulevard d'Arago, 75014 Paris, France*
[2] *Observatoire astronomique de Strasbourg, 11 rue de l'Universite, 67000 Strasbourg, France*
[3] *Horizon, CNRS, 98 bis boulevard d'Arago, 75014 Paris, France*

arXiv:astro-ph/0512381v2 17 Jan 2006

Typeset 5 February 2008; Received / Accepted

ABSTRACT
We investigate statistically the dynamical consequences of cosmological fluxes of matter and related moments on progenitors of today's dark matter haloes. These haloes are described as open collisionless systems which do not undergo strong interactions anymore. Their dynamics is described via canonical perturbation theory which accounts for two types of perturbations: the tidal field corresponding to flybys and accretion of dark matter through the halo's outer boundary.

The non-linear evolution of both the entering flux and the particles of the halo is followed perturbatively. The dynamical equations are solved linearly, order by order, projecting on a biorthogonal basis to consistently satisfy the field equation. Since our perturbative solution of the Boltzmann Poisson is explicit, we obtain, as a result, expressions for the N-point correlation function of the halo's response to the perturbative environment. It allows statistical predictions for the ensemble distribution of the inner dynamical features of haloes. We demonstrate the feasibility of the implementation via a simple example in the appendix. We argue that the fluid description accounts for the dynamical drag and the tidal stripping of incoming structures. We discuss the realm of non-linear problems which could be addressed statistically by such a theory, such as differential dynamical friction, tidal stripping and the self gravity of objects within the virial sphere.

The secular evolution of open galactic haloes is investigated: we derive the kinetic equation which governs the quasi-linear evolution of dark matter profile induced by infall and its corresponding gravitational correlations. This yields a Fokker Planck-like equation for the angle-averaged underlying distribution function. This equation has an explicit source term accounting for the net infall through the virial sphere. Under the assumption of ergodicity we then relate the corresponding source, drift and diffusion coefficients for the ensemble-average distribution to the underlying cosmic two-point statistics of the infall and discuss possible applications.

The internal dynamics of sub-structures within galactic haloes (distortion, clumps as traced by Xray emissivity, weak lensing, dark matter annihilation, tidal streams ..), and the implication for the disk (spiral structure, warp *etc...*) are then briefly discussed. We show how this theory could be used to (i) observationally constrain the statistical nature of the infall (ii) predict the observed distribution and correlations of substructures in upcoming surveys, (iii) predict the past evolution of the observed distribution of clumps, and finally (iv) weight the relative importance of the intrinsic (via the unperturbed distribution function) and external (tidal and/ or infall) influence of the environment in determining the fate of galaxies. We stress that our theory describes the *perturbed* distribution function (mean profile removed) directly in phase space.

Key words: Galaxies: haloes, kinematics and dynamics, statistics , Cosmology: Dark Matter

1 INTRODUCTION

It now appears clearly that the dynamical (azimuthal instabilities, warps, accretion), physical (heating, cooling) and chemical (metal-poor cold gas fluxes) evolution of galaxies are processes which are partly driven by the boundary conditions imposed by their cosmological environment. It is therefore of prime importance to formulate the effects of such an interaction in a unified framework.

Modern digital all-sky surveys, such as the SDSS, 2MASS or the 2dF provide for the first time the opportunity to build statistically relevant constraints on the dynamical states of galaxies which can be used as observational input. Other projects, like Gaia or Planck, will provide small-scale information on our Galaxy and its environment and will soon allow detailed confrontation of the predictions of models with the observations. We ought to be able to draw conclusions on the internal dynamics of the halo and its inner components and constrain their statistical properties.

Unfortunately, it is difficult to study the response of haloes to moderate amplitude perturbations. Current N-body techniques suffer from resolution limitations (due to particle number and drift in orbit integration, see e.g. Power et al. (2003), Binney (2004), for a discussion of such effects) that hide to some extent linear collective effects which dominate the response of the halo (Weinberg (1998b), Murali (1999))[1]. Simulations on galactic scales are also often carried without any attempt to represent the cosmological variety arising from the possible boundary conditions (the so-called cosmic variance problem). This is because the dynamical range required to describe both the environment and the inner structure is considerable, and can only be achieved for a limited number of simulations (e.g. Knebe et al. (2004), Gill et al. (2004), Diemand et al. (2004)). By contrast, the method presented below circumvents this difficulty while relying on an *explicit* treatment of the inner dynamics of the halo, in the perturbative regime. Specifically, our purpose is to develop a tool to study the dynamics of an open stellar system and apply it to the dynamic of a halo which is embedded into its cosmological environment. One can think of this project as an attempt to produce a semi-analytic explicit re-simulation tool, in the spirit of what is done in N-body simulations with zoomed-in initial conditions.

The concept of an initial power spectrum describing the statistical properties of the gravitational perturbations has proved very useful in cosmological studies (e.g. Peebles (1980), Bernardeau et al. (2002)). The underlying paradigm, that gravity drives cosmic evolution, is likely to be a good description at the megaparsec scale. We show below that a similar approach to galactic haloes is still acceptable, and marginally within the reach of our modeling capabilities. The description of the boundary is significantly more complex, but the inner dynamics of hot components is better behaved. Here, we describe a stable system which undergoes small interactions, rather than an unstable system in comoving coordinates undergoing catastrophic multi-scale collapse.

The purpose of this investigation is to derive analytically the dynamical response of a galactic halo, induced by its (relatively weak) interaction with its near environment. Interaction should be understood in a general sense and involve tidal potential interactions (like that corresponding to a satellite orbiting around the galaxy), or an infall where an external quantity (virialized or not) is advected into the galactic halo.

With a suitable formalism, we derive the propagation of an external perturbation from the near galactic environment down to the scale of the galactic disk through the dark matter halo. We essentially solve the coupled collisionless Boltzmann-Poisson equations as a Dirichlet initial value problem to determine the response of the halo to infall and tidal field. The basis over which the response is projected can be customized to, say, the universal profile of dark matter haloes, which makes it possible to consistently and efficiently solve the coupled dynamical and field equations , so long as the entering fluxes of dark matter amounts to a small perturbation in mass compared to the underlying equilibrium.

In a pair of companion papers, Aubert & Pichon (2005a,b) described the statistical properties of the infalling distribution of dark matter at the virial radius, R_{200} as a function of cosmic time between redshift $z = 1$ and today. These papers focused on a description of the one- and two-point statistics of the infall towards well formed $L_\star$ dark matter haloes. All measurements were carried for 15 000 haloes undergoing minor mergers. The two-point correlations were measured both angularly and temporally for the flux densities, and over the whole 5D phase space for the expansion coefficients of the source.

Together with the measurements presented there, we show in this paper that the formalism described below will allow astronomers to address globally and coherently dynamical issues on galactic scales. Most importantly it will allow them to tackle problems in a *statistically representative* manner. This investigation has a broad field of possible applications. Galaxies are subject to boundary conditions that reflect motions on larger scales and their dynamics may constrain the cosmology through the rate of merging events for example, or the mass distribution of satellites. Halo transmission and amplification also fosters communication between spatially separated regions, (see *e.g.* Murali (1999)) and continuously excites the disk structure. For example, spirals can be induced by encounters with satellites and/or by mass injection (e.g. Toomre & Toomre (1972), Howard & Byrd (1990)), while warps results from torque interactions with the surrounding matter (López-Corredoira et al. (2002), Jiang & Binney (1999)). Therefore the proportion of spirals and warps contains information on the structure's formation and environment. The statistical link between the inner properties of galactic haloes, and their cosmic boundary can be reversed to attempt and constrain the nature of the infall while investigating the one and two point statistics of the induced perturbations. This is best done by transposing down to galactic scales the classical cosmic probes for the large-scale structures (lensing, SZ, *etc...*) which have been used successfully

[1] it has been argued that shadowing (Earn & Tremaine (1991)) will in practice allow for another orbit to correct for the drift, but this is of no help to resonant processes because it requires that the *same* orbit does not diffuse for a few libration periods.

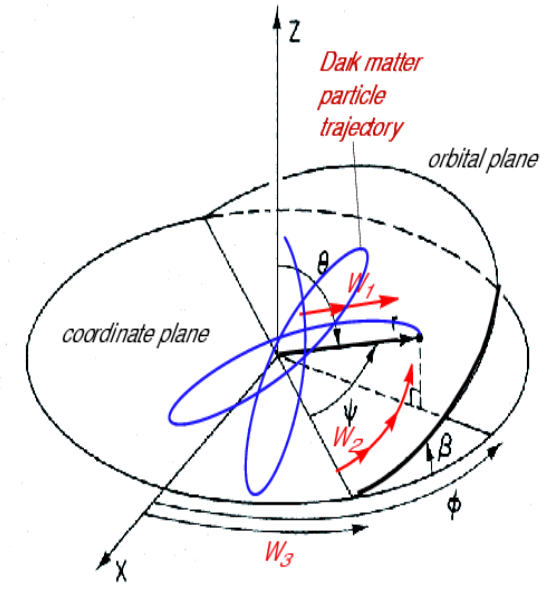

Figure 1. The action angle, $(\mathbf{I}, \mathbf{w})$, - spherical coordinate, $(\mathbf{r}, \mathbf{v})$, transformation. The dark matter particle at running spherical coordinate (r, θ, ϕ) describes a rosette in the orbital plane orthogonal to its momentum, $\mathbf{L}$. The line of node of the orbital plane intersects the $x-y$ plane at a constant (in spherical symmetry) angle w_3 with respect to the x axis. The orbital plane is at an angle $\beta = \mathrm{acos}(L_z/L)$ to the $x-y$ plane. The particle polar coordinate in the orbital plane w.r.t. this line of node is ψ. The angle coordinates, w_2, is measured along ψ but varies linearly with time by construction. Finally the radial angle w_1 varies with radius between peri-apse and apo-apse. (Strongly inspired from Fig 1 of Tremaine & Weinberg (1984)).

to characterize the power-spectrum of fluctuations on larger scales.

The outline of this paper is the following: we describe in Section 2 the linear response of a spherical halo which undergoes cosmological infall of dark matter, and compute the induced correlations in the inner halo; Section 3 presents the second-order perturbative response of the galactic halo to the infalling flux; (Appendix D gives the higher order corrections to the dynamics and addresses the issue of dynamical friction). Section 4 derives the Fokker-Planck equation that the cosmic mean halo profile obeys in such an open environment. Section 5 describes briefly possible astrophysical applications. In particular, it is discussed how the statistical analysis of mean and variance properties of galactic haloes and galaxies can be compared to the quantitative prediction of the concordant ΛCDM cosmogony on those scales. We also show how to revert in time observed tidal features within our Galaxy, or in external galaxies. The last section draws conclusions and discusses prospects for future work.

2 THE SPHERICAL HALO: LINEAR RESPONSE

In the following section, we extend to *open* spherical stellar systems the formalism developed by Kalnajs (1976) (for stellar disks), Aoki et al. (1979) (for gaseous disks), Fridman & Poliachenko (1984), Tremaine & Weinberg (1984) and e.g. Palmer & Papaloizou (1987), Murali (1999), Vauterin & Dejonghe (1996), Bertin et al. (1994) by adding a source term to the collisionless Boltzmann equation. Since the formalism is otherwise fairly standard, we will present it relatively swiftly. In a nutshell, the dynamical equations are solved linearly while projecting over a biorthogonal basis to consistently satisfy the Poisson equation (*e.g.* Kalnajs (1971) Kalnajs (1976) Kalnajs (1977)). The dynamical equation of an open system characterized by its distribution function, F, together with the field equation, read formally:

$$\partial_t \mathrm{F} + \{\mathrm{H} + \psi^e, \mathrm{F}\} = s^e\,, \quad \text{and} \quad \nabla^2\Psi = 4\pi\mathcal{G}\int \mathrm{d}\mathbf{v}\mathrm{F}\,, \tag{1}$$

where H is the Hamiltonian of the system, $\{\ \}$ is the usual Poisson bracket and (Ψ, ψ^e, s^e) stands for the potential, the perturbing exterior potential and incoming source term. The latter, $s^e(\mathbf{r}, \mathbf{v}, t)$ accounts for the entering dark matter *at the virial radius* and is discussed in detail below (Section 2.3, see also Aubert et al. (2004) and Aubert & Pichon (2005a)). In a somewhat unconventional manner, $\psi^e(\mathbf{r}, t)$ refers here to the external potential, *i.e.* the tidal potential created by the perturbations *outside the outer boundary of the halo* (, i.e. R_{200}).

Let us expand the Hamiltonian and the distribution function, F, as:

$$\mathrm{F} = F + \varepsilon f\,, \quad \text{and} \quad \mathrm{H} = H_0 + \varepsilon\psi\,, \tag{2}$$

where we assume that everywhere in phase space $\varepsilon \triangleq m/M \ll 1$ i.e. that the mass of the perturbation, m, is small compared to the mass, M, of the unperturbed halo. In Eq. (2), f represents the small response to the perturbations, F represents the equilibrium state and ψ the small response in potential. Putting Eq. (2) into Eq. (1) and reordering in ε yields the linearized Boltzmann equation :

$$\frac{\mathrm{d}f}{\mathrm{d}t} + \frac{\mathrm{d}H_0}{\mathrm{d}\mathbf{I}}\cdot\frac{\mathrm{d}f}{\mathrm{d}\mathbf{w}} - \left(\frac{\mathrm{d}\psi}{\mathrm{d}\mathbf{w}} + \frac{\mathrm{d}\psi^e}{\mathrm{d}\mathbf{w}}\right)\cdot\frac{\mathrm{d}F}{\mathrm{d}\mathbf{I}} = s^e, \tag{3}$$

where $\mathbf{I}$ and $\mathbf{w}$ are conjugate canonical variables which are described in the following section.

2.1 The Boltzmann equation in action-angle

The most adequate representation of multiply-periodic integrable systems relies on the action-angle variables[2], since resonant processes will dominate the response of the live halo, and are best expressed in those variables. We will use vector notation for simplicity. The details of the computation of these variables is discussed in Appendix B following work by Murali (1999) (see also Fig. (1)). This achieves separation of variable between the phase space canonical variables (angle and actions) on the one hand, and time on the other hand. We denote as usual the set of action variables by $\mathbf{I}$ and angle variables by $\mathbf{w}$ (see Appendix B). The rates of change of angles is $\boldsymbol{\omega} \triangleq \mathrm{d}\mathbf{w}/\mathrm{d}t$. Along the multi-periodic orbits, any field, Z, can be Fourier-expanded with respect to the angles as:

$$Z(\mathbf{r}, \mathbf{v}, t) = \sum_{\mathbf{k}} Z_{\mathbf{k}}(\mathbf{I}, t)\exp(\imath\mathbf{k}\cdot\mathbf{w}). \tag{4}$$

Conversely

[2] Note that $(\mathbf{w}, \mathbf{I})$ are canonical variables, and as such preclude nothing about the evolution of the system. They simplify the expression of the linearized equations, order by order.

$$Z_{\mathbf{k}}(\mathbf{I},t) = \frac{1}{(2\pi)^3}\int \mathrm{d}\mathbf{w}\exp(-\imath\mathbf{k}\cdot\mathbf{w})Z(\mathbf{r},\mathbf{v},t)\,, \tag{5}$$

where $\mathbf{k}\triangleq(k_1,k_2,k_3)$ is the Fourier triple index conjugate to the three angles $\mathbf{w}\triangleq(w_1,w_2,w_3)$. Given Eqs. (1)-(2), the linearized Boltzmann equation in such a representation is:

$$\frac{\partial f_{\mathbf{k}}(\mathbf{I},t)}{\partial t}+\imath\mathbf{k}\cdot\boldsymbol{\omega}f_{\mathbf{k}}(\mathbf{I},t) = \imath\mathbf{k}\cdot\frac{\mathrm{d}F}{\mathrm{d}\mathbf{I}}(\psi_{\mathbf{k}}(\mathbf{I},t)+\psi^e_{\mathbf{k}}(\mathbf{I},t))+s^e_{\mathbf{k}}(\mathbf{I},t). \tag{6}$$

Here ψ is the potential perturbation created by the halo's inner density fluctuations and ψ^e the potential perturbation created by external fly byes. The gravitational field of incoming particles is accounted for by the source term s^e. The solution to Eq. (6) may then be written as:

$$\begin{aligned} f_{\mathbf{k}}(\mathbf{I},t) &= \int_{-\infty}^{t}\exp(\imath\mathbf{k}\cdot\boldsymbol{\omega}(\tau-t))\times \\ &\left[\imath\mathbf{k}\cdot\frac{\mathrm{d}F}{\mathrm{d}\mathbf{I}}\left[\psi_{\mathbf{k}}(\mathbf{I},\tau)+\psi^e_{\mathbf{k}}(\mathbf{I},\tau)\right]+s^e_{\mathbf{k}}(\mathbf{I},\tau)\right]\mathrm{d}\tau. \end{aligned} \tag{7}$$

Eq. (7) assumes that the perturbation has been switched on a long time ago in the past so that all transients have damped out.[3]

2.2 Self-consistency

Eq. (7) can be integrated over velocities and summed over $\mathbf{k}$ to get the density perturbation:

$$\begin{aligned} \rho(\mathbf{r},t) &= \sum_{\mathbf{k}}\int_{-\infty}^{t}\mathrm{d}\tau\int\mathrm{d}\mathbf{v}\,\exp(\imath\mathbf{k}\cdot\boldsymbol{\omega}(\tau-t)+\imath\mathbf{k}\cdot\mathbf{w})\times \\ &\left[\imath\mathbf{k}\cdot\frac{\mathrm{d}F}{\mathrm{d}\mathbf{I}}\left[\psi_{\mathbf{k}}(\mathbf{I},\tau)+\psi^e_{\mathbf{k}}(\mathbf{I},\tau)\right]+s^e_{\mathbf{k}}(\mathbf{I},\tau)\right]. \end{aligned} \tag{8}$$

Let us expand the potential and the density over a bi-orthogonal complete set of basis functions such that:

$$\psi(\mathbf{r},t)=\sum_{\mathbf{n}}a_{\mathbf{n}}(t)\psi^{[\mathbf{n}]}(\mathbf{r})\,,\quad \rho(\mathbf{r},t)=\sum_{\mathbf{n}}a_{\mathbf{n}}(t)\rho^{[\mathbf{n}]}(\mathbf{r})\,, \tag{9}$$

$$\nabla^2\psi^{[\mathbf{n}]}=4\pi G\rho^{[\mathbf{n}]}\,,\quad \int\psi^{[\mathbf{n}]*}(\mathbf{r})\rho^{[\mathbf{p}]}(\mathbf{r})\mathrm{d}\mathbf{r}=\delta^{\mathbf{n}}_{\mathbf{p}}\,, \tag{10}$$

(where $\psi^{[\mathbf{n}]*}(\mathbf{r})$ is the complex conjugate of $\psi^{[\mathbf{n}]}(\mathbf{r})$). We naturally expand the external potential on the same basis (Kalnajs (1971)) as:

$$\psi^e(\mathbf{r},t)=\sum_{\mathbf{n}}b_{\mathbf{n}}(t)\psi^{[\mathbf{n}]}(\mathbf{r}). \tag{11}$$

Thus, the coefficients $a_{\mathbf{n}}$ are representative of the density and potential perturbations in the halo itself, at $r<R_{200}$, while the coefficients $b_{\mathbf{n}}$ represent the potential created in the halo by density fluctuations at $r>R_{200}$. Taking advantage of bi-orthogonality Eq. (8) is multiplied by $\psi^*_{\mathbf{p}}(\mathbf{r})$ and integrated over $\mathbf{r}$, which yields:

$$\begin{aligned} a_{\mathbf{p}}(t) &= \sum_{\mathbf{k}}\int_{-\infty}^{t}\mathrm{d}\tau\iint\mathrm{d}\mathbf{v}\mathrm{d}\mathbf{r}\exp(\imath\mathbf{k}\cdot\boldsymbol{\omega}(\tau-t)+\imath\mathbf{k}\cdot\mathbf{w})\psi^{[\mathbf{p}]*}(\mathbf{r})\times \\ &\left[\sum_{\mathbf{n}}\imath\mathbf{k}\cdot\frac{\mathrm{d}F}{\mathrm{d}\mathbf{I}}\left[a_{\mathbf{n}}(\tau)+b_{\mathbf{n}}(\tau)\right]\psi^{[\mathbf{n}]}_{\mathbf{k}}(\mathbf{I})+s^e_{\mathbf{k}}(\mathbf{I},\tau)\right]. \end{aligned} \tag{12}$$

[3] Mathematically, we only retain the particular solution to Eq. (6), while assuming that the homogeneous solution did not hit long-lived resonances.

We may now swap from position-velocity to action-angle variables. Since this transformation is canonical $\mathrm{d}\mathbf{v}\mathrm{d}\mathbf{r}=\mathrm{d}\mathbf{w}\mathrm{d}\mathbf{I}$. In Eq. (12) only $\psi^{[\mathbf{p}]}(\mathbf{r})$ depends on $\mathbf{w}$, so we may carry the $\mathbf{w}$ integration over $\psi^{[\mathbf{p}]*}$, which yields $\psi^{[\mathbf{p}]*}_{\mathbf{k}}(\mathbf{I})$. Eq. (12) then becomes :

$$\begin{aligned} a_{\mathbf{p}}(t) &= (2\pi)^3\sum_{\mathbf{k}}\int_{-\infty}^{t}\mathrm{d}\tau\int\mathrm{d}\mathbf{I}\exp(\imath\mathbf{k}\cdot\boldsymbol{\omega}(\tau-t))\times \\ &\left[\sum_{\mathbf{n}}\imath\mathbf{k}\cdot\frac{\mathrm{d}F}{\mathrm{d}\mathbf{I}}\left[a_{\mathbf{n}}(\tau)+b_{\mathbf{n}}(\tau)\right]\psi^{[\mathbf{p}]*}_{\mathbf{k}}(\mathbf{I})\psi^{[\mathbf{n}]}_{\mathbf{k}}(\mathbf{I})+s^e_{\mathbf{k}}(\mathbf{I},\tau)\,\psi^{[\mathbf{p}]*}_{\mathbf{k}}(\mathbf{I})\right]. \end{aligned} \tag{13}$$

At this point, it seems natural to expand the source term on a basis too, but unlike the previous one, this basis should also describe velocity space. We admit for now that such a basis $\phi_n(\mathbf{r},\mathbf{v})$ exists, and write:

$$s^e(\mathbf{r},\mathbf{v},t)=\sum_{\mathbf{n}}c_{\mathbf{n}}(t)\phi^{[\mathbf{n}]}(\mathbf{r},\mathbf{v})\,,\quad \text{so} \tag{14}$$

$$s^e_{\mathbf{k}}(\mathbf{I},\tau)\;=\sum_{\mathbf{n}}c_{\mathbf{n}}(\tau)\sigma^{[\mathbf{n}]e}_{\mathbf{k}}(\mathbf{I}), \tag{15}$$

where $\sigma^{[\mathbf{n}]e}_{\mathbf{k}}(\mathbf{I})$ is the angle transform of $\phi^{[\mathbf{n}]}(\mathbf{r},\mathbf{v})$ (see Eq. (24) below). The coefficients $c_{\mathbf{n}}$ are representative of the mass exchange between the halo and the external world. The sum in Eq. (15) spans velocity space as well as configuration space, and therefore involve significantly more terms. Such an expansion is performed in Aubert & Pichon (2005a) to constrain the source function measured in cosmological simulations. Calling $\mathbf{a}(\tau)=[a_1(\tau),\cdots,a_{\mathbf{n}}(\tau)\cdots]$, $\mathbf{b}(\tau)=[b_1(\tau),\cdots,b_{\mathbf{n}}(\tau)\cdots]$, and $\mathbf{c}(\tau)=[c_1(\tau),\cdots,c_{\mathbf{n}}(\tau)\cdots]$, we define two matrices, $\mathbf{K}$ and $\mathbf{Q}$. The matrix $\mathbf{K}$ has elements $K_{\mathbf{p},\mathbf{n}}$ defined by:

$$K_{\mathbf{p},\mathbf{n}}(\tau)=(2\pi)^3\sum_{\mathbf{k}}\int\mathrm{d}\mathbf{I}\exp(\imath\mathbf{k}\cdot\boldsymbol{\omega}\tau)\imath\mathbf{k}\cdot\frac{\mathrm{d}F}{\mathrm{d}\mathbf{I}}\psi^{[\mathbf{p}]*}_{\mathbf{k}}(\mathbf{I})\psi^{[\mathbf{n}]}_{\mathbf{k}}(\mathbf{I}), \tag{16}$$

which depend only on the halo equilibrium state. The matrix $\mathbf{Q}$ has elements

$$Q_{\mathbf{p},\mathbf{n}}(\tau)=(2\pi)^3\sum_{\mathbf{k}}\int\mathrm{d}\mathbf{I}\exp(\imath\mathbf{k}\cdot\boldsymbol{\omega}\tau)\sigma^{[\mathbf{n}]e}_{\mathbf{k}}(\mathbf{I})\,\psi^{[\mathbf{p}]*}_{\mathbf{k}}(\mathbf{I}), \tag{17}$$

which depend only on the source's expansion basis. Equation (13) then becomes:

$$\mathbf{a}(t)=\int_{-\infty}^{t}\mathrm{d}\tau\,(\mathbf{K}(\tau-t)\cdot[\mathbf{a}(\tau)+\mathbf{b}(\tau)]+\mathbf{Q}(\tau-t)\cdot\mathbf{c}(\tau))\,. \tag{18}$$

The kernels $\mathbf{K}$ and $\mathbf{Q}$ are functions of the equilibrium state distribution function, F, and of the two bases, $\phi^{[\mathbf{n}]}(\mathbf{r},\mathbf{v})$, and $\psi^{[\mathbf{n}]}(\mathbf{r})$ only. They may be computed once and for all for a given equilibrium model. Assuming linearity and knowing $\mathbf{K}$ and $\mathbf{Q}$, one can see that the properties of the environments (represented by $\mathbf{b}$ and $\mathbf{c}$) are *propagated* to the inner dynamical properties of collisionless systems (described by $\mathbf{a}$). We may perform a "half" Fourier transform with respect to time. In the limit where the transients may be neglected, which implies that the system should be stable, this transform amounts to a Laplace transform with $p=\imath\omega+\epsilon^+$. Temporal convolutions are then replaced by matrix multiplications and Eq. (18) becomes:

$$\hat{\mathbf{a}}(\omega)=(\mathbf{1}-\hat{\mathbf{K}}(\omega))^{-1}\cdot\left[\hat{\mathbf{K}}(\omega)\cdot\hat{\mathbf{b}}(\omega)+\hat{\mathbf{Q}}(\omega)\cdot\hat{\mathbf{c}}(\omega)\right]. \tag{19}$$

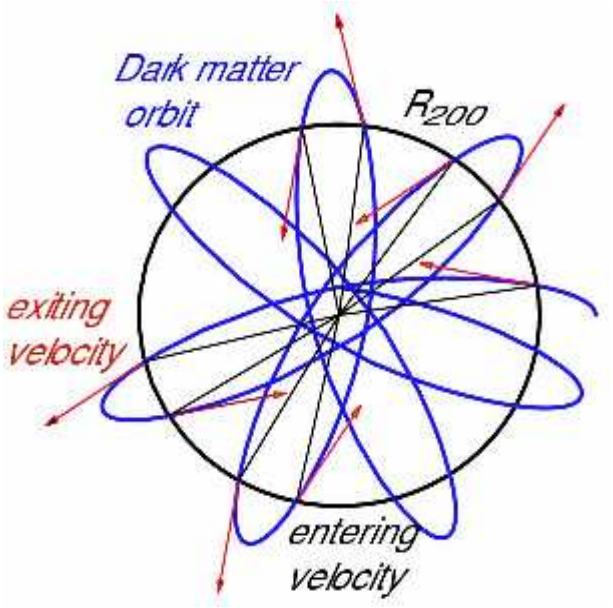

Figure 2. A typical rosette orbit in its orbital plane; the intersection with the R_{200} sphere is shown, together with the corresponding velocity vectors, both entering and exiting. The net flux of such quantities enters Eq. (25) and characterize the source of infall perturbing the halo. Note that by construction, in the linear regime all infalling material re-exits R_{200}, since the perturbation evolves along the unperturbed orbits. This is to be contrasted to the situation presented in Fig. (3) where dynamical friction is qualitatively accounted for.

In this expression, $\mathbf{1}$ is the identity matrix, and $\hat{\mathbf{K}}$ and $\hat{\mathbf{Q}}$ include Heaviside functions before Fourier transform to account for causality (see Aubert et al. (2004) for details). Section D3 gives an explicit expression for $\hat{\mathbf{K}}(\omega)$. Note the difference between $\boldsymbol{\omega}$, the angular frequency of the orbits, defined above Eq. (6), and ω, the half Fourier transform variable associated with time which appears in Eq. (19). Here $\mathbf{b}$ and $\mathbf{c}$ could be given deterministic functions of time, or stochastic random fields (characterized statistically in Aubert & Pichon (2005a)). In contrast, $\mathbf{a}$ describes the detailed response of the halo in phase space within R_{200}.

2.2.1 *Higher moments*

The second moment is obtained by multiplying (7) by $\mathbf{v}$ and by performing an integration over velocities. Summing over $\mathbf{k}$ leads to:

$$\rho\bar{\mathbf{v}}(\mathbf{r},t) = \sum_{\mathbf{k}} \int_{-\infty}^{t} \mathrm{d}\tau \int \mathrm{d}\mathbf{v} \exp(\imath\mathbf{k}\cdot\boldsymbol{\omega}(\tau-t)+\imath\mathbf{k}\cdot\mathbf{w}) \times \left[\imath\mathbf{k}\cdot\frac{\mathrm{d}F}{\mathrm{d}\mathbf{I}}\mathbf{v}\left[\psi_{\mathbf{k}}(\mathbf{I},\tau)+\psi^{e}_{\mathbf{k}}(\mathbf{I},\tau)\right]+\mathbf{v}s^{e}_{\mathbf{k}}(\mathbf{I},\tau)\right]. \quad (20)$$

Using the same biorthonormal expansion as above, we may express the mass flux as a function of the coefficients $a_{\mathbf{n}}$ and $b_{\mathbf{n}}$ (associated with the potential perturbations of external origin). If we define the following new tensors:

$$K_{[2],\mathbf{n}}(\mathbf{r},\tau) = \sum_{\mathbf{k}} \int \mathrm{d}\mathbf{v} \exp(\imath\mathbf{k}\cdot\boldsymbol{\omega}\tau+\imath\mathbf{k}\cdot\mathbf{w})\,\mathbf{v}\,\imath\mathbf{k}\cdot\frac{\mathrm{d}F}{\mathrm{d}\mathbf{I}}\psi^{[\mathbf{n}]}_{\mathbf{k}}(\mathbf{I}), \quad (21)$$

and a similar expression for $Q_{[2],\mathbf{n}}(\mathbf{r},\tau)$, involving the source's expansion basis, the mass flux may be written as a convolution:

$$\rho\bar{\mathbf{v}}(\mathbf{r},t) = \int_{-\infty}^{t}\mathrm{d}\tau\,(\mathbf{K}_2(\mathbf{r},\tau-t)\cdot[\mathbf{a}(\tau)+\mathbf{b}(\tau)]+\mathbf{Q}_2(\mathbf{r},\tau-t)\cdot\mathbf{c}(\tau)).$$

After half Fourier transforming with respect to time, we get

$$\rho\hat{\bar{\mathbf{v}}} = \hat{\mathbf{K}}_{[2]}(\mathbf{r},\omega)\cdot(\mathbf{1}-\hat{\mathbf{K}})^{-1}\cdot\left[\hat{\mathbf{b}}+\hat{\mathbf{Q}}\cdot\hat{\mathbf{c}}\right]+\hat{\mathbf{Q}}_{[2]}(\mathbf{r},\omega)\cdot\hat{\mathbf{c}}. \quad (22)$$

We will return to Eq. (22) in Section 5.

2.3 Sinks, sources and tidal field

Let us now turn to an explicit description of the source term (s^e, hence $\mathbf{c}$), and the tidal field (ψ^e, hence $\mathbf{b}$) entering Eq. (6). We consider here a source at the virial radius corresponding to cosmic infall. Note however that we might have considered just as well sinks reflecting the presence of a super massive black hole at the center of the host galaxy or the deflection/absorption of orbits due to a galactic disk.

2.3.1 *Source of infall at R_{200}*

A possible Ansatz for the source term consistent with the first two velocity moments of the entering matter has been proposed by Aubert et al. (2004). Following them $s^e(\mathbf{r},\mathbf{v},t)$ can be written as

$$s^e(\mathbf{r},\mathbf{v},t) \triangleq \sum_{\mathbf{m}} Y_{\mathbf{m}}(\boldsymbol{\Omega})\delta_{\mathrm{D}}(r-R_{200})\left(\sum_{\boldsymbol{\alpha}} c_{\mathbf{n}}(t)g_{\boldsymbol{\alpha}}(\mathbf{v})\,Y_{\mathbf{m}}(\boldsymbol{\Omega})\right),$$

where $\mathbf{m}$ stands for the two harmonic numbers, (ℓ,m) and $Y_{\mathbf{m}}(\boldsymbol{\Omega}) \triangleq Y^m_\ell(\boldsymbol{\Omega})$ is the usual spherical harmonic. The Dirac function $\delta_{\mathrm{D}}(r-R_{200})$ appears because the source terms are located at the virial radius in our representation[4]. This equation corresponds to the parameterization of $\phi^{[\mathbf{n}]}$ as:

$$\begin{aligned}\phi^{[\mathbf{n}]}(\mathbf{r},\mathbf{v}) &= g_{\boldsymbol{\alpha}}(\mathbf{v})\,Y_{\mathbf{m}}(\boldsymbol{\Omega})\delta_{\mathrm{D}}(r-R_{200}),\\ &\triangleq g_{\alpha}(v)\,Y_{\mathbf{m}}(\boldsymbol{\Omega})Y_{\mathbf{m}'}(\boldsymbol{\Gamma})\delta_{\mathrm{D}}(r-R_{200}), \end{aligned} \quad (23)$$

of Gaussian functions, $g_{\boldsymbol{\alpha}}$, covering the radial velocity component and spherical harmonics for the angle distribution, $\boldsymbol{\Gamma}$, of the velocity vector and orientation, $\boldsymbol{\Omega} = (\theta,\phi)$ of the infall (see Aubert & Pichon (2005a) for details). Here we have $\boldsymbol{n} \triangleq [\boldsymbol{m},\boldsymbol{\alpha}] \triangleq [\boldsymbol{m},\boldsymbol{m}',\alpha] \triangleq [\ell,m,\ell',m',\alpha]$. From Eq. (15)

$$\sigma^{[\mathbf{n}]e}_{\mathbf{k}}(\mathbf{I}) \triangleq \frac{1}{(2\pi)^3}\int \mathrm{d}^3\mathbf{w}\exp(-\imath\mathbf{k}\cdot\mathbf{w})\phi^{[\mathbf{n}]}(\mathbf{r},\mathbf{v}). \quad (24)$$

With Eq.(23), Eq. (24) becomes

$$\sigma^{[\mathbf{n}]e}_{\mathbf{k}}(\mathbf{I}) = \frac{1}{(2\pi)^3}\int \mathrm{d}^3\mathbf{w}\exp(-\imath\mathbf{k}\cdot\mathbf{w})\,Y_{\mathbf{m}}[\boldsymbol{\Omega}(\mathbf{I},\mathbf{w})]\times g_{\boldsymbol{\alpha}}(\mathbf{v}[\mathbf{I},\mathbf{w}])\delta_{\mathrm{D}}(r(\mathbf{I},\mathbf{w})-R_{200}). \quad (25)$$

[4] This choice is mainly justified by the measurments performed in Aubert et al. (2004) and Aubert & Pichon (2005a) and stands as a good compromise between a relaxed halo inside this boundary and a low contribution of the orbits of relaxed particles to the flux.

We can make use of the $\delta_{\rm D}$ function occurring in Eq. (25) since $w_r \triangleq \tilde{w}_r(r,\mathbf{I})$ (given by Eq. (B1)). Therefore Eq. (25) reads:

$$\sigma^{[\mathbf{n}]e}_{\mathbf{k}}(\mathbf{I}) = \int \frac{\mathrm{d}^2\mathbf{w}}{(2\pi)^3} \int \mathrm{d}w_r \exp\left(-\imath \mathbf{k}\cdot\mathbf{w}\right) Y_{\mathbf{m}}[\mathbf{\Omega}(\mathbf{I},\mathbf{w})] \times g_{\boldsymbol{\alpha}}(\mathbf{v}[\mathbf{I},\mathbf{w}]) \frac{1}{|\partial\tilde{w}_r/\partial r|^{-1}} \delta_{\rm D}(w_r - \tilde{w}_r[R_{200},\mathbf{I}]) \,, \quad (26)$$

$$= \int \frac{\mathrm{d}^2\mathbf{w}}{(2\pi)^3} \exp\left(-\imath \mathbf{k}\cdot\mathbf{w}\right) Y_{\mathbf{m}}[\mathbf{\Omega}(\mathbf{I},\mathbf{w},\tilde{w}_r[R_{200},\mathbf{I}])] \times g_{\boldsymbol{\alpha}}(\mathbf{v}[\mathbf{I},\mathbf{w},\tilde{w}_r(R_{200},\mathbf{I})]) \frac{\omega_r(\mathbf{I})}{|\dot{r}(R_{200},\mathbf{I})|} \exp\left(-\imath k_r\cdot\tilde{w}_r[R_{200},\mathbf{I}]\right) \,.$$

In Eq. (26) we sum over all intersections of the orbit $\mathbf{I}$ with the R_{200} sphere, at the radial phase corresponding to that intersection with a weight corresponding to $\omega_r/|\dot{r}|$ (see Fig. (2)). Note that Eq. (26) involves $\mathrm{d}^2\mathbf{w} \triangleq \mathrm{d}w_2\mathrm{d}w_3$.

2.3.2 *Tidal excitation from beyond R_{200}*

The tidal potential is given as a boundary condition on the virial sphere and deprojected in volume. Let us call $b'_{\ell m}(t)$ the harmonic coefficients of the expansion of the external potential on the virial sphere. We expand the potential over the biorthogonal basis, $(u^{\ell m}_n, d^{\ell,m}_{n'})$ (see Appendix B), so that

$$\psi^e(r,\mathbf{\Omega},t) = \sum_{n,\ell,m} b'_{\ell m}(t)\, Y^m_\ell(\mathbf{\Omega}) \left(\frac{r}{R_{200}}\right)^\ell , = \sum_{\mathbf{n}} b_{\mathbf{n}}(t)\psi^{[\mathbf{n}]}(\mathbf{r}) \,, \quad (27)$$

where $\psi^{[\mathbf{n}]}(\mathbf{r}) \triangleq Y^m_\ell(\mathbf{\Omega}) u^{\ell m}_j(r)$. The first equality in Eq. (27) corresponds to the inner solution of the three-dimensional potential whose boundary condition is given by $Y^\ell_m(\mathbf{\Omega}) b'_{\ell m}$ on the sphere of radius R_{200} (defined below). Since the basis is biorthogonal, it follows that

$$b_{\mathbf{n}}(t) = \left(\int d^{\ell m}_n(r) \left(\frac{r}{R_{200}}\right)^\ell \mathrm{d}r \right) b'_{\ell m}(t) \,. \quad (28)$$

It is therefore straightforward to recover the coefficient of the 3D external potential from that of the potential on the sphere.

2.4 Induced correlations in the halo

Our purpose is to characterize *statistically* the response of the dark matter halo to tidal perturbation and infall. This is best done by computing the N-point statistics of the perturbed density field. Let us start with the two-point correlation. From Eq.(19) the variance-covariance matrix of the response is given by

$$\left\langle \hat{\mathbf{a}}\cdot\hat{\mathbf{a}}^{*\top} \right\rangle = \left\langle \left[\hat{\mathbf{K}}\cdot\hat{\mathbf{b}} + \hat{\mathbf{Q}}\cdot\hat{\mathbf{c}}\right]\cdot(\mathbf{1}-\hat{\mathbf{K}})^{-1}\cdot (\mathbf{1}-\hat{\mathbf{K}})^{-1*\top}\cdot\left[\hat{\mathbf{K}}\cdot\hat{\mathbf{b}} + \hat{\mathbf{Q}}\cdot\hat{\mathbf{c}}\right]^{\top *} \right\rangle. \quad (29)$$

This expression of the $\mathbf{n}\times\mathbf{n}$ matrix, $\langle \hat{\mathbf{a}}\cdot\hat{\mathbf{a}}^{*\top}\rangle$ involves autocorrelation terms like the components of $\langle \hat{\mathbf{b}}\cdot\hat{\mathbf{b}}^{*\top}\rangle$ (the tidal field) and $\langle \hat{\mathbf{c}}\cdot\hat{\mathbf{c}}^{*\top}\rangle$ (the source of infall), but also cross-correlation terms such as the components of $\langle \hat{\mathbf{b}}\cdot\hat{\mathbf{c}}^{*\top}\rangle$. For a spherical harmonic basis, the induced density perturbation reads (see Eq. (B2) in Appendix B)

$$\rho(r,\mathbf{\Omega},t) = \sum_{\mathbf{n}} a_{\mathbf{n}}\rho_{\mathbf{n}}(\mathbf{r}) = \sum_{n\ell m} a^n_{\ell m}(t) Y^m_\ell(\mathbf{\Omega}) d^n_{\ell m}(r) \,, \quad (30)$$

The functions $d^n_{\ell m}(r)$ depend on the chosen basis. An example is given by Eq. (B3). Again, $\mathbf{n}$ stands here for n,ℓ,m, respectively the radial and the two angular 'quantum numbers'. As a consequence the two-point correlation function for the perturbed density reads

$$\left\langle \rho(r,\mathbf{\Omega}+\Delta\mathbf{\Omega},t+\Delta t)\rho(r',\mathbf{\Omega},t)\right\rangle = \sum_{n\ell m n'\ell' m'} Y^m_\ell(\mathbf{\Omega}) \times Y^{m'*}_{\ell'}(\mathbf{\Omega}+\Delta\mathbf{\Omega}) d^n_{\ell m}(r) d^{n'}_{\ell' m'}(r') \langle a^n_{\ell m}(t) a^{n'*}_{\ell' m'}(t+\Delta t)\rangle. \quad (31)$$

The statistical averages, $\langle a^n_{\ell m}(t) a^{n'*}_{\ell' m'}(t+\Delta t)\rangle$ are given by the temporal inverse Fourier transform of Eq. (29). If the perturbation is stationary and statistically rotationally invariant $\langle a^n_{\ell m}(t) a^{n'}_{\ell' m'}(t+\Delta t)\rangle \triangleq C^{nn'}_\ell(\Delta t)\delta^{m'}_m\delta^{\ell'}_\ell$. The correlation function then obeys

$$\left\langle \rho(r,\mathbf{\Omega}+\Delta\mathbf{\Omega},t+\Delta t)\rho(r',\mathbf{\Omega},t)\right\rangle = \sum_{nn'\ell m} P_\ell(\cos(\gamma)) d^n_{\ell m}(r) d^{n'}_{\ell m}(r') C^{nn'}_\ell(\Delta t) \,, \quad (32)$$

where γ stands for the angle between $\mathbf{\Omega}$ and $\mathbf{\Omega}'$. Evaluating Eq. (32) for $\gamma = 0$, $\Delta t = 0$, $r = r'$ gives a measure of the cosmic variance of the amplitude of the response of the halo as a function of radius r. The full-width half maximum (FWHM) of $\langle \rho(r,\mathbf{\Omega}+\Delta\mathbf{\Omega},t)\rho(r,\mathbf{\Omega},t)\rangle$ is a measure as a function of time, t, and radius, r, of the angular extent of the ensemble average mean polarization. Conversely, the FWHM of $\langle \rho(r,\mathbf{\Omega},t)\rho(r+\Delta r,\mathbf{\Omega},t)\rangle$ is a measure of its radial extent in the direction $\mathbf{\Omega}$. Note that Eq. (7) together with (18) yield a description of the response both in position and velocity. For instance, Eq. (22) allow us to predict the induced correlations amongst streams. Applications of Eqs. (29)-(32) (and their non-linear generalization in Section 3.2) will be discussed in greater details in Section 5. The actual implementation of Eqs. (29)-(**??**)s carried in a simplified framework in Section B4.

2.4.1 *Link with propagators*

Let us emphasize that the splitting of the gravitational field into two components, one originating outside of R_{200}, and one from the inside, via point particles obeying the distribution $s^e(\mathbf{r},\mathbf{v},t)$ is somewhat *ad hoc* from the point of view of the linear dynamics. It is convenient from the point of view of the measurements, and crucial for the non-linear evolution (described below), or the ensemble average, as shown above [5]. It allows us to specify the statistical characteristics of the infall without having to refer to the properties of the object on which this infall occurs.

We discuss in appendix A the formulation of the response of a self-gravitating sphere in terms of a propagator (*i.e.* the Green function of the collisionless Boltzmann-Poisson equation).

[5] One should account for the fact that ψ_e should be switched on long before any particles enter R_{200} since no particle is created at the boundary.

This formulation is mathematically equivalent to the approach described above, but there we relied on Gauss's theorem to reproject all the information beyond R_{200} back onto the virial sphere. This information involves two contributions: one relative to particles beyond R_{200}, which contribute to the tidal field, the other relative to particles entering R_{200} which contribute to $s^e(\mathbf{\Omega}, \mathbf{v})$)

The main asset of this formulation is to localize the boundary, which is possible since the interaction is purely gravitational, at the expense of having *two* sources of different nature. In particular, this implies that the environment may be characterized once and for all, independently of the detailed nature of the inner halo.

In this section, we assumed that the polarisation of the halo was *linear*. This hopefully provided some insight for some aspects of the dynamics, but effectively ignores non-linear phenomena such as dynamical friction or tidal stripping. Let us now expand perturbation theory to higher orders.

3 NON-LINEAR PERTURBATIVE RESPONSE

In the following, we describe, using perturbation theory, the non linear response of the halo to material entering at the virial sphere. It is assumed that the perturbation is first-order in the hierarchy, and that the halo is dynamically stable. This should warrant the validity of the expansion. We use the angle-action variables of the *unperturbed* system as canonical variables and investigate the non-linear evolution of the infall and the tidal excitation.
In essence, the key is to expand the potential onto the biorthogonal potential density basis which allows us to decouple position-velocity and time (i.e. perform a separation of variable), and solve in turns each order of the perturbation expansion.

3.1 Perturbative expansion

Recall that the dynamical equation of an open system characterized by its distribution function, F is given by Eq. (1). Let us expand again F as

$$\mathrm{F} = F + \sum_{\mathrm{n}} \varepsilon^{\mathrm{n}} f^{(\mathrm{n})}, \quad \text{and} \quad \mathrm{H} = H_0 + \sum_{\mathrm{n}} \varepsilon^{\mathrm{n}} \psi^{(\mathrm{n})}, \tag{33}$$

where the unperturbed equilibrium is characterized by the distribution function, $F(\mathbf{I})$. Note that (n), the order of the expansion should not be confused with $\mathbf{n} \triangleq (n, \ell, m)$. Finally, it is assumed that the external perturbation enters as a first-order only, *i.e.* $s^e \propto \varepsilon$ and $\psi^e \propto \varepsilon$. In short, the rewriting of Eq. (1) to order ε^{n} yields:

$$\frac{\partial f^{(\mathrm{n})}_{\mathbf{k}}}{\partial t} + \imath \mathbf{k} \cdot \boldsymbol{\omega} f^{(\mathrm{n})}_{\mathbf{k}} = \left(\frac{\partial F}{\partial \mathbf{I}} \cdot \imath \mathbf{k} [\, \psi^{(\mathrm{n})}_{\mathbf{k}} + \delta^1_{\mathrm{n}} \psi^e_{\mathbf{k}}] - \sum_{k=1}^{\mathrm{n}-1} \{\psi^{(k)}, f^{(\mathrm{n}-k)}\}_{\mathbf{k}} + \delta^1_{\mathrm{n}} s^e_{\mathbf{k}} \right). \tag{34}$$

In the following, we solve Eq. (34) recursively, order by order, to recover the perturbative response of the halo to the tidal interaction and infall. We expand both the potentials and the source term over a biorthogonal basis, so that, with $^{(\mathrm{n})}$ referring to the order in the hierarchy and $^{[\mathbf{p}]}$ to the label in the basis

$$\psi^{(\mathrm{n})}_{\mathbf{k}}(\mathbf{I}, t) = \sum_{\mathbf{p}} a^{(\mathrm{n})}_{\mathbf{p}}(t) \psi^{[\mathbf{p}]}_{\mathbf{k}}(\mathbf{I}), \quad \psi^e_{\mathbf{k}}(\mathbf{I}, t) = \sum_{\mathbf{p}} b_{\mathbf{p}}(t) \psi^{[\mathbf{p}]}_{\mathbf{k}}(\mathbf{I}), \qquad s^e_{\mathbf{k}}(\mathbf{I}, t) = \sum_{\mathbf{p}} c_{\mathbf{p}}(t) \sigma^{[\mathbf{p}]}_{\mathbf{k}}(\mathbf{I}). \tag{35}$$

Recall also that the superscript, $^{[\mathbf{p}]}$, in Eq. (35) spans discretely a 3D or 5D space depending on the type of function basis. The first-order solution for $a_{\mathbf{p}}$ was given Eq. (13). Let us turn to the higher order equations.

3.1.1 *Second-order perturbation theory*

The second-order equation for $a^{(2)}_{\mathbf{p}}$ reads

$$\begin{aligned} a^{(2)}_{\mathbf{p}}(t) \quad = \quad & (2\pi)^3 \sum_{\mathbf{n}} \int_{-\infty}^{t} \mathrm{d}\tau \, a^{(2)}_{\mathbf{n}}(\tau) \left(\sum_{\mathbf{k}} \int \mathrm{d}\mathbf{I} \psi^{[\mathbf{n}]}_{\mathbf{k}}(\mathbf{I}) \psi^{[\mathbf{p}]*}_{\mathbf{k}}(\mathbf{I}) \, \frac{\partial F}{\partial \mathbf{I}} \cdot \imath \mathbf{k} \exp(\imath \mathbf{k} \cdot \boldsymbol{\omega} [\tau - t]) \right) + \\ & (2\pi)^3 \int_{-\infty}^{t} \mathrm{d}\tau \sum_{\mathbf{k}} \int \mathrm{d}\mathbf{I} \exp(\imath \mathbf{k} \cdot \boldsymbol{\omega} [\tau - t]) \left\{ f^{(1)}(\tau, \mathbf{w}, \mathbf{I}), \psi^{(1)}(\tau, \mathbf{w}, \mathbf{I}) \right\}_{\mathbf{k}} \psi^{[\mathbf{p}]*}_{\mathbf{k}}(\mathbf{I}), \end{aligned} \tag{36}$$

where $\{f^{(1)}, \psi^{(1)}\}$ is the Poisson bracket of the perturbation to first-order. Now for a set (f, ψ) we have

$$\{f, \psi\}_{\mathbf{k}} = \int \mathrm{d}\mathbf{w} \exp(-\imath \mathbf{k} \cdot \mathbf{w}) \left\{ \sum_{\mathbf{k}_1} f_{\mathbf{k}_1}(\mathbf{I}) \exp(\imath \mathbf{k}_1 \cdot \mathbf{w}), \sum_{\mathbf{k}_2} \psi_{\mathbf{k}_2}(\mathbf{I}) \exp(\imath \mathbf{k}_2 \cdot \mathbf{w}) \right\}. \tag{37}$$

Therefore

$$\{f,\psi\}_{\mathbf{k}} = \sum_{\mathbf{k}_1+\mathbf{k}_2=\mathbf{k}} \left(\psi_{\mathbf{k}_2} \frac{\partial f_{\mathbf{k}_1}}{\partial \mathbf{I}} \cdot \imath \mathbf{k}_2 \; - f_{\mathbf{k}_1} \frac{\partial \psi_{\mathbf{k}_2}}{\partial \mathbf{I}} \cdot \imath \mathbf{k}_1 \right) \triangleq \sum_{\mathbf{k}_1+\mathbf{k}_2=\mathbf{k}} [\![f_{\mathbf{k}_1}, \psi_{\mathbf{k}_2}]\!] \; , \tag{38}$$

where the sum is over $\mathbf{k}_1$ with $\mathbf{k}_2 = \mathbf{k} - \mathbf{k}_1$. Given Eq. (7), Eq. (36) may be rearranged as

$$\begin{aligned} a^{(2)}_{\mathbf{p}}(t) \quad = \quad & (2\pi)^3 \sum_{\mathbf{q}_1} \int_{-\infty}^{t} \mathrm{d}\tau_1 \, a^{(2)}_{\mathbf{q}_1}(\tau_1) \left(\sum_{\mathbf{k}} \int \mathrm{d}\mathbf{I} \psi^{[\mathbf{q}_1]}_{\mathbf{k}}(\mathbf{I}) \psi^{[\mathbf{p}]*}_{\mathbf{k}}(\mathbf{I}) \; \frac{\partial F}{\partial \mathbf{I}} \cdot \imath \mathbf{k} \exp(\imath \mathbf{k} \cdot \boldsymbol{\omega}[\tau_1 - t]) \right) + \\ & (2\pi)^3 \int^{t} \mathrm{d}\tau_1 \int^{\tau_1} \mathrm{d}\tau_2 \left(\sum_{\mathbf{k}} \int \mathrm{d}\mathbf{I} \exp(\imath \mathbf{k} \cdot \boldsymbol{\omega}[\tau_1 - t]) \sum_{\mathbf{q}_1, \mathbf{q}_2} [a^{(1)}_{\mathbf{q}_1}(\tau_1) + b_{\mathbf{q}_1}(\tau_1)] \times \right. \\ & \left. \sum_{\mathbf{k}_1+\mathbf{k}_2=\mathbf{k}} \left[\!\!\left[\exp(\imath \mathbf{k}_1 \cdot \boldsymbol{\omega}[\tau_2 - \tau_1]) \left[\frac{\partial F}{\partial \mathbf{I}} \cdot \imath \mathbf{k}_1 \; [a^{(1)}_{\mathbf{q}_2}(\tau_2) + \; b_{\mathbf{q}_2}(\tau_2)] \psi^{[\mathbf{q}_2]}_{\mathbf{k}_1}(\mathbf{I}) + c_{\mathbf{q}_2}[\tau_2] \sigma^{e,[\mathbf{q}_2]}_{\mathbf{k}_1}(\mathbf{I}) \right] , \psi^{[\mathbf{q}_1]}_{\mathbf{k}_2} \right]\!\!\right] \psi^{[\mathbf{p}]*}_{\mathbf{k}} \right) . \end{aligned} \tag{39}$$

Note that the r.h.s. of Eq.(39) is linear in $\mathbf{a}^{(2)}$ while it is quadratic in $\mathbf{a}^{(1)}$, $\mathbf{b}^{(1)}$, $\mathbf{c}^{(1)}$, involving products such as $\mathbf{a}\,\mathbf{a}$, $\mathbf{a}\,\mathbf{c}$, $\mathbf{b}\,\mathbf{c}$ and so on. More generally, the perturbation theory at order (n) is linear in $a^{(n)}$. Note also that Eq. (39) involves a double ordered time integral over τ_1 and τ_2 of the source coefficient, $c_{\mathbf{q}_1}(\tau_1)$ and $c_{\mathbf{q}_2}(\tau_2)$, which accounts for the fact that, non-linearly, the relative phase of the accretion events matter (Eq. (D12) gives the analog to Eq. (39) in the complex frequency plane). Eq (39) includes in particular a term like

$$\exp(\imath(\mathbf{k}_1+\mathbf{k}_2)\cdot\boldsymbol{\omega}[\tau_1-t])\exp(\imath\mathbf{k}_1\cdot\boldsymbol{\omega}[\tau_2-\tau_1])\psi^{[\mathbf{p}]*}_{\mathbf{k}_1+\mathbf{k}_2} \sum_{\mathbf{q}_1,\mathbf{q}_2} \left(\frac{\partial \sigma^{e,[\mathbf{q}_2]}_{\mathbf{k}_1}}{\partial \mathbf{I}} \psi^{[\mathbf{q}_1]}_{\mathbf{k}_2} - \frac{\partial \psi^{[\mathbf{q}_1]}_{\mathbf{k}_2}}{\partial \mathbf{I}} \sigma^{e,[\mathbf{q}_2]}_{\mathbf{k}_1} \right) \left(a^{(1)}_{\mathbf{q}_1}(\tau_1) + b_{q_1}(\tau_1) \right) c_{q_2}(\tau_2) \tag{40}$$

which involves the rate of change of the source term with respect to action variation (via $\partial \sigma^{e,[\mathbf{q}_2]}_{\mathbf{k}_1} / \partial \mathbf{I}$) modulated twice over time as $\exp(\imath(\mathbf{k}_1+\mathbf{k}_2)\cdot\boldsymbol{\omega}[\tau_1-t])\exp(\imath\mathbf{k}_1\cdot\boldsymbol{\omega}[\tau_2-\tau_1])$.

The second order solution can be synthetically written by introducing tensors $\mathbf{K}_2$ and $\mathbf{Q}_2$ similar to those defined in Eq. (16) and Eq. (17) to express the first order solution as Eq. (18). These latter tensors will now be referred to as $\mathbf{K}_1$ and $\mathbf{Q}_1$. Specifically, the components of these tensors are defined as:

$$(\mathbf{K}_1)_{\mathbf{p},\mathbf{q}_1}[\tau_1 - t] \triangleq (\mathbf{K})_{\mathbf{p},\mathbf{q}_1}[\tau_1 - t] = (2\pi)^3 \sum_{\mathbf{k}} \int \mathrm{d}\mathbf{I} \exp(\imath \mathbf{k} \cdot \boldsymbol{\omega}[\tau_1 - t]) \psi^{[\mathbf{p}]*}_{\mathbf{k}} \, \psi^{[\mathbf{q}_1]}_{\mathbf{k}} \; \frac{\partial F}{\partial \mathbf{I}} \cdot \imath \mathbf{k} \, , \tag{41}$$

$$(\mathbf{K}_2)_{\mathbf{p},\mathbf{q}_1,\mathbf{q}_2}[\tau_1 - t, \tau_2 - \tau_1] = (2\pi)^3 \sum_{\mathbf{k}} \int \mathrm{d}\mathbf{I} \exp(\imath \mathbf{k} \cdot \boldsymbol{\omega}[\tau_1 - t]) \sum_{\mathbf{k}_1+\mathbf{k}_2=\mathbf{k}} \left[\!\!\left[\exp(\imath \mathbf{k}_1 \cdot \boldsymbol{\omega}[\tau_2 - \tau_1]) \frac{\partial F}{\partial \mathbf{I}} \cdot \imath \mathbf{k}_1 \; \psi^{[\mathbf{q}_2]}_{\mathbf{k}_1}, \psi^{[\mathbf{q}_1]}_{\mathbf{k}_2} \right]\!\!\right] \psi^{[\mathbf{p}]*}_{\mathbf{k}} \, , \tag{42}$$

while $\mathbf{Q}_i$ involves replacing $\psi^{[\mathbf{q}]}_{\mathbf{k}} \, \partial F / \partial \mathbf{I} \cdot \mathbf{k}$ by $\sigma^{e,[\mathbf{q}]}_{\mathbf{m}}$. For instance,

$$(\mathbf{Q}_2)_{\mathbf{p},\mathbf{q}_1,\mathbf{q}_2}[\tau_1 - t, \tau_2 - \tau_1] = (2\pi)^3 \sum_{\mathbf{k}} \int \mathrm{d}\mathbf{I} \exp(\imath \mathbf{k} \cdot \boldsymbol{\omega}[\tau_1 - t]) \sum_{\mathbf{k}_1+\mathbf{k}_2=\mathbf{k}} \left[\!\!\left[\exp(\imath \mathbf{k}_1 \cdot \boldsymbol{\omega}[\tau_2 - \tau_1]) \sigma^{e,[\mathbf{q}_2]}_{\mathbf{k}_1}, \psi^{[\mathbf{q}_1]}_{\mathbf{k}_2} \right]\!\!\right] \psi^{[\mathbf{p}]*}_{\mathbf{k}} \, ,$$

This implies in particular that $\mathbf{Q}_1 \triangleq \mathbf{Q}$ given by Eq. (17). Note that each component of $\mathbf{K}_2$ has the same complexity as $\mathbf{K}_1$, i.e. the perturbation theory is linear order by order; on the other hand it involves *all* the couplings in configuration space, hence the double sum in $\mathbf{k}$. With these definitions, Eqs. (13) and (39) read formally

$$\mathbf{a}^{(1)} = \mathbf{K}_1 \cdot [\mathbf{a}^{(1)}_1 + \mathbf{b}] + \mathbf{Q}_1 \cdot \mathbf{c} \, , \tag{43}$$

$$\mathbf{a}^{(2)} = \mathbf{K}_1 \cdot \mathbf{a}^{(2)} + \mathbf{K}_2 \cdot [\mathbf{a}^{(1)} + \mathbf{b}] \otimes [\mathbf{a}^{(1)} + \mathbf{b}] + \mathbf{Q}_2 \cdot [\mathbf{a}^{(1)} + \mathbf{b}] \otimes \mathbf{c} \, . \tag{44}$$

where the dot operator is not merely a tensor contraction, but also involves a time convolution. For example, $\mathbf{Z}$ being a given field:

$$(\mathbf{K}_1 \cdot \mathbf{Z})_{\mathbf{p}}(t) \triangleq \sum_{\mathbf{q}} \int_{-\infty}^{t} \mathrm{d}\tau (K_1)_{\mathbf{p},\mathbf{q}}(\tau - t) Z_{\mathbf{q}}(\tau) \, , \tag{45}$$

and similarly the higher order contraction rule over the fields $\mathbf{Z}^1 \otimes \cdots \otimes \mathbf{Z}^{\mathrm{n}}$ is defined as:

$$(\mathbf{K}_{\mathrm{n}} \cdot \mathbf{Z}^1 \otimes \cdots \otimes \mathbf{Z}^{\mathrm{n}})_{\mathbf{p}}(t) \triangleq \sum_{\mathbf{q}_1,\cdots\mathbf{q}_{\mathrm{n}}} \int^{t} \mathrm{d}\tau_1 \cdots \int^{\tau_{\mathrm{n}-1}} \mathrm{d}\tau_{\mathrm{n}} (K_{\mathrm{n}})_{\mathbf{p},\mathbf{q}_1,\cdots\mathbf{q}_n}(\tau_1 - t, \cdots, \tau_{\mathrm{n}} - \tau_{\mathrm{n}-1}) Z^1_{\mathbf{q}_1}(\tau_1) \cdots Z^{\mathrm{n}}_{\mathbf{q}_{\mathrm{n}}}(\tau_{\mathrm{n}}) \, . \tag{46}$$

Note that the order of the argument does matter. (*i.e.* Eq. (46) defines a non-commutative algebra). Note also that the sum of the order in each term corresponds to the order of the perturbation. For instance, in Eq. (44), the second term involves the product of two first-order terms, while the first term is a single second-order term. Note finally that the contraction for the $\mathbf{Q}_{\mathrm{n}}$ involve a summation over 5 indices, $\ell, m, \alpha, \ell', m'$, (whereas contraction over $\mathbf{K}_{\mathrm{n}}$ involves only 3 indices: n, ℓ, m). We illustrate and discuss in Fig. (5) through synthetic diagrams the corresponding expansion. (See also Fig. (D1) in Appendix D for an expansion to higher order).

In appendix D, we show in Eqs. (D3)-(D4) how to rewrite Eq. (44) to order n.
As for all expansion schemes, the issue of the truncation arises. Depending on the physical process investigated, the truncation order may vary. For instance, it may be legitimate to truncate the perturbation to second-order since the second-order is the first-order for which dynamical friction is taken into account.

3.2 Non-linear two-point correlation functions

Let us now re-address the computation of the two-point correlation function (*cf.* Section 2.4) of the response of the halo to tidal excitation and infall while accounting for the non-linearities described in Section 3.1.1. First, let us reshuffle the hierarchy in a format which is best suited for the statistical average of the non-linear response.

3.2.1 *Reordering in* **b** *and* **c**

Let us define $\mathcal{F}(\omega,t) \triangleq \exp(\imath\omega t)$ the Fourier operator, so that $\mathcal{F}\cdot\mathbf{Z}$ and $\mathcal{F}^\top\cdot\mathbf{Z}$ are respectively the half-Fourier and inverse half-Fourier transform of their argument $\mathbf{Z}$. Calling

$$\mathbf{R}_1 \triangleq \mathcal{F}^\top\cdot(\mathbf{1}-\hat{\mathbf{K}}_1)^{-1}\cdot\mathcal{F}\,, \tag{47}$$

Eq. (44) (and its generalization Eq. (D3)) reads like a recursion:

$$\mathbf{a}^{(\mathrm{n})} \triangleq \mathbf{R}_1\cdot\mathcal{K}[\mathbf{a}^{(\mathrm{n}-1)}\cdots,\mathbf{a}^{(1)},\mathbf{b},\mathbf{c}]\,,\qquad \text{for}\quad \mathrm{n}\geqslant 2\,, \tag{48}$$

where $\mathcal{K}$ stands formally for some combination of $\mathbf{K}_\mathrm{n}$ and $\mathbf{Q}_\mathrm{n}$. Note that $\mathbf{K}_1$ accounts for the self-gravity of the halo. If the halo is very hot, this self-gravity may be neglected altogether and $\mathbf{R}_1\rightarrow\mathbf{1}$. If not, we may define $\mathbf{K}'_i\triangleq\mathbf{R}_1\cdot\mathbf{K}_i$, $\mathbf{Q}'_i\triangleq\mathbf{R}_1\cdot\mathbf{Q}_i$, and rewrite the recursive relations Eq. (48) with $\mathbf{K}_1\triangleq 0$. For instance:

$$\mathbf{a}^{(1)} = \mathbf{R}_1\cdot(\mathbf{K}_1\cdot\mathbf{b}+\mathbf{Q}_1\cdot\mathbf{c}) = \mathbf{K}'_1\cdot\mathbf{b}+\mathbf{Q}'_1\cdot\mathbf{c}\,, \tag{49}$$

which we can rearrange as:

$$\mathbf{a}^{(1)} \triangleq A_b\cdot\mathbf{b}+A_c\cdot\mathbf{c} \tag{50}$$

where $A_b\triangleq\mathbf{K}'_1$ and $A_c\triangleq\mathbf{Q}'_1$. Let us also introduce $\mathbf{K}''_1 = \mathbf{K}'_1+\mathbf{1}$. Similarly, the contribution of b's and c's to the second order term for a can be expressed as:

$$\mathbf{a}^{(2)} \triangleq A_{bb}\cdot\mathbf{b}\otimes\mathbf{b}+A_{cc}\cdot\mathbf{c}\otimes\mathbf{c}+A_{cb}\cdot\mathbf{c}\otimes\mathbf{b}+A_{bc}\cdot\mathbf{b}\otimes\mathbf{c}\,. \tag{51}$$

where

$$\begin{aligned} A_{bb} &= \mathbf{K}'_2\circ\mathbf{K}''_1\,,\quad A_{cc}=\mathbf{K}'_2\circ\mathbf{Q}'_1+\mathbf{Q}'_2\circ[\mathbf{Q}'_1,\mathbf{I}]\,, \\ A_{cb} &= \mathbf{K}'_2\circ[\mathbf{Q}'_1,\mathbf{K}''_1]\,,\quad A_{bc}=K'_2\circ[\mathbf{K}''_1,\mathbf{Q}'_1]+\mathbf{Q}'_2\circ[\mathbf{K}''_1,\mathbf{I}]\,. \end{aligned} \tag{52}$$

Here the bracket, [,] accounts for the differential composition, so that,

$$\begin{aligned} A_{cb}\cdot\mathbf{b}\otimes\mathbf{b} &= \mathbf{K}'_2\cdot(\mathbf{Q}'_1\cdot\mathbf{b})\otimes(\mathbf{K}''_1\cdot\mathbf{b}) \\ &= \mathbf{R}_1\cdot\mathbf{K}_2\cdot(\mathbf{R}_1\cdot\mathbf{Q}_1\cdot\mathbf{b})\otimes([\mathbf{1}+\mathbf{R}_1]\cdot\mathbf{K}_1\cdot\mathbf{b}). \end{aligned}$$

In appendix D1.2, we also show how to write an equation similar to Eq. (51) for the third order contribution and more generally for an arbitrary order (see Eq.D8).

3.2.2 *Non-linear correlators*

We may now complete the calculation of, say, the two-point correlation function of the density, C_2^ρ :

$$C_2^\rho \triangleq \langle\rho(x_1)\rho(x_2)\rangle = \sum_\mathrm{n}\sum_{p=1}^{\mathrm{n}}\varepsilon^\mathrm{n}\langle\rho^{(p)}(x_1)\rho^{(\mathrm{n}-p)}(x_2)\rangle\,, \tag{53}$$

where $x_i = (\mathbf{r}_i,\tau_i)$, i=1,2. Following Eq. (35), let us also expand the response in density, ρ, over the basis function $\{\rho^{[\mathbf{q}]}(\mathbf{r})\}_\mathbf{q}$, so that

$$C_2^\rho = \sum_\mathrm{n}\varepsilon^\mathrm{n}\sum_{p=1}^{\mathrm{n}}\sum_{\mathbf{q}_1,\mathbf{q}_2}\rho^{[\mathbf{q}_1]}(\mathbf{r}_1)\rho^{[\mathbf{q}_2]}(\mathbf{r}_2)\langle a^{(p)}_{\mathbf{q}_1}(\tau_1)a^{(\mathrm{n}-p)}_{\mathbf{q}_2}(\tau_2)\rangle\,.$$

Now, given Eq. (49) and (51), we may rearrange this equation as:

$$C_2^\rho = \varepsilon^2\sum_{\mathbf{q}_1,\mathbf{q}_2}\rho^{[\mathbf{q}_1]}(\mathbf{r}_1)\rho^{[\mathbf{q}_2]}(\mathbf{r}_2)\left[C_2^{\{2\}}+\varepsilon C_2^{\{3\}}+\ldots\right]\,. \tag{54}$$

where $C_2^{\{2\}}$ is a simple reshuffling of Eq. (29), i.e:

$$\begin{aligned} C_2^{\{2\}} = {} & A_b{\times}A_b\cdot\langle\mathbf{b}\otimes\mathbf{b}\rangle + A_c{\times}A_c\cdot\langle\mathbf{c}\otimes\mathbf{c}\rangle + A_b{\times}A_c\cdot\langle\mathbf{b}\otimes\mathbf{c}\rangle + \\ & A_c{\times}A_b\cdot\langle\mathbf{c}\otimes\mathbf{b}\rangle\,, \end{aligned} \tag{55}$$

and:

$$\begin{aligned} C_2^{\{3\}} = {} & (A_{bb}{\times}A_b + A_b{\times}A_{bb})\cdot\langle\mathbf{b}\otimes\mathbf{b}\otimes\mathbf{b}\rangle + \\ & (A_{cc}{\times}A_c + A_c{\times}A_{cc})\cdot\langle\mathbf{c}\otimes\mathbf{c}\otimes\mathbf{c}\rangle + \\ & (A_{bc}{\times}A_c + A_b{\times}A_{bc})\cdot\langle\mathbf{b}\otimes\mathbf{c}\otimes\mathbf{c}\rangle + \\ & (A_{bb}{\times}A_c + A_b{\times}A_{bc})\cdot\langle\mathbf{b}\otimes\mathbf{b}\otimes\mathbf{c}\rangle + \\ & (A_{cb}{\times}A_b + A_c{\times}A_{bb})\cdot\langle\mathbf{c}\otimes\mathbf{b}\otimes\mathbf{b}\rangle\,. \end{aligned} \tag{56}$$

The $\times$ operator is non-commutative and guaranties that the order is preserved in the dot contraction. Recall that $A_b\triangleq\mathbf{K}'_1$ and $A_c\triangleq\mathbf{Q}'_1$, while A_{bb}, A_{cc}, A_{cb} and A_{bc} are given by Eq. (53) (or in terms of the underlying distribution function, $F_0(\mathbf{I})$, and the basis function, $\psi^{[\mathbf{n}]}(\mathbf{r})$ via Eqs (41), (42) and (47) through the definitions of $\mathbf{K}_1,\mathbf{Q}_1,\mathbf{K}_2$ and $\mathbf{Q}_2$). It follows from Eq. (56) that the non-linear two-point correlation will involve at least the three-point correlation of the incoming flux and of the external potential. We will see in Section 5 that this is a generic consequence of mode coupling. Now the three point correlation of the incoming flux, **c**, and the tidal field, **b** may be reexpressed in terms of the mean and the two-point correlations of those fields while relying on Wick's theorem, since we showed in Aubert & Pichon (2005a) that these fields were approximately Gaussian. Appendix D2 presents formally the generalization of Eqs. (55)-(56) for the N-point correlation function to arbitrary order.

Equations such as Eq. (44) or its reordered version Eq. (51) might look deceivingly simple. One should nevertheless keep in mind that the perturbation theory involves an exponentially growing number of terms. This is probably best realized by looking at diagrams such as Fig. (D2) (presented in the appendix) while keeping in mind that *each* straight line represents a triple sum over $\mathbf{k} = (k_1,k_2,k_3)$ and a time integral (see also Appendix B). The prospect of achieving resummation (in the spirit of what was achieved by *e.g.* Bernardeau (1992) for the gravitational instability of the large-scale structures) given the relative complexity of the double source expansion is slim. Yet it might be possible to construct scaling rules (see Fry (1984)) since gravity is

also here the driving force. Let us stress once again that the perturbative expansion accounts explicitly, within its convergence radius, for all aspects of the non-linear physics taking place within the R_{200} sphere.

3.3 Implication for dynamical friction and tidal stripping

One of the possible assets of this perturbative formulation is that the incoming flux may describe a virialized object which has a finite extent, and as such will undergo internal phase mixing reflecting the fact that different points in the object will describe different orbits, at different frequencies (see Fig. (3)). In the perturbative regime, dynamical friction will also account for both the overall drag of the object, but also its tidal stripping (*i.e.* the fact that the less bound component of the object will undergo a differential more efficient friction). Specifically, the deflection of perturbed trajectories will correctly describe the balance (or lack thereof) between the self-gravity of the entering flow and its tendency to be torn by the differential gravitational field of the halo (which imposes the unperturbed different orbital trajectories). As such, the flow paradigm implemented in this paper and in Aubert et al. (2004), Aubert & Pichon (2005a) should allow for the appropriate level of flexibility in defining what a structure is and how time-dependent the concept is, within the self-gravitating halo (see also Section 3.3.1).

Let us briefly discuss how to identify substructures within the halo.

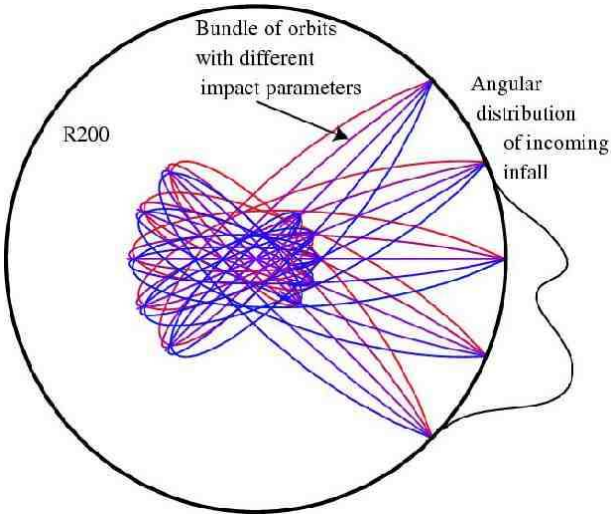

Figure 3. displays qualitatively a bundle of orbits (in their orbital plane) which undergo dynamical friction and phase mixing within the R_{200} radius. As expected, dark matter describing orbits which initially are at the same position, but with "slightly" different initial impact parameters will end up in quite different regions at later time. On the right the curve represents a possible angular distribution of a given entering object (for which the kinematic and angular spread has been greatly exaggerated). The caustics corresponding to the successive rebound of the orbits is clearly visible here (Fillmore & Goldreich (1984)). Note that the amplitude of the friction force was *ad hoc*, and the self-gravity within the bundle was *not* taken into account.

3.3.1 *Substructure counts and distribution*

The identification of substructures within a given halo is a very promising but difficult topic (see e.g. Springel et al. (2001),Gill et al. (2004) Aubert et al. (2004)) . Once the boundary flow has been propagated inwards, we have in principle access to the full distribution function of the perturbation as a function of time. When the field $f(\mathbf{v},\mathbf{r},t)$ is known inside R_{200}, we may attempt to identify collapsed objects and apply some form of count in cell statistics in order to characterize their spatial distribution as a function of time. This would allow us in particular to put aside objects which have been disrupted by tidal stripping or phase mixing (indeed 10 % of the mass of the halo is believed to remain in the form of virialized objects, while 90 % is disrupted by the tidal field). Recall that the disruption process is in principle well described by the perturbative expansion.

The criterion for the detection of objects must be carried while accounting for both the density contrast and the corresponding velocities (see also Arad et al. (2004)). Indeed, we do not wish to identify as objects local overdensities which may just correspond to caustics or local wave reinforcement. Here we are interested in the temporal coherence of objects.

For this purpose, we may coarse-grain the perturbed distribution function both in position and velocity, with some given smoothing function, $W(\mathbf{r}/\mathcal{R}_s,\mathbf{v}/\mathcal{V}_s)$, and then apply some thresholding ($W\circ f > f_{\rm min}$ where $\circ$ stands for convolution) on the amplitude of the distribution function, defining a set of connex regions. For each of these regions, we may then compute the energy of the corresponding clump. If it is negative, the clump will be labeled as bound for the corresponding threshold ($f_{\rm min}$), and coarse-graining parameters ($\mathcal{R}_s,\mathcal{V}_s$). Note that since the response only involves the *perturbed* density, one need not subtract the mean potential, (which is quite a difficult task in general).

Once the bound regions are identified, we may compute the corresponding mass and assign it to the bottom of the local potential well. This procedure may be applied for a range of threshold values, and standard statistical tools for discrete sources but in spherical geometry. We may in particular construct in this manner the mass function of satellites as a function of radius, or, say the two-point correlation function versus mass and cosmic time. Both issues are subjects of strong discussions when addressed through standard N-body simulations.

This time-dependent identification of virialized objects is useful because of biasing, *i.e.* the fact that most observational tracers will only be sensitive to the more massive tail of the mass function of virialized objects.

Conversely, we may want to label regions which match the thresholding but not the requirement on binding energy, *i.e.* identify caustics, cusps, and shells (Fillmore & Goldreich (1984)). We may then characterize statistically the mean distance between the apoapses (see Fig. (3)), which will in general depend on $\mathcal{R}_s$,$\mathcal{V}_s$ and $f_{\rm min}$ but also on the underlying equilibrium, via $F(\mathbf{I})$ and on the statistical properties of $\mathbf{c}$ through, say the distribution of impact parameters. Note in closing that the competing effects of phase mixing, tidal stripping and dynamical friction all assume that the underlying basis function reaches sufficiently high spatial frequencies to resolve these phenomena. In practice, since the projection of the response (both linearly and non linearly) is

achieved over a basis which has a truncation frequency, $\ell_{\max}$, there is a finite time scale, $T_{\max} \propto \ell_{\max}/\langle\omega\rangle$ above which phase mixing would induce winding at unresolved scales (here $\langle\omega\rangle$ represents the typical frequency of the dark matter in that region). Since the dynamical time is shorter in the inner region of the galaxy, such a threshold is going to be reached there first. Beyond this critical time, the dynamics is inaccurately modeled for the corresponding clump. This issue will be important for the non linear coupling of clumps, since substructures entering the halo at later times will be dragged by streamers which are beyond the accuracy threshold[6].

4 QUASI-LINEAR EVOLUTION OF HALO PROFILE

The previous sections dealt with the halo polarization while considering that perturbations were transients. In practice, a halo undergoes recursive excitations from its environment that will induce departures from its equilibrium state so that it won't remain static. In Appendix C we derive a quasi linear formalism for the collisionless open Boltzmann equation in order to take this effect in account. This follows in essence the work of Weinberg (1993), Weinberg (2001a), or Ma & Bertschinger (2004), though the derivation differs. We introduce here an explicit expression, valid at low redshift, for the source of stochastic "noise". We account explicitly for the correlation induced by the entering material (as characterized by Aubert & Pichon (2005a)) rather than rely on some *ad hoc* assumption on its nature. We also account consistently for the mean secular infall which adiabatically restructures the mean profile.

4.1 Context and derivation

Gilbert (1970) gives a very elegant derivation from first principles of the secular equation based on a $1/N$ (N being the number of particles in the system) expansion of the collisional relaxation equations presented by Bogolyubov & Gurov (1947). Weinberg (1993), Weinberg (2001a) and Ma & Bertschinger (2004) rely on the same expansion scheme to derive their kinetic equation for the mean halo profile.

Weinberg (1993) focuses on the secular collective relaxation of a system induced by the finite number of particles within a multi-periodic uniform medium, hence transposing to collisionless stellar dynamics the derivation of Lenard-Balescu (Lenard (1961), Balescu (1963)) applied originally to plasma physics in order to describe the secular convergence of such systems towards thermalisation.

Weinberg (2001a) derives a similar result for the spherical halo in angle and action variables, while relying on the Kramers-Moyal (Risken (1989)) expansion, which corresponds to a Markovian description based on the transition probability of a change in action induced by the interaction with a dressed particle cloud. His Fokker-Planck coefficients differ slightly from Eqs. (C13)-(C14) given in the Appendix in that the spectral properties of $\langle \hat{b}_{\mathbf{n}} \hat{b}_{\mathbf{n}'} \rangle$ are postulated in his case, while $\mathbf{c} \triangleq 0$.

Ma & Bertschinger (2004) construct a Fokker-Planck equation for the mean profile of a halo in a cosmic environment while relying on the constrained random field of peaks in the standard cosmological model to derive the drift and diffusion coefficients from first principles. Their derivation is dynamically accurate to second-order in the perturbation theory (in position-velocity space) and relate the kinetic coefficients to the properties of the underlying linear power spectrum. In contrast to the theory presented here, their kinetic equation describes the very early phase of halo formation, whereas we focus here on the quasi-linear evolution (in angle action space) of fully relaxed equilibria at low redshift.

In Appendix C, we account explicitly for the nature of the perturbation's power spectrum as defined in Aubert & Pichon (2005a) and present an explicit derivation for the Fokker-Planck equation obeyed on secular time scales by the distribution function in angle action. It is natural to use these variables to describe a relaxed collisionless halo since they allow to split the dynamics into a secular (phase averaged) and a fluctuating part.

Even though individual dark matter particles obey a collisionless dynamics, the phase average ("ensemble average") distribution for the open system satisfies a collisional kinetic equation where the clumpiness of the *open* medium breaks the mean field approximation (see also Ma & Bertschinger (2004)). Indeed, individually, clumps and tidal remnants deflect the actions of the underlying distribution in a stochastic (but correlated) manner, so that in the mean ensemble sense, the coarse-grained distribution (*i.e.* the distribution averaged over the angles) obeys a collisional diffusion of the Fokker-Planck type. In this formulation, the graininess of the system (as defined by the second-order closure of the BBGKY hierarchy of the N-point distribution) corresponds to the mean number of clumps expected in the halo, while the detailed (kinetic and angular) power spectrum of the gravitational fluctuations is given by the cosmogony.

It is usual in plasma physics to take a two-time scale approach to the Boltzmann equation. The short time scale describes the system's dynamics on the dynamical (orbital) time scale, while the longer time scale corresponds to the secular evolution. The Action-Angle variables are best suited here. This time scale separation procedure leads to the following system of equations:

$$\frac{\partial f}{\partial t} + \boldsymbol{\omega} \cdot \frac{\partial f}{\partial \mathbf{w}} - \frac{\partial \psi}{\partial \mathbf{w}} \cdot \frac{\partial F}{\partial \mathbf{I}} = \frac{\partial \psi_e}{\partial \mathbf{w}} \cdot \frac{\partial F}{\partial \mathbf{I}} + s_e, \tag{57}$$

$$\frac{\partial F}{\partial T} = \left\langle \left[\frac{\partial \psi}{\partial \mathbf{w}} + \frac{\partial \psi_e}{\partial \mathbf{w}} \right] \cdot \frac{\partial f}{\partial \mathbf{I}} \right\rangle_T - \left\langle \left[\frac{\partial \psi}{\partial \mathbf{I}} + \frac{\partial \psi^e}{\partial \mathbf{I}} \right] \cdot \frac{\partial f}{\partial \mathbf{w}} \right\rangle_T + S_e, \tag{58}$$

In Eq. (57) and (58) s_e and S_e stand for the perturbative and secular advected source terms, while f stands for the fluctuating distribution and F stands for the secular distribution function (see Appendix C for details). The bracket around the quadratic terms stands for a time average over a secular time, T which is long compared to dynamical time, t (taken by a dark matter particle to describe its orbit). If we fix $F(\mathbf{I}, T)$, Eq. (57) corresponds exactly to Eq. (6) whose solution was described in Section 2.1. This formal solution may then be injected in the quadratic terms of Eq. (58). Following

[6] these limitations are also clearly encountered in classical N-body simulations

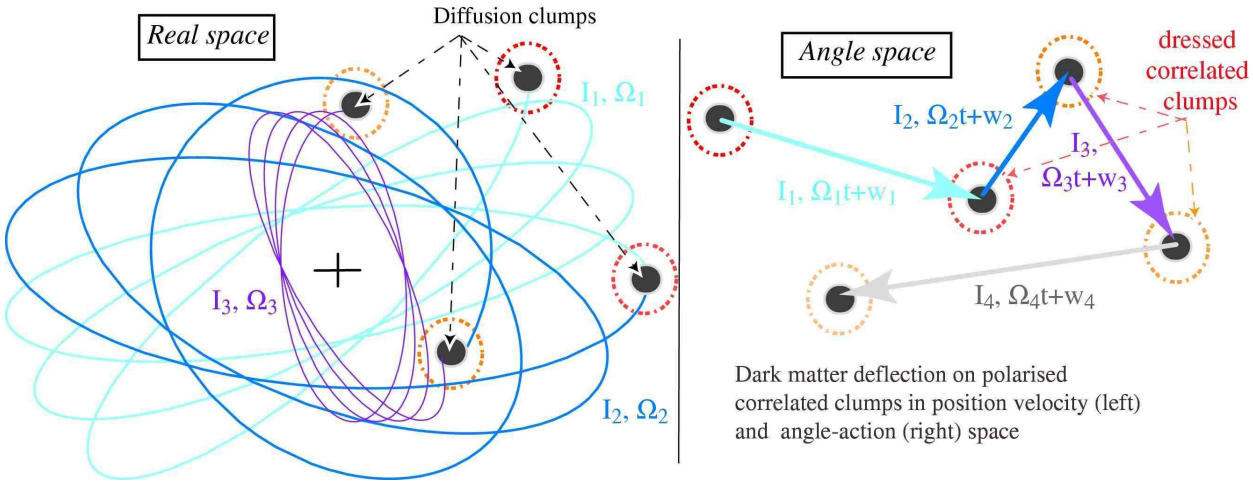

Figure 4. *Left panel* schematic representation of the successive deflection of a given orbit on correlated clumps within the halo in position space. Each clump is represented with its polarisation cloud. The gray scale coding in the cloud reflects their spatial and temporal correlation within the clumps. During the deflections, the orbital parameters change (though the individual change is here grossly exaggerated). *Right panel:* the same orbit as viewed in angle-action variables. The dynamics in these variable is straightforward (it corresponds to straight lines obeying $\mathbf{w} = \boldsymbol{\omega}(\mathbf{I})t + \mathbf{w}_0$) and the diffusion process resembles Brownian motion obeying a Langevin equation the particle receiving a random kick at each deflection, represented by a change in colour which reflects the fact that the "collision" is instantaneous in constrast to the time interval separating two collisions

this route, we show in Appendix C how to rearrange Eq. (58) as a Fokker Planck equation:

$$\frac{\partial F}{\partial T} = \langle \mathrm{D}_0(\mathbf{I})\rangle - \langle \mathbf{D}_1(\mathbf{I})\rangle \cdot \frac{\partial F}{\partial \mathbf{I}} - \langle \mathbf{D}_2(\mathbf{I})\rangle : \frac{\partial^2 F}{\partial \mathbf{I}^2}, \tag{59}$$

where D_0, $\mathbf{D}_1$ and $\mathbf{D}_2$ are given by Eqs. (C13)-(C15), while : stand for the total contraction. Note that Eq. (59), in contrast to Eq. (58) refers this time to the driving equation for the mean halo profile since we invoqued ergodicity to replace time averages by ensemble averages (see Appendix C for details). The D_0 term enters here because the halo is an open system, which may receive or lose mass. The drift term with the factor $\mathbf{D}_1$ accounts for the dynamical friction induced by the polarization cloud around the tidal remnants; the diffusion term with the factor $\mathbf{D}_2$ arises because of the fluctuations in the potential (both tidal and associated with the infalling dark matter) induced by the clumps. The diffusion term will in general induce a spreading of the energy distribution by accelerating some orbits to higher energies while decelerating some other ones. The polarization cloud will in general induce a drag on the clumps, represented by the $\mathbf{D}_1$ term. Note that the former should be independent of the mass of the clump (since the energy is exchanged via the mean field) while the latter will not (since more massive clump polarize the medium more). From the point of view of the entering dark matter, the net effect is therefore a segregation process in which the more massive clumps fall in (as discussed by Gilbert (1970)).

According to Risken (1989), the corresponding Langevin (Langevin (1908)) equation reads (when the source term, D_0 is *omitted*)

$$\frac{\partial \mathbf{I}}{\partial t} = \boldsymbol{\Delta}_1(\mathbf{I}) + \boldsymbol{\Delta}_2(\mathbf{I}) \cdot \boldsymbol{\xi}(t)\,. \tag{60}$$

Here $\boldsymbol{\Delta}_1(\mathbf{I})$ and $\boldsymbol{\Delta}_2(\mathbf{I})$ are given in terms of $\mathbf{D}_1(\mathbf{I})$ and $\mathbf{D}_2(\mathbf{I})$ by

$$\boldsymbol{\Delta}_2 = \mathbf{D}_2^{1/2}, \quad \text{and} \quad \boldsymbol{\Delta}_1 = \mathbf{D}_1 - \mathbf{D}_2^{1/2} : \nabla_{\mathbf{I}} \mathbf{D}_2^{1/2},$$

where $[\mathbf{D}_2]^{1/2}$ stands for the square root of the matrix $\mathbf{D}_2$ which is computed via diagonalization, provided the eigenvalues are positive. The 3D random field, $\boldsymbol{\xi}(t)$, should have spectral properties which reflect the stochastic properties of $\mathbf{b}$ and $\mathbf{c}$. The probability distribution of the solution to the stochastic equation, Eq. (60), obeys the Fokker Planck Equation, Eq. (59). In this form, the effect of diffusion on the departure from phase mixed equilibrium is easily interpreted.

4.2 Prospects for universal halo profiles

As has been suggested and illustrated by Weinberg (2001a) and Ma & Bertschinger (2004), it would be very worthwhile to use Eq. (59) and predict the asymptotic dark matter profile, (and, say the cosmic evolution of the concentration parameter) which will be shaped in part by encounters and interlopers.

Note that the diffusion coefficients, D_i are relatively straightforward to compute for a given halo model, $F(\mathbf{I})$ *but* Eq. (59) corresponds to an evolution equation for $F(\mathbf{I})$ and will in practice require re evaluating the coefficients for different values of F.

Let us now draw constraints on the stationary solutions of Eq. (59). Again (following Section 5), this may be done in one of two ways: take D_0, $\mathbf{D}_1$ and $\mathbf{D}_2$ as given function of the actions, and deduce what equation F should obey from requiring that Eq. (59) has a stationary solution. (this is the route first explored by Weinberg (2001b)); or, if we assume that a given model, say a universal profile, should correspond to the asymptotic solution of Eq. (59), we may find the relationship relating the corresponding asymptotic $\mathbf{D}_i$ coefficients.

For simplicity, let us illustrate this second point while neglecting here the fact that the diffusion coefficients depend

on the distribution function, and restricting ourselves briefly to an isotropic distribution, $F(E,T)$. Calling:

$$H(E) = \left(\langle \mathbf{D}_1 \rangle \cdot \boldsymbol{\omega} + \langle \mathbf{D}_2 \rangle : \frac{\partial \boldsymbol{\omega}}{\partial \mathbf{I}} \right) / \left(\langle \mathbf{D}_2 \rangle : \boldsymbol{\omega} \otimes \boldsymbol{\omega} \right), \qquad (61)$$

$$\text{and} \quad Q(E) = \frac{\langle \mathrm{D}_0 \rangle}{\langle \mathbf{D}_2 \rangle : \boldsymbol{\omega} \otimes \boldsymbol{\omega}}, \qquad (62)$$

the stationary solution ($\partial F/\partial T = 0$) to Eq. (59) reads formally:

$$F(E) = \int_0^E \exp\left[-\int_{e_2}^{e_3} H[e_1] de_1 \right] \times \left\{ \int^{e_3} Q[e_4] \exp\left[\int_{e_2}^{e_4} H[e_1] de_1 \right] de_4 \right\} de_3. \qquad (63)$$

This distribution function should satisfy the self-consistency requirement that

$$\rho(r) = 2\sqrt{2} \int_{-\psi}^{0} F(E) \sqrt{E+\psi} \mathrm{d}E, \quad \nabla^2 \psi(r) = 4\pi G \rho(r). \qquad (64)$$

Imposing that $F(E)$ obeys Eqs. (62)-(64) yields a non-linear integral equation for the $\mathbf{D}_i$, *i.e.* a (admittedly indirect) constraint on the angular correlation of the external field. Section 5 describes other means of constraining the power spectrum of the infalling dark matter. Weinberg (2001b) found iteratively the corresponding solution while making some assumptions on the spectral properties of $\mathbf{b}$ in the régime where $\mathbf{c} = 0$. In the light of his investigation, he concluded that the tidal excitation drives the halo towards a less steep profile. It will be interesting to explore this venue with a realistic accounting of the source of infall. The setting here would be that the satellite problem and the cusp problem of dark matter haloes might be the two sides of the same coin, so that the evolution towards a universal profile might be triggered by the actual infall of substructures.

Let us now return to the perturbative dynamics described in Section 2, 3 and explore its implications for galaxies.

5 APPLICATIONS: HALO POLARIZATION, DISK DYNAMICS AND INVERSION

Aubert & Pichon (2005a,b) provided a detailed statistical description of how dark matter falls onto a $L^\star$ galactic halo: how much mass is accreted as a function of time, how is it accreted *i.e.* in what form, with what velocity distribution, along which direction, and for how long? Putting the theory described here and the tabulated measurements from that paper together, allows us to address globally, and coherently dynamical issues on galactic scales in a *statistically representative* manner. With the help of the theory presented in Section 2, 3, we are now in a position to ask ourselves: what are the expected features of a halo/galaxy induced by their cosmic environment. Specifically, we may now "simply" propagate the cosmological framework and its statistics to observables (describing the departure from spherical symmetry/stationarity) on galactic scales. On these scales, the realm of astrophysical applications for the perturbative open solution of the Poisson-Boltzmann equations is extremely wide. It is clearly beyond the scope of this paper to attempt an exhaustive inventory. Rather, we shall here focus on a few specific issues, for which we show how the open perturbative framework improves our understanding, and allows for a statistical investigation.

In particular, we shall restrict ourselves to settings where the detailed geometry of the infall matters, since the theory described above does account for the configuration and the time lag involved in the accretion on top of $L^\star$ galaxies.

Recall that the purpose of the statistical propagation is threefold: (i) constrain the properties of the infall on the basis of the *observed* distribution for the properties of galaxies and their environment; (ii) *predict* some of the statistical properties of galaxies which are not directly observable, while relying on the properties of the infall. (iii) weigh the relative importance of the intrinsic properties of the disk+halo compared to the strength of the environment.

We will distinguish three classes of problems; first we will describe how to transpose to galactic scales (Section 5.1) the classical probes used in cosmology to trace the large-scale structures. We will then explore in Section 5.2 the implication for the properties of external galaxies, and in Section 5.3 for the structures within the Milky Way halo. Finally, we will elaborate in Section 5.4 on the prospect of inverting the upcoming data sets for the *past* history of our own Galaxy and for field galaxies in the local group.

5.1 Cosmic probes in the neighbourhood of galaxies: $R_{200}/10 < R < R_{200}$

A series of observational probes of the statistical properties of the density field have been devised over the years, such as weak lensing, galaxy counts, the SZ effect, X-ray or γ-ray emissivity maps. In the light of large galactic surveys which are available today, it becomes quite desirable to apply these probes in the neighborhood of galactic haloes in order to study the dark matter distribution within the R_{200} radius. Some of these tracers are only sensitive to the baryon density, which need not trace directly the dark matter density. In this section, we will systematically assume for simplicity a simple biasing, though this assumption may be lifted (at the expense of extra non-linearities, see Section E3) provided the biasing law is known (*i.e.* the observables are assumed to scale like the dark matter density, or some power of it); we refer to Section 3.3.1 for a brief discussion of thresholding, which is bound to be important in practice.

The calculation described in the previous sections, together with the statistical measurements described in Aubert et al. (2004); Aubert & Pichon (2005a,b) *should* allow us to make statistical predictions about observables which may be expressed in terms of the distributions of clumps within the galactic haloes, either via their gravitational potential, their projected density or even their velocity distributions (*e.g.* Galactic streams).

We will consider in turns observable which may be approximated as linear functions of the *perturbed* fields, either in projected coordinates on the plane of the sky, or as seen by an observer at the galactic center. We will also consider observables which involve quadratic functions of this field (*e.g.* the square of the electron density), or even more non-linear functions of the dark matter distribution within the virial ra-

dius (such as the locus of virialized clumps, which dissolve at a function of time). We will in particular build the two-point statistics for these observables, since the mean of the perturber is often zero by construction. Finally we will also consider metals lines in absorptions systems, which involve the cross-correlation of the density and the velocity fields. Note that all these measurements could in principle be carried as a function of redshift, or a function of the mass of the halo, or while varying the anisotropy of the equilibrium for the halo (by varying $F(\mathbf{I})$ in *e.g.* $\mathbf{K}$ in Eq. (41)). Note finally that some tracers correspond to the scales of clusters, and we will assume here that the measurements presented in Aubert & Pichon (2005a) could be reproduced for these objects (whereas the theory described here is scale independent provided the system is dynamically relaxed and spherical).

In this section, we will focus on a couple of probes which are supposed to scale linearly with the dark matter density in the main text (weak lensing, SZ effect), and postpone to appendix E a presentation of other probes (X-ray emissivity, dark matter disintegration, metal lines in absorption spectra).

Note that all probes described below are a departure from the mean profile of galactic haloes (just as cosmic perturbation theory describes the growth of structure as a departure form the mean density/expansion of the universe) and as such, assume that we have a good understanding of this profile. This will undoubtedly turn out to be a serious observational constraint when attempting to ensemble average galaxies of various size and properties.

5.1.1 *Weak lensing in stacked haloes*

Weak lensing corresponds to the deflection of light emitted from background galaxies by the gravitational potential of structures between those galaxies and the observer. It has recently been used quite successfully to constrain the statistical distribution of the large-scale structures. On smaller scales, the effects of substructures in haloes on the lensing measurments have been demonstrated by e.g. Dalal & Kochanek (2002), Kochanek & Dalal (2004).

In the weak lensing régime (Peacock (1999)), the relationship between the observed convergence and the underlying projected dark matter profile is approximated to be linear. Hence we may straightforwardly propagate our statistical predictions for the clumpy dark matter distribution around a dark matter halo (or within the neighborhood of clusters of galaxies provided some readjustment of the theoretical predictions described in Aubert et al. (2004); Aubert & Pichon (2005a) on these larger scales).

The cumulative deflection angle, $\boldsymbol{\alpha}(\boldsymbol{\theta}, w) \triangleq \delta\mathbf{x}/r_k(w)$ by which light is deflected is given by

$$\boldsymbol{\alpha}(\boldsymbol{\theta}, w) = \frac{2}{c^2}\int \mathrm{d}w' \frac{r_k(w'-w)}{r_k(w)} \nabla_\perp \psi(r_k(w')\boldsymbol{\theta}, w')\,, \tag{65}$$

where r_k is the angular comoving distance, $\mathrm{d}w \triangleq \mathrm{d}r/\sqrt{1-kr^2}$ ($k = 0, \pm 1$) and $\mathbf{x}$ the transverse comoving distance. Defining the convergence, $\kappa(\boldsymbol{\theta})$ by

$$\kappa(\boldsymbol{\theta}) = \frac{1}{2}\nabla_{\boldsymbol{\theta}} \cdot \boldsymbol{\alpha}(\boldsymbol{\theta})\,, \tag{66}$$

the mean ensemble average convergence of the rescaled halo, $\langle\kappa(\theta)\rangle$, reads:

$$\langle\kappa(\theta)\rangle = \frac{1}{c^2}\int \mathrm{d}w' \frac{r_k(w'-w)}{r_k(w)} \nabla^2_\perp \psi_{\mathrm{NFW}}(r_k(w')\theta, w')\,. \tag{67}$$

Now recall that (*cf.* Eq. (9) where $\psi^{[\mathbf{n}]}$ is given by Eqs. (B2)-(B3) in Appendix B2.)

$$\delta\psi(\mathbf{r}) = \sum_{\mathbf{n}} a_{\mathbf{n}} \psi^{[\mathbf{n}]}(\mathbf{r})\,, \quad \text{hence} \quad \delta\kappa(\boldsymbol{\theta}) = \sum_{\mathbf{n}} a_{\mathbf{n}} \kappa^{[\mathbf{n}]}(\boldsymbol{\theta})\,, \tag{68}$$

where

$$\kappa^{[\mathbf{n}]}(\boldsymbol{\theta}) = \frac{1}{c^2}\int \mathrm{d}w' \frac{r_k(w'-w)}{r_k(w)} \nabla^2 \psi^{[\mathbf{n}]}(r_k(w')\boldsymbol{\theta}, w')\,. \tag{69}$$

It follows that the correlation function of the relative convergence obeys

$$\frac{\langle\delta\kappa(\boldsymbol{\theta})\delta\kappa(\boldsymbol{\theta}')\rangle}{\langle\kappa(\theta)\rangle^2} = \frac{1}{\langle\kappa(\theta)\rangle^2}\sum_{\mathbf{n},\mathbf{n}'} \langle a_{\mathbf{n}} a_{\mathbf{n}'}\rangle \kappa^{[\mathbf{n}]}(\boldsymbol{\theta})\kappa^{[\mathbf{n}']}(\boldsymbol{\theta}')\,. \tag{70}$$

Hence, the statistical properties of the relative convergence will depend on the statistical distribution of the clumps of the halo through the $\{a_{\mathbf{n}}\}$ coefficients which are given in Eq. (29) in terms of $b_{\mathbf{n}}$ and $c_{\mathbf{n}}$.

In practice one has to devise an observational strategy, given the expected size of the caustics of subclumps within haloes of galaxies or clusters, the number of background sources, and the expected number of foreground objects (*i.e.* galaxies or clusters).

Finally, it is believed that one in a hundred large ellipticals on the sky should undergo strong lensing. In the long run, the statistical properties of such a non-linear signal will be worth investigating within the framework described in this paper (following the non-linear steps described in say, Section E3).

5.1.2 *Thermal S-Z effect of stacked haloes*

When the photons of the cosmic microwave background enter the hot dense gaz within the clusters and galactic haloes, they interact with the electrons of the gaz. The diffusion process transfers the energy of the photons to the electrons which in turn reemit this energy at a higher frequency. The corresponding spectral redistribution induces a local temperature decrement seen in the temperature map of the clusters, known as the thermal Sunyaev-Zeldovich effect (see e.g. Peacock (1999)). The temperature decrement (at low frequency) reads as a function of the distance to the cluster center, $\mathbf{R}$:

$$\frac{\Delta T(\mathbf{R})}{T_{\mathrm{CMB}}} = -2\frac{k_{_B}\sigma_{\mathrm{T}}}{m_e c^2}\int \mathrm{d}z n_e(z, \mathbf{R}) T_e(z, \mathbf{R})\,, \tag{71}$$

where m_e, n_e and T_e are respectively the mass, the numerical density and the temperature of the electrons, while σ_{T} is the Thomson scattering section ($6.65 \times 10^{-25}\mathrm{cm}^2$), c the speed of light, $k_{_B}$ Boltzmann's constant, and T_{CMB} is the Cosmic microwave background temperature.

Let us assume that the variation in temperature is small compared to the variation of the electron number density[7]. Let us also assume that the electron density is proportional to the dark matter density (constant biasing) as mentioned above. Let us define the departure from the cosmic average for the profile as:

$$\delta\Delta T(\mathbf{R}) = \Delta T(\mathbf{R}) - \langle \Delta T \rangle(R)\,. \tag{72}$$

The relative fluctuation of the temperature decrement reads:

$$\frac{1}{\langle \Delta T \rangle^2(R)} \langle \delta\Delta T(\mathbf{R}) \delta\Delta T(\mathbf{R}') \rangle = \frac{1}{\Sigma_{\rm NFW}(R)^2} \sum_{\mathbf{n},\mathbf{n}'} \langle a_{\mathbf{n}} a_{\mathbf{n}'} \rangle \times \int \mathrm{d}z \int \mathrm{d}z' \rho^{[\mathbf{n}]}(\mathbf{R}, z) \rho^{[\mathbf{n}']}(\mathbf{R}', z')\,, \tag{73}$$

where $\Sigma_{\rm NFW}$ is the mean rescaled projected dark matter mass profile. Note that the double integral in Eq. (73) is carried over known functions and is just a geometric factor which will depend on R, ΔR, and $\Delta\Theta$ only. Again, the knowledge of the statistics of the $\{a_{\mathbf{n}}\}$ (which in turn only depend on the equilibrium, F_0, and the statistics of $b_{\mathbf{n}}$ and $c_{\mathbf{n}}$ at R_{200}, see Eq. (19) or (29)) therefore allows us to predict the statistical properties of the relative fluctuations in the temperature decrement. ALMA will soon provide detailed SZ maps of clusters for which it should be possible to apply these techniques.

Let us note in passing that the kinetic S-Z effect of stacked haloes may also be investigated following the same route

$$\frac{\Delta T(\mathbf{R})}{T_{\rm CMB}} = -2 \frac{k_B \sigma_{\rm T}}{m_e c^2} \int \mathrm{d}z n_e(z, \mathbf{R}) v_z(z, \mathbf{R}). \tag{74}$$

In closing, let us note that maps of SZ effects within our own Galaxy will be available with the upcoming Planck satellite, and will provide statistical information on the small-scale distribution of local clumps. Recall finally that appendix E presents other statistical probes of the outer structures found in galactic haloes (X-ray emissivity, dark matter disintegration, metal lines in absorption spectra). Most of these probes could be used to say, probe the shape of the density profile in the outer parts of galaxies, or the biasing law relating dark matter to stars or gas.

5.2 Galactic structure: $R < R_{200}/10$

In the previous section, we investigated the dynamical consequences of the cosmic infall in the outer region of the halo. Let us now turn to the regions of the halo where we expect to find the galaxies themselves. At lower redshift, the galaxies essentially come in two flavours, ellipticals and spirals. The response of ellipticals should follow closely that of the dark matter halo since both components are hot enough not to undergo gravitational instabilities. In effect, describing an embedded "spherical" elliptical galaxy within a dark matter halo amounts to changing the distribution function to account for the presence of the elliptical and its possibly distinct kinematics. Note that, as mentioned before the above theory could be amended to account perturbatively for the possible triaxiality of the elliptical (Binney & Spergel (1984)).

For a disk or a very flattened spheroid, the situation becomes quite different. The cooler disk is likely to be either drawn beyond its stability threshold by the perturbation, or will respond much more strongly to the perturber than its dark halo. Hence we need to model the disk component differently. The proto-galactic environment is likely to be extremely noisy, particularly in outer regions, so that the halo may perturb the disk by transmitting numerous disturbances into the inner galaxy. Moreover, the inner halo may continue to oscillate as it settles after the coalescence of advected objects. Halo oscillations may easily perturb the disk through the time-dependent gravitational potential. Conversely, the structural integrity of observed disks set limits on the degree of disequilibrium in the proto-galactic halo.

Within the realm of features found in galactic disks, a fraction are known to be the result of instabilities (*e.g.* galactic bars), while others have been shown to correspond to transients (*e.g.* galactic warps).

With the advent of modern systematic surveys, it is possible to construct distributions corresponding to, say, the fraction of spirals which fall within some Hubble type, or the fraction of warps whose inclination is larger than some angle, On the disk scale, we may construct the PDF of, say, the pitch angle of dynamically induced spirals, or the PDF of the extent of the bar, its amplitude, or less directly observed the PDF of pattern speeds. Some of these processes depend crucially on gas physics and will not be addressed here.

5.2.1 *Pitch angle distribution for spirals*

For stellar disks, the stars obey formally the same equation as Eqs. (6)-(11), but this time the modes may be unstable, and sometimes the disk cannot be treated in isolation from the live halo in which it is embedded. On the other hand, it is often well approximated as an infinitely thin structure; such a 2D system becomes integrable again with two actions, $\mathrm{d}\mathbf{J} \triangleq \mathrm{d}J_r \mathrm{d}L_{z_{\rm D}}$. Here J_r is the radial action of the stars in the plane of the disk, and $L_{z_{\rm D}}$ is the momentum of the stars in the disk. Following Weinberg (1998a) and adding some source of infall at R_{200}, we may describe the coupled system disk + halo in the complex plane as

$$\begin{pmatrix} \hat{\mathbf{a}}_{\rm D} \\ \hat{\mathbf{a}}_{\rm H} \end{pmatrix} = \begin{pmatrix} \hat{\mathbf{K}}_{\rm DD} & \hat{\mathbf{K}}^*_{\rm DH} \\ \hat{\mathbf{K}}_{\rm DH} & \hat{\mathbf{K}}_{\rm HH} \end{pmatrix} \cdot \begin{pmatrix} \hat{\mathbf{a}}_{\rm D} \\ \hat{\mathbf{a}}_{\rm H} + \hat{\mathbf{b}} \end{pmatrix} + \begin{pmatrix} 0 \\ \hat{\mathbf{Q}} \end{pmatrix} \cdot \begin{pmatrix} 0 \\ \hat{\mathbf{c}} \end{pmatrix},$$

where $\hat{\mathbf{K}}_{\rm HH}$ is given by Eq. (D15), while

$$\left(\hat{\mathbf{K}}_{\rm DD}\right)_{\mathbf{p},\mathbf{q}} = \sum_{\mathbf{k}} \int \mathrm{d}\mathbf{J} \frac{\psi^{\mathrm{D},[\mathbf{p}]}_{\mathbf{k}}(\mathbf{J}) \psi^{\mathrm{D},[\mathbf{q}]*}_{\mathbf{k}}(\mathbf{J})}{\mathbf{k}\cdot\boldsymbol{\omega}_{\rm D} - \omega}\, \mathbf{k} \cdot \frac{\partial F_{\rm D}}{\partial \mathbf{J}},$$

and a similar expression involving $\psi^{[\mathbf{p}]}_{\mathbf{k}}(\mathbf{J}) \psi^{\mathrm{D},[\mathbf{q}]*}_{\mathbf{k}}(\mathbf{J})$ for the cross term, $\hat{\mathbf{K}}_{\rm DH}$. See Pichon & Cannon (1997) for details relative to the disk. Here $\hat{\mathbf{a}}_{\rm D}$ and $\hat{\mathbf{a}}_{\rm H}$ are the coefficient of the expansion for the disk and the halo respectively, $F_{\rm D}$ is the distribution function of stellar stars within the disk, $\{\psi^{\mathrm{D},[\mathbf{q}]}(r)\}_{\mathbf{q}}$ the potential basis function over which the disk response is projected, and $\boldsymbol{\omega}_{\rm D}$ the angular frequencies of the stars in the disk.

Let us first assume that the unperturbed disk is stable. Solving the coupled equation for $[\hat{\mathbf{a}}_{\rm H}, \hat{\mathbf{a}}_{\rm D}]$ yields (after half

[7] Note that we may lift this assumption at the cost of nonlinearities, provided we may rely on an equation of state to relate it to the underlying density

inverse Fourier transform) the temporal evolution of the spiral response as a function of time for a given tidal field, $\mathbf{b}(t)$ and a given infall history, $\mathbf{c}(t)$. The pitch angle, $\mathcal{I}$ of the spiral, defined by $\tan(\mathcal{I}) = 1/\pi \int_0^\pi \mathrm{d}\theta \mathrm{d}\log\mathcal{R}/\mathrm{d}\theta$ (where $\mathcal{R}(\theta)$ corresponds to the crest of the spiral wave), is a non-linear function of $\mathbf{a}_\mathrm{D}$, which we may write formally as $\mathcal{I}[\mathbf{a}_\mathrm{D}]$. Hence we may ask ourselves what it's cosmic mean, $\langle\mathcal{I}[\mathbf{a}_\mathrm{D}]\rangle$ is, given that $\hat{\mathbf{a}}_\mathrm{D}(\omega)$ obeys

$$\hat{\mathbf{a}}_\mathrm{D}(\omega) = \hat{\mathbf{K}}_\mathrm{HD}\cdot[\mathbf{b}+\mathbf{Q}\cdot\mathbf{c}] \Big/ \mathrm{Det}\begin{vmatrix} \mathbf{1}-\hat{\mathbf{K}}_\mathrm{DD} & \hat{\mathbf{K}}^*_\mathrm{DH} \\ \hat{\mathbf{K}}_\mathrm{DH} & \mathbf{1}-\hat{\mathbf{K}}_\mathrm{HH}\end{vmatrix}.$$

Note that $\mathcal{I}[\mathbf{a}_\mathrm{D}]$ will depend on the statistical properties of $\mathbf{b}$, $\mathbf{c}$ and also on the distribution function for the halo, $F(\mathbf{I})$, and the distribution function for the disk, $F_\mathrm{D}(\mathbf{J})$. More generally, we may in this manner construct the full PDF of the pitch angle, as a function of say, cosmic time, (or relative mass in the disk or ...) following the same route as sketched in Section E3.

If the disk is intrinsically unstable, we must then add to the driven response described above the unstable modes. The amplitude of the response will then depend on exactly when each unstable mode has been exited. Such a prescription is beyond the scope of this paper, but could be addressed statistically through the description of a phase transition.

5.2.2 *Warp excitation*

As mentioned earlier (López-Corredoira et al. (2002), Jiang & Binney (1999)), warps are intrinsically stable modes of thin disks which respond to their environment. The action of the torque applied on the disk of a galaxy is different for different angular and radial positions of the perturbation. The warp's orientation and its amplitude are functions of the external potential.

The work done by the presence of perturbations on the stellar system is

$$\frac{\mathrm{d}E}{\mathrm{d}t} = -\int \mathrm{d}\mathbf{r}\nabla(\psi+\psi^e)\cdot\rho\mathbf{v} = -\int \mathrm{d}\mathbf{r}(\psi+\psi^e)\nabla(\rho\mathbf{v}), \quad (75)$$

where $\psi+\psi^e$ is the total potential perturbation (self-response + external component).

Using Eq. (20) and Eq. (75)

$$\langle\frac{\mathrm{d}E}{\mathrm{d}t}\rangle = -\sum_{\mathbf{n},\mathbf{n}'}\int \mathrm{d}\mathbf{r}\langle[a_{\mathbf{n}'}(t)+b_{\mathbf{n}'}(t)]\,\nabla\psi_\mathbf{n}(\mathbf{r})\cdot\times$$

$$\int_{-\infty}^{t}\mathrm{d}\tau K_{[2],\mathbf{n}}(\mathbf{r},\tau-t)\,[a_\mathbf{n}(\tau)+b_\mathbf{n}(\tau)]+Q_{[2],\mathbf{n}}(\mathbf{r},\tau-t)c_\mathbf{n}(\tau)\rangle.$$

The power spectra of potential fluctuations drive the energy rate of change through the cross-correlation between the source and the potential.

Note in closing that the framework described in this paper should allow us in the future to address the possibility of warps induced by the accretion of gas.

5.3 Substructures in our own Galactic halo

Let us now turn to the Milky Way. Our knowledge of the structure of its halo has increased dramatically in the course of the last decade with the advent of systematic imaging and spectroscopic surveys (*e.g.* SDSS, 2dF), both in the optical and at longer wavelengths (*e.g.* 2MASS), and this observational investigation will undoubtedly continue with efforts such as RAVE, or the upcoming launch of GAIA. This has led to the discovery of quite a few substructures within our halo, both in projection on the plane of the sky (tidal tails) as star counts but also via kinematical features (streams). The extent of the upcoming systematic stellar surveys will allow for a systematic analysis of the dynamical properties of Galactic substructures.

5.3.1 *Extent of tidal tails and streams in proper motion & galactic coordinates*

The number of stars, $\mathrm{d}N$, in the solid angle defined by the Galactic longitudes and latitudes $(\ell,b)\triangleq\boldsymbol{\ell}$ (within $\mathrm{d}\ell\mathrm{d}(\sin b)$), with proper motions $(\mu_\ell,\mu_b)\triangleq\boldsymbol{\mu}$ (within $\mathrm{d}\mu_b\mathrm{d}\mu_\ell$) at time t is given by (Pichon et al. (2002)):

$$\mathrm{d}N \triangleq A_\lambda(\boldsymbol{\mu},\boldsymbol{\ell},t)\,\mathrm{d}\boldsymbol{\mu}\mathrm{d}\boldsymbol{\ell} = \left\{\iint \mathrm{d}u_r \mathrm{r}^4\mathrm{d}\mathrm{r} f(\mathrm{r},\mathbf{u},t)\right\}\mathrm{d}\boldsymbol{\mu}\mathrm{d}\boldsymbol{\ell}, \quad (76)$$

The variables $\mathrm{r},\mathbf{u}$ are the vector position and velocity coordinates (u_r,u_ℓ,u_b) in phase space relative to the Local Standard of Rest, while $\mathbf{r}=(R,\Phi,z)$ and $\mathbf{v}=(v_R,v_\Phi,v_z)$ are those relative to the Galactic centre. In particular, the radius r (within dr) corresponds to the distance along the line of sight in the direction given by the Galactic longitudes and latitudes (ℓ,b) (within the solid angle $\mathrm{d}\ell\cos(b)\mathrm{d}b$).

These velocities are given as a function of the velocities measured in the frame of the sun by

$$\begin{aligned}
v_\Phi &= \frac{1}{R}(r_\odot\sin(b)\sin(\ell)u_b - r_\odot\cos(b)\sin(\ell)u_r - \\
&\quad r_\odot\cos(\ell)u_\ell + r\cos(b)\,(u_\ell-\sin(\ell)u_\odot)+(r_\odot+r\cos(b)\cos(\ell))\,v_\odot)\,,\\
v_R &= \frac{1}{R}\{(r\,\cos(b)-r_\odot\,\cos(\ell))\,\sin(b)\,u_b - r_\odot\,\sin(\ell)\,u_\ell - \\
&\quad \cos(b)\,(r\,\cos(b)-r_\odot\,\cos(\ell))\,u_r + \\
&\quad r_\odot\,u_\odot - r\,\cos(b)\cos(\ell)\,u_\odot + r\,\cos(b)\,\sin(\ell)\,v_\odot\}\,,\\
v_z &= \sin(b)\,u_r+\cos(b)\,u_b+w_\odot\,, \qquad (77)
\end{aligned}$$

where

$$\begin{aligned}
&\Phi = \tan^{-1}\left(\frac{\mathrm{r}\,\cos(b)\,\sin(\ell)}{R}, \frac{r_\odot-\mathrm{r}\,\cos(b)\,\cos(\ell)}{R}\right),\\
&R=\sqrt{r_\odot^2-2r_\odot\mathrm{r}\,\cos(b)\,\cos(\ell)+\mathrm{r}^2\cos(b)^2}, \quad \text{and}\\
&z=\mathrm{r}\sin(b)\,. \qquad (78)
\end{aligned}$$

R measures the projected distance (in the meridional plane) to the Galactic centre, Φ the angle in the meridional plane between the star and the Galactic centre, while z is the height of the star. Here $u_\odot,v_\odot,w_\odot$ and $r_\odot$ are respectively the components of the Sun's velocity and its distance to the Galactic centre.

Recall that Eq. (7) together with Eq. (19) provides us with the full phase space distribution of the infall as a function of the actions of the unperturbed halo. Let us call $f_\mathbf{n}$, the phase space basis defined by

$$f_\mathbf{n}(\mathbf{r},\mathbf{v},\tau)\triangleq\sum_\mathbf{k}\exp(\imath\mathbf{k}\cdot\boldsymbol{\omega}\tau+\imath\mathbf{k}\cdot\mathbf{w})\,\mathbf{v}\;\imath\mathbf{k}\cdot\frac{\mathrm{d}F}{\mathrm{d}\mathbf{I}}\psi^{[\mathbf{n}]}_\mathbf{k}(\mathbf{I}), \quad (79)$$

so that the perturbation at time t and position $(\mathbf{r},\mathbf{v})$ reads

$$f(\mathbf{r},\mathbf{v},t)=\sum_{\mathbf{n}}\int^{t}\mathrm{d}\tau f_{\mathbf{n}}(\mathbf{r},\mathbf{v},\tau-t)a_{\mathbf{n}}(\tau)\,. \tag{80}$$

We may now seek the characteristic signature in observed phase space (today *i.e.* at $t=0$), of a given perturbation.

$$A(\boldsymbol{\ell},\boldsymbol{\mu})=\sum_{\mathbf{n}}\!\!\int\!\mathrm{d}\tau a_{\mathbf{n}}(\tau)\!\!\int\!\mathrm{d}\mathrm{r}\mathrm{r}^4\!\!\int\!\mathrm{d}u_r f_{\mathbf{n}}(\mathbf{r}[\boldsymbol{\ell},\mathrm{r}],\mathbf{v}[\mathrm{r}\boldsymbol{\mu},u_r],\tau)\,, \tag{81}$$

where $\mathbf{v}[\mathrm{r}\boldsymbol{\mu},u_r]$ is given by Eq. (77), and $\mathbf{r}[\boldsymbol{\ell},\mathrm{r}]$ is given by Eq. (78). In particular, we may compute the autocorrelation of the kinematic count defined by

$$C_{\mathrm{A}}^{\boldsymbol{\mu}}(\Delta\boldsymbol{\ell},\Delta\boldsymbol{\mu})\triangleq\langle A(\boldsymbol{\ell}+\Delta\boldsymbol{\ell},\boldsymbol{\mu}+\Delta\boldsymbol{\mu})A(\boldsymbol{\ell},\boldsymbol{\mu})\rangle\,. \tag{82}$$

It involves an integral over time of the autocorrelation of the coefficients, $\langle a_{\mathbf{n}}(\tau)a_{\mathbf{n}'}(\tau')\rangle$ as

$$C_{\mathrm{A}}^{\boldsymbol{\mu}}=\sum_{\mathbf{n},\mathbf{n}'}\iint\mathrm{d}\tau\mathrm{d}\tau'\langle a_{\mathbf{n}}(\tau)a_{\mathbf{n}'}(\tau')\rangle\iint\mathrm{r}^4\mathrm{d}\mathrm{r}\mathrm{r}'^4\mathrm{d}\mathrm{r}'\iint\mathrm{d}u_r\mathrm{d}u'_r\times$$
$$f_{\mathbf{n}}(\mathbf{r}[\boldsymbol{\ell},\mathrm{r}],\mathbf{v}[\mathrm{r}\boldsymbol{\mu},u_r],\tau)f_{\mathbf{n}'}(\mathbf{r}[\boldsymbol{\ell}+\Delta\boldsymbol{\ell},\mathrm{r}],\mathbf{v}[\mathrm{r}'\boldsymbol{\mu}+\mathrm{r}'\Delta\boldsymbol{\mu},u'_r],\tau').$$

Recall that $\langle a_{\mathbf{n}}(\tau)a_{\mathbf{n}'}(\tau')\rangle$ can be reexpressed in terms of the coefficients of $\langle\hat{\mathbf{b}}\cdot\hat{\mathbf{b}}^{*\top}\rangle$ and $\langle\hat{\mathbf{c}}\cdot\hat{\mathbf{c}}^{*\top}\rangle$ and $\langle\hat{\mathbf{b}}\cdot\hat{\mathbf{c}}^{*\top}\rangle$ via Eq. (29). The width of the correlation, $C_{\mathrm{A}}^{\boldsymbol{\mu}}(\Delta\boldsymbol{\ell},\Delta\boldsymbol{\mu})$, both in velocity space and in position space accounts for the expected cosmic size of structures within the Galactic halo.

5.3.2 *Angular extend of tidal tails*

The marginal distribution over proper motions of Eq. (76) yields the projection on the sky of the perturbation:

$$A(\boldsymbol{\ell},t)\;\triangleq\;\iint A(\boldsymbol{\ell},\boldsymbol{\mu},t)\,\mathrm{d}\boldsymbol{\mu}=\!\!\iiint\mathrm{d}u_r\mathrm{r}^4\mathrm{d}\mathrm{r}f(\mathrm{r},\mathbf{u},t)\,\mathrm{d}\boldsymbol{\mu}\,, \tag{83}$$

which can be derived from Eq. (81) but is also found directly via integration over the density as

$$A(\boldsymbol{\ell},t)=\sum_{\mathbf{n}}a_{\mathbf{n}}(t)\int\tilde{\rho}_{\mathbf{n}}(\mathrm{r},\boldsymbol{\ell})\mathrm{r}^2\mathrm{d}\mathrm{r}\,,\quad\text{given}$$
$$\tilde{\rho}_{\mathbf{n}}(\mathrm{r},\boldsymbol{\ell})\triangleq\rho_{\mathbf{n}}(R(\mathrm{r},\boldsymbol{\ell}),\Phi(\mathrm{r},\boldsymbol{\ell}),z(\mathrm{r},\boldsymbol{\ell}))\,, \tag{84}$$

where $\rho_{\mathbf{n}}$ is given by Eq. (9) and *e.g.* $R(\mathrm{r},\boldsymbol{\ell})$ is given by Eq. (78). Note the generic difference between Eq. (81) and (84): the former involves the explicit cumulative knowledge of $a_{\mathbf{n}}(\tau)$ for all τ since it involves a kinematical (inertial) quantity, $\boldsymbol{\mu}$, while the latter only require the knowledge of the current $a_{\mathbf{n}}(t)$. This difference is weaker than it seems in practice, since self-gravity implies that $a_{\mathbf{n}}(t)$ depends in turn on the previous $a_{\mathbf{n}}(\tau)$ via Eq. (18). The corresponding angular correlation reads

$$C_{\mathrm{A}}(\Delta\boldsymbol{\ell})\quad\triangleq\quad\langle A(\boldsymbol{\ell}+\Delta\boldsymbol{\ell})A(\boldsymbol{\ell})\rangle=$$
$$\sum_{\mathbf{n},\mathbf{n}'}\langle a_{\mathbf{n}}(t)\,a_{\mathbf{n}'}(t)\rangle\iint\mathrm{d}\mathrm{r}\,\mathrm{d}\mathrm{r}'\,\mathrm{r}'^2\mathrm{r}^2\tilde{\rho}_n[\mathrm{r},\boldsymbol{\ell}]\tilde{\rho}_n[\mathrm{r}',\boldsymbol{\ell}+\Delta\boldsymbol{\ell}]\,. \tag{85}$$

The FWHM of the correlation defined by Eq. (85) corresponds to the"cosmic" width of tidal stream projected on the sky.

5.4 Past history of galaxies : dynamical inversion

Let us now see how the theoretical framework presented in Section 2 and Section 3 may be applied to invert observed properties of galaxies back in time and constrain the past infall and the tidal field on a given dark matter halo. In short, the idea is to notice that the perturbation theory provides an explicit relationship between the response and the excitation of the inner halo which we can tackle as an integral equation for the source. [8] Let us present first the inversion for our Milky Way (Section 5.4.1), and discuss briefly extra galactic stellar streams.

5.4.1 *The Galactic inverse problem*

Let us rewrite formally Eq. (81) as $A(\boldsymbol{\ell},\boldsymbol{\mu})=\mathcal{A}^{\boldsymbol{\ell},\boldsymbol{\mu}}\cdot\mathbf{a}$, where the dot product accounts for *both* the summation over $\mathbf{n}$ and the integration over τ (*cf.* Eq. (45)). Let us assume that we have access to kinematic star counts, *i.e.* to a set of measurements $\{A_i\triangleq A(\boldsymbol{\ell}_i,\boldsymbol{\mu}_i)\}_{i\leqslant n}$. We want to minimize

$$\chi^2=\sum_i\Big(A_i-\mathcal{A}_i^{\boldsymbol{\ell},\boldsymbol{\mu}}\cdot\mathbf{R}_1\cdot(\mathbf{K}\cdot\mathbf{b}+\mathbf{Q}\cdot\mathbf{c})\Big)^2\,, \tag{86}$$

subject to some penalty function. Recall that $\mathbf{R}_1$ is given by Eq. (47) and accounts for the self-gravity of the halo. Let us formally rewrite again $\mathcal{A}_i^{\boldsymbol{\ell},\boldsymbol{\mu}}\cdot\mathbf{R}_1\cdot(\mathbf{K}_1\cdot\mathbf{b}+\mathbf{Q}_1\cdot\mathbf{c})\triangleq\mathbf{M}\cdot\tilde{\mathbf{b}}$, with $\tilde{\mathbf{b}}=[\mathbf{b},\mathbf{c}]$. Let us also write $\mathbf{A}=(A_i)_{i\leqslant n}$. The solution to the linear minimization, Eq. (86) reads

$$\tilde{\mathbf{b}}\triangleq\mathbf{M}_\lambda^{(-1)}\cdot\mathbf{A}=(\mathbf{M}^\top\cdot\mathbf{M}+\lambda\mathbf{P})^{-1}\cdot\mathbf{M}^\top\cdot\mathbf{A}\,, \tag{87}$$

where $\mathbf{P}$ is some penalty which should impose smoothness for $\mathbf{b}$ and $\mathbf{c}$ both angularly and as a function of time. For instance, For the $\mathbf{b}$ field we could use (see, *e.g.* Pichon et al. (2002)):

$$P[b_{\ell m}]=\sum_\ell[(\ell+1)\ell]^2\int\mathrm{d}\omega\omega^2|\hat{C}_\ell|,\quad\text{where}\quad\hat{C}_\ell(\omega)\triangleq\langle|\hat{b}_{\ell m}|^2\rangle\,,$$

(so that large ω and ℓ are less likely in the solution) and a similar expression for the $\mathbf{c}$ field which should also impose smoothing along velocities. The penalty coefficient, λ, should be tuned so as to provide the appropriate level of smoothing. In practice, it might be necessary to impose further non-linear constrains on the solution, $\tilde{\mathbf{b}}$, such as requiring that the excitation is locally as compact and connex as possible on the R_{200} sphere. This can be done via some form of non-linear band pass filter in the prior, in order to limit the effective degrees of freedom in $\tilde{\mathbf{b}}$.

Accounting for non-linearities.

The non-linear solution, Eq. (51) may be formally rewritten as $\mathbf{a}_2\triangleq\mathbf{M}_2\cdot\tilde{\mathbf{b}}\otimes\tilde{\mathbf{b}}$, so that the perturbative inverse reads

$$\tilde{\mathbf{b}}\triangleq\mathbf{M}_\lambda^{(-1)}\cdot\mathbf{A}-\mathbf{M}_\lambda^{(-1)}\cdot\mathbf{M}_2\cdot(\mathbf{M}_\lambda^{(-1)}\cdot\mathbf{A})\otimes(\mathbf{M}_\lambda^{(-1)}\cdot\mathbf{A})\,, \tag{88}$$

(where $\mathbf{M}_\lambda^{(-1)}$ is defined by Eq. (87)) provided the regime for the perturbative expansion applies. If not, we may still find the best non-linear solution to the penalized likelihood problem of jointly minimizing $||\mathbf{A}-\mathbf{M}\cdot\tilde{\mathbf{b}}-\mathbf{M}_2\cdot\tilde{\mathbf{b}}\otimes\tilde{\mathbf{b}}||^2+\lambda\mathbf{P}$, while using Eq. (88) as a starting point.

When proper motions measurements are not available (*i.e.* we only have access to star counts), Eqs. (86)-(88) still

[8] Since our treatment of the dynamics (including the self -consistent gravity polarisation) is linear order by order, we may in principle recover the history of the excitation.

apply with some straightforward modifications, but the conditioning of the problem should decrease significantly, since the dynamics is less constrained.

For a data set such as GAIA, we shall have access to the full 6-dimensional description of phase space for some of the stars (via radial velocity measurements and parallax) or at least 5 dimensional measurements $(\ell, b, \mu_\ell, \mu_b, u_r)$.

Recall that in practice, the fields, **b** and **c** are respectively three-dimensional (2 angles and time) and 5 -dimensional (2 angles, time and 3 velocities). Consequently the inverse problem is generically very ill-conditioned since data space is either two (ℓ, b), four $(\ell, b, \mu_\ell, \mu_b)$, five -dimensional $(\ell, b, \mu_\ell, \mu_b, \pi)$, or six dimensional $(\ell, b, \mu_\ell, \mu_b, \pi, v_r)$. In fact it is anticipated that the conditioning is even poorer because the dynamical evolution involves damped modes, implying an exponential decay (which corresponds to a major challenge for extrapolation). It remains that the weakly damped modes should be tractable back in time up to some horizon, which will depend on the nature of the halo (via the conditioning of $\mathbf{M}_\lambda$ defined in Eq. (87)), the volume of data, and the signal to noise ratio in the measurements.

Let us close this discussion of the inverse problem by emphasizing again the true complexity of the implementation: Eq. (87), and its non-linear counterpart, Eq. (88), include via the dot product large sums over **n** and integrals over τ. $\mathbf{M}$ and $\mathbf{M}_2$ are functions of $\mathcal{A}^{\ell,\mu}$ (which require a couple of integrals) and A_{bb} *etc...* which are themselves functions of $\mathbf{K}_i$ (Eq. (53)) (which involves the underlying distribution function, $F_0(\mathbf{I})$, and the basis function, $\psi^{[\mathbf{n}]}(\mathbf{r})$ via Eqs (41), (42) and (47)).

Streamers (or tidal tails) in external galaxies may also be integrated backwards through the same procedure. It will involve the deprojection of the stream and of the underlying halo.

In contrast to the Galactic inverse problem, it will in principle be possible to reproduce the inversion process on a statistical set of haloes, which would allow us to compare directly to the predicted statistical properties of the **b** and the **c** (though clearly the bias introduced by the penalised inversion would have to be accounted for).

This completes our rapid survey of possible applications for the perturbative treatment of the dynamics of an open halo.

6 CONCLUSION

In the last few years, with the observational convergence towards the concordant cosmological model, a significant fraction of the interest has shifted towards smaller scales. Indeed it now becomes possible to project down to these scales some of the predictions of the model. This in turn offers the prospect of transposing there what has certainly been a key asset of modern cosmology, both observationally and theoretically: statistics. This is a requirement both from the point of view of the (often understated) variety of objects falling onto an $L_\star$ galaxy, but also because of the sheer size of the configuration space for infall. It is also a requirement from the point of view of the non-linear dynamics within the dark matter halo in order to account for the relative time ordering of accretion events. was pointless to describe continuous infall, haloes are typically not in fully phase mixed equilibria, and the resulting fluctuation spectrum may seed or excite the observed properties of galaxies.

In this paper, we aimed at constructing a self-consistent description of dynamical issues for dark matter haloes embedded in a moderately active cosmic environment. It relied entirely on the assumption that the statistics of the infall is well-characterized, as described in Aubert & Pichon (2005a,b), and that the mass of the infalling material (or to a lesser extend that of the fly-by) should be small compared to the mass of the halo. It also assumed that the halo was spherical and static or evolving adiabatically (Section 4). The emphasis was on the theoretical framework, rather than the details of the actual implementation. In other words, we aimed at describing a self-consistent setting which allows us to propagate the cosmological environment into the core of galactic haloes.

In Section 2, we derived the dynamical equations governing the linear evolution of the induced perturbation by direct infall or tidal excitation of a spherically symmetric (integrable) stationary dark matter halo. The simplified geometry of the initial state allowed us to focus on the specificities of an open system. Specifically, we revisited the influence of the external perturbations on the spherical halo, and extended the results of the literature by considering an advection term in the Boltzmann equation. This approach was compared to the classical Green solution in Appendix A. Note that both the intrinsic properties of the halo, via the distribution function, F (Eq. (16)), and the environment, via (s^e, ψ^e) (Eq. (17)), of the infall and the tidal distortion were accounted for. Clearly the subclass of problems corresponding to tidal perturbations only will turn out to be easier to implement at first. Appendix B presents the details of the angle action variables on the sphere together with an explicit expression for the kernel, $\mathbf{K}$, and carried out a test case implementation of the statistical propagation of an ensemble of radial excitations with a powerspectrum scaling like ν^{-2}.

In Section 3, we derived the non-linear response of the galactic halo to second-order (Eq. (44)) in the perturbation (and to order n in Appendix D together with the corresponding N-point correlation function) to account for tidal stripping and dynamical friction. The dynamics was "solved" iteratively, in the spirit of the successful approach initiated in cosmology by Fry (1984) and considerably extended by Bernardeau (1992). In particular we presented and illustrated a set of diagrams (Fig. (5), (D1)), each corresponding to the contribution of the perturbation expansion. Though the actual implementation of the non-linear theory is going to be CPU intensive, we argue that it will improve our understanding of the competing dynamical processes within a galactic halo. In particular, we discussed how this explicit theory of non-linear dynamics provides the setting in which substructure evolution (and destruction) will have to be carried, in order to account for *e.g.* tidal stripping.

In Section 4 we presented the Fokker-Planck equation governing the quasi-linear evolution of the mean profile of the ensemble averaged halo embedded in its cosmic environment. Specifically we showed how the infall, drift and diffusion coefficients (Eqs. (C13)-(C15)) are related to the two-point correlation of the tidal field, and incoming fluxes. Ap-

pendix C gives a derivation of this equation from first principles, while in the main text, we focused on the bibliographic context and possible applications. The key physical ingredient behind this secular evolution theory was the stochastic fluctuation caused by the incoming cosmic substructures. The key technical assumption was that the two time scales corresponding to the relaxation processes and the dynamical evolution decouple. Hence we could assume a hierarchy in time so that the distribution function is constant in time when computing the polarization.

Finally, in Section 5 we considered in turn a few classical probes of the large-scale structures which had been used in the past to constrain the main cosmological parameters and the initial power spectrum, which we transposed to the galactocentric context. Note that these are built upon observables, hence they may be used to constrain the boundary power spectrum of the $a_{\mathbf{n}}$. Since Eq. (65), (71), (E1), and (E10) involve different combinations of $\langle a_{\mathbf{n}} a_{\mathbf{n}'} \rangle$, they will constrain them at different scales with different biases, which should ultimately allow us to better characterize the power spectrum. This situation is the direct analog of the cosmic situation, where the different tracers (weak lensing, Ly-α forest, CMB etc..), constrain different scales of the cosmological power spectrum (with different biases). Note also that our knowledge of the statistical properties of the boundary (via the $b_{\mathbf{n}}$ and $c_{\mathbf{n}}$ coefficients) together with some assumptions on the equilibrium F_0 allows us to generate given realizations of the $a_{\mathbf{n}}$ as shown in Aubert & Pichon (2005a) and therefore virtual observables for any of these data sets, for the purpose of *e.g.* validating inverse methods. We investigated the consequences of the infall down to galactic scales and showed how it could be used to account for the observed distribution of disk properties (spiral winding, warps *etc...*). We demonstrated how the analytical model (both linear and non-linear) are quite useful when attempting to"invert" the observations for the past accretion history a given galaxy. This stems mainly from the fact that perturbation theory provides an explicit scheme for the response of the system, in contrast to the algorithmic procedure corresponding to N-body simulations.

Again let us emphasize that Eq. (18) and its non-linear generalization (D3) and (C7) yield in principle the detailed knowledge of the full *perturbed* distribution (inside R_{200}) at later times. (This is to be contrasted to the situation in N-body simulations where the response of the system is partially hidden by the mean profile of the halo, which requires first identifying substructures (Aubert et al. (2004))). Hence we should be in a position to weigh the relative importance of the environment (via s^e and ψ^e) against the inner properties of the galaxy: the unperturbed distribution function of the halo, $F(\mathbf{I})$, (its level of anisotropy, the presence of a central cusp *etc...*) the disk, (its mass, its profile, its distribution function, $F(\mathbf{J})$ *etc...*).

The work presented here derives from the fact that it was realized that the biorthogonal projection pioneered by Kalnajs (1976) could be applied order by order to the perturbative expansion of the dynamical equations. Yet this in turn required the knowledge of the relative phases involved in the perturbation, which involves characterizing the properties of the perturber. The characterization only made sense statistically in order to retain the generality of the approach of Kalnajs (1976). Hence the emphasis on statistics.

6.1 discussion & Prospects

Our purpose in this paper was to address in a statistically representative manner dynamical issues on galactic scales. We also advocated using perturbation theory in angle-actions in order to explicitly propagate this cosmic boundary inwards in phase space. As was demonstrated in the paper (and shown quantitatively in Section B4), this task remains in many respects quite challenging.

One of the limitations of the above method is the reliance on numerous expansions combined to the special care required in their implementation. One could argue that this level of sophistication might not be justified in the light of the weakness of some of the assumptions. Indeed, we are limited to systems with spherical geometry whereas galaxies most likely come in a variety of shapes. This assumption could be lifted provided we compute the modified actions of the flattened spheroidal equilibrium using perturbation theory for the equilibrium in the spirit of Binney & Spergel (1984), but implies a higher level of complexity; (it would also require statistically specifying the orientation of the halo relative to the infall, as discussed in part in Aubert et al. (2004)). We assumed here that the perturbation was relatively light, which excludes a fraction of cosmic event which might dominate the distribution of some of the observables.

Section 4.2, Section 5 and Appendix E presented a few possible applications for the framework described here and in Aubert & Pichon (2005a). These galactic probes would need to be further investigated, in particular in terms of observational and instrumental constraints. The biasing specific to each tracer should be accounted for. The second-order perturbation theory needs to be implemented in practice together with the diffusion coefficients of Section 4, following Section B and extending Section B4. Similarly, the identification and evolution of substructures within the halo mentioned in Section 3.3.1 deserves more work. In Aubert et al. (2004), we showed that the accretion onto L* haloes was anisotropic; the dynamical implication of this anisotropy will require some specific work in the future.

We will need to demonstrate against N-body simulations the relevance of perturbation theory for dynamical friction; in particular, we should explore the regime in which the second-order truncation is appropriate, and at what cost ? Note that truncated perturbation theory implies that modes will ring forever. At some stage, one will therefore have to address the problem of energy dissipation.

Implementing a realistic treatment of the infalling gas will certainly be amongst the more serious challenges ahead of us. This is a requirement both from the point of view of the dynamics but also from the point of view of converting the above predictions into baryon-dependent observables. The description of the gas will require a proper treatment of the various cooling processes, which can be quite important on galactic scales. In particular, the thickening of galactic disks is most likely the result of a fine-tuning between destructive processes such as the tidal disruption of compact substructures on the one hand, and the adiabatic coplanar infall of

cold gas within the disk. In fact, the nonlinear theory presented in Section 3 and Section 4 could be extended to the geometry of disks to account for the adiabatic polarization towards the plane of the disk.

Note that we assumed here that transients corresponding to the initial conditions where damped out so that the response of the system was directly proportional to the excitation. The underlying picture is that of a calmer past, which in fact is very much in contradiction with both our measurements and common knowledge on the more violent past accretion history of galaxies. Indeed, infalling subclumps will contribute via the external tidal potential at some earlier time, and the larger the lookback time, the relatively stronger the importance of the perturbation (since the intensity of infall is in fact an increasing function of lookback time). We are therefore facing a partially divergent boundary condition. Because of the characteristics of hierarchical clustering, the actual bootstrapping of the analytical framework is therefore challenging. This could be a problem in particular for non linear dynamics, where the coupling of transients may turn out to be as important as the driven response. The importance of these shortcomings will need to be addressed in the future.

Finally let us note that the theory described in Section 2, Section 3 and Section 4 describe perturbative solutions to the collisionless Boltzmann Poisson equation in angle-action variables, and as such are not specific to the description of dark matter haloes. It could straightforwardly be transposed to other situations or geometries provided the system remains integrable. As mentioned in Section 2.3, the stellar dynamics around a massive black hole would seem to be an obvious context in which this theory could be applied. For instance, we might want to investigate the capture of streams of stars by an infalling black hole. In a slightly different context, note in passing that the above theory could also be applied to celestial mechanics, since an angle-action expansion corresponds to an all eccentricity scheme.

Let us close this paper by a summary of the pros and cons of the theory presented here.

Possible assets:

- fixed boundary: localized statistics;
- fluid description : no *a priori* assumption on the possibly time- dependent nature of the objects;
- non-linear explicit treatment of the dynamics: proper account of the self-gravity of incoming objects and statistical accounting of causality;
- dynamically-consistent statistically-representative treatment of the cosmic environment;
- customized description of resonant processes within the halo via angle action variables of universal profile;
- ability to construct one- and two-point statistics for a wide range of galactic observables.
- theoretical framework for dynamical inversion and secular evolution

Possible drawbacks:

- weak perturbation w.r.t. spherical stationary equilibrium: not representative of *e.g.* equal mass mergers;
- complex time dependent 5D boundary condition;
- *ad hoc* position of the boundary;
- no obvious truncation of two-entry perturbation theory;
- no account of baryonic processes;
- inconsistency in relative strength of merging events versus time;
- non-Gaussian environment probably untractable;
- finite temporal horizon given finite $\ell_{\rm max}$;
- no statistical accounting of linear instabilities.

Acknowledgments

We are grateful to E. Bertschinger, J. Binney, S. Colombi, J. Devriendt, J. Heyvaerts, A. Kalnajs, J. Magorrian, D. Pogosyan, S. Prunet, A. Siebert, S. Tremaine, & E. Thiébaut for useful comments and helpful suggestions. We are especially grateful to J. Heyvaerts for carefull reading of the manuscript and for introducing us to the quasi-linear formalism. We thank the anonymous referee for constructive remarks. Support from the France-Australia PICS is gratefully acknowledged. DA thanks the Institute of Astronomy and the MPA for their hospitality and funding from a Marie Curie studentship.

REFERENCES

Aoki S., Noguchi M., Iye M., 1979, Astron. Soc. of Japan Publications, 31, 737
Arad I., Dekel A., Klypin A., 2004, MNRAS , 353, 15
Aubert D., Pichon C., 2005a, in prep.
Aubert D., Pichon C., 2005b, in prep.
Aubert D., Pichon C., Colombi S., 2004, MNRAS , 352, 376
Balescu R., 1963, Statistical Mechanics of Charged Particles.. Wiley, New York
Bernardeau F., 1992, ApJ , 392, 1
Bernardeau F., Colombi S., Gaztañaga E., Scoccimarro R., 2002, Phys. Rep., 367, 1
Bertin G., Pegoraro F., Rubini F., Vesperini E., 1994, ApJ , 434, 94
Binney J., 2004, MNRAS , 350, 939
Binney J., Spergel D., 1984, MNRAS , 206, 159
Binney J., Tremaine S., 1987, Galactic dynamics. Princeton, NJ, Princeton University Press, 1987, 747 p.
Bogolyubov N., Gurov K., 1947, Zh. Eksp. Teor. Fiz., 17, 615
Dalal N., Kochanek C. S., 2002, ApJ , 572, 25
Diemand J., Moore B., Stadel J., 2004, MNRAS , 353, 624
Earn D. J. D., Tremaine S., 1991, in Dynamics of Disc Galaxies Exact Solutions for Hamiltonian Systems Using Integer Arithmetic. pp 137–+
Fillmore J. A., Goldreich P., 1984, ApJ , 281, 9
Fridman A. M., Poliachenko V. L., 1984, Shock and Vibration
Fry J. N., 1984, ApJ , 279, 499
Gilbert I. H., 1970, ApJ , 159, 239
Gill S. P. D., Knebe A., Gibson B. K., 2004, MNRAS , 351, 399
Gill S. P. D., Knebe A., Gibson B. K., Dopita M. A., 2004, MNRAS , 351, 410
Hernquist L., 1990, ApJ , 356, 359
Hernquist L., Ostriker J. P., 1992, ApJ , 386, 375
Howard S., Byrd G. G., 1990, AJ , 99, 1798

Ichimaru S., 1973, Basic Principles of Plasma Physics: A Statistical Approach . (Reading: Addison-Wesley)
Jiang I., Binney J., 1999, MNRAS , 303, L7
Kalnajs A. J., 1971, ApJ , 166, 275
Kalnajs A. J., 1976, ApJ , 205, 745
Kalnajs A. J., 1977, ApJ , 212, 637
Klimontovich Y., 1967, The Statistical Theory of Non-Equilibrium Processes in a Plasma . (Cambridge: MIT Press)
Knebe A., Gill S. P. D., Gibson B. K., Lewis G. F., Ibata R. A., Dopita M. A., 2004, ApJ , 603, 7
Kochanek C. S., Dalal N., 2004, ApJ , 610, 69
López-Corredoira M., Betancort-Rijo J., Beckman J. E., 2002, AAP , 386, 169
Langevin P., 1908, Comptes Rendu, 146, 530
Lenard A., 1961, J. Math. Phys., 2, 682
Ma C., Bertschinger E., 2004, ApJ , 612, 28
Murali C., 1999, ApJ , 519, 580
Palmer P. L., Papaloizou J., 1987, MNRAS , 224, 1043
Peacock J. A., 1999, Cosmological physics. Cosmological physics. Publisher: Cambridge, UK: Cambridge University Press, 1999. ISBN: 0521422701
Peebles P. J. E., 1980, The large-scale structure of the universe. Research supported by the National Science Foundation. Princeton, N.J., Princeton University Press, 1980. 435 p.
Pichon C., Cannon R. C., 1997, MNRAS , 291, 616
Pichon C., Siebert A., Bienaymé O., 2002, MNRAS , 329, 181
Pichon C., Vergely J. L., Rollinde E., Colombi S., 2001, MNRAS , 326, 597
Power C., Navarro J. F., Jenkins A., Frenk C. S., White S. D. M., Springel V., Stadel J., Quinn T., 2003, MNRAS , 338, 14
Press W. H., Teukolsky S. A., Vetterling W. T., Flannery B. P., 1992, Numerical recipes in C. The art of scientific computing. Cambridge: University Press, |c1992, 2nd ed.
Risken H., 1989, The Fokker-Planck equation. Methods of solution and applications. Springer Series in Synergetics, Berlin, New York: Springer, |c1989, 2nd ed.
Seguin P., Dupraz C., 1994, AAP , 290, 709
Springel V., White S. D. M., Tormen G., Kauffmann G., 2001, MNRAS , 328, 726
Stoehr F., White S. D. M., Springel V., Tormen G., Yoshida N., 2003, MNRAS , 345, 1313
Toomre A., Toomre J., 1972, ApJ , 178, 623
Tremaine S., Weinberg M. D., 1984, MNRAS , 209, 729
Vauterin P., Dejonghe H., 1996, AAP , 313, 465
Weinberg M. D., 1989, MNRAS , 239, 549
Weinberg M. D., 1993, ApJ , 410, 543
Weinberg M. D., 1998a, MNRAS , 299, 499
Weinberg M. D., 1998b, MNRAS , 297, 101
Weinberg M. D., 2001a, MNRAS , 328, 321
Weinberg M. D., 2001b, MNRAS , 328, 321

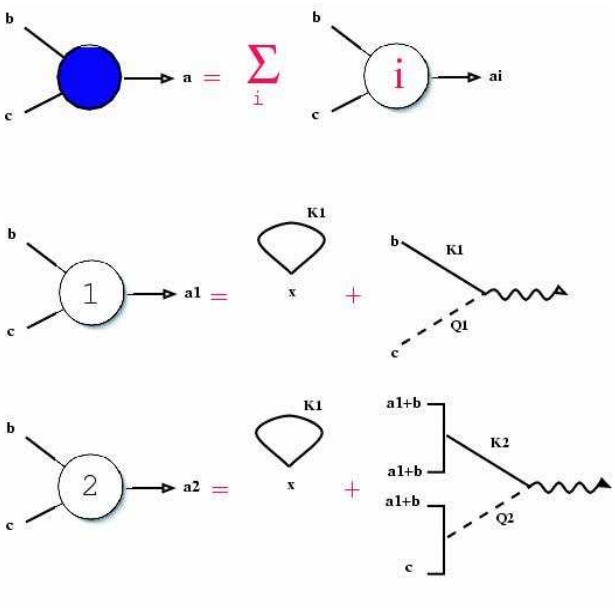

Figure 5. diagrammatic representation of the expansion to second-order given in Eqs. (43)-(44). The top diagram states that one should sum over all orders in the coupling in order to model the non-linear response of the halo; The second diagram from the top stands for Eq. (43) and the third for Eq. (44). The loops correspond to the self-coupling i.e. the self-gravity response of the halo to the perturbing flow. The second diagram corresponds to the "propagation" of the double excitation (see also Appendix A for a discussion of the distribution function propagator in angle-action variables): the input are the external potential, ψ^e (through its $b_{\mathbf{n}}$ coefficients) and the source, s^e (expanded over the $c_{\mathbf{n}}$ coefficients); the output is the coefficient of the expansion of the inner potential. The coupling is achieved via the operator K_i and Q_i defined by Eqs. (42)-(3.1.1) and (D4), while the contraction is achieved by Eq. (45), (46) and is represented by the wiggly horizontal line.

APPENDIX A: LINEAR PROPAGATOR IN ACTION ANGLE

As mentioned in Section 2.4.1, it is useful to regard the open collisionless system as a segmentation of the source for the propagator (ie the Green function of the coupled Poisson Boltzmann equation), where one distinguishes two contributions for the initial distribution: the contribution at R_{200} with $v_r < 0$ (what we describe as the source term in Eq. (6)) and the contribution beyond R_{200} or at R_{200} with $v_r > 0$ (what we describe as the tidal field in the main text). In order to make this comparison, let us derive generally (without any reference to a boundary for now) the Green function satisfying the *linearized* Boltzmann Poisson equation. Let us call $G(\mathbf{w},\mathbf{I},t|\mathbf{w}',\mathbf{I}',t')$ this Green function; it obeys:

$$\frac{\partial G}{\partial t}+\boldsymbol{\omega}\cdot\nabla_{\mathbf{w}}G+\frac{\partial F}{\partial \mathbf{I}}\cdot\nabla_{\mathbf{w}}\int\frac{\mathrm{d}\mathbf{r}''}{|\mathbf{r}''-\mathbf{r}|}d\mathbf{v}''G(\mathbf{r}'',\mathbf{v}'',t|\mathbf{w}',\mathbf{I}',t')=\delta_{\rm D}(\mathbf{w}-\mathbf{w}')\delta_{\rm D}(\mathbf{I}-\mathbf{I}')\delta_{\rm D}(t-t')\,, \tag{A1}$$

so that the distribution function at $(\mathbf{I},\mathbf{w},t)$ reads

$$f(\mathbf{w},\mathbf{I},t)=\int\mathrm{d}t'\int\mathrm{d}\mathbf{w}'\int\mathrm{d}\mathbf{I}'G(\mathbf{w},\mathbf{I},t|\mathbf{w}',\mathbf{I}',t')f(\mathbf{w}',\mathbf{I}',t')\,. \tag{A2}$$

Let us define the linear propagator, $U_{\omega,\mathbf{k},\mathbf{w}_0}(\mathbf{I}|\mathbf{I}')$, as:

$$U_{\omega,\mathbf{k},\mathbf{w}_0}(\mathbf{I}|\mathbf{I}')=\frac{\delta_{\rm D}(\mathbf{I}-\mathbf{I}')}{\mathbf{k}\cdot\boldsymbol{\omega}-\omega}-\sum_{\mathbf{n},\mathbf{n}'}\frac{\partial F}{\partial\mathbf{I}}\cdot\mathbf{k}\frac{\psi^{[\mathbf{n}]}_{\mathbf{k}}(\mathbf{I})}{(\mathbf{k}\cdot\boldsymbol{\omega}-\omega)}\left((\mathbf{1}-\hat{\mathbf{K}}[\omega])^{-1}\right)_{\mathbf{n},\mathbf{n}'}\sum_{\mathbf{k}'}\frac{\psi^{[\mathbf{n}']}_{\mathbf{k}'}(\mathbf{I}')}{(\mathbf{k}'\cdot\boldsymbol{\omega}'-\omega)}\,\exp(\imath\mathbf{w}_0\cdot[\mathbf{k}-\mathbf{k}'])\,, \tag{A3}$$

so that the distribution function, $f(\mathbf{I},\mathbf{w},t)$, at time t, with action $\mathbf{I}$ and angles $\mathbf{w}$ induced by the propagation of the distribution at earlier time t', with action $\mathbf{I}'$, and angles $\mathbf{w}'$ reads

$$f(\mathbf{I},\mathbf{w},t)=\int\mathrm{d}t'\int\mathrm{d}\mathbf{I}'\int\mathrm{d}\mathbf{w}'\sum_{\mathbf{k}}\int\mathrm{d}\omega\exp(\imath\omega[t-t']-\imath\mathbf{k}\cdot[\mathbf{w}-\mathbf{w}'])U_{\omega,\mathbf{k},\mathbf{w}_0}(\mathbf{I}|\mathbf{I}')f(\mathbf{I}',\mathbf{w}',t')\,. \tag{A4}$$

It is interesting to contrast Eq. (A3) to the propagator found by Ichimaru (1973) for the uniform plasma. In particular, the gradient of the density profile breaks the stationarity in $\mathbf{w}-\mathbf{w}_0$ of the propagator, Eq. (A3). Note also that the first term on the r.h.s. of Eq. (A3) corresponds to free streaming inside the halo (*i.e.* dark matter particles describing their unperturbed orbits), and reads in real space

$$G_{\rm free}(\mathbf{I},\mathbf{w},t|\mathbf{I}',\mathbf{w}',t')=\sum_{\mathbf{k}}\int\mathrm{d}\omega\exp(\imath\omega[t-t']-\imath\mathbf{k}\cdot[\mathbf{w}-\mathbf{w}'])\frac{\delta_{\rm D}(\mathbf{I}-\mathbf{I}')}{\mathbf{k}\cdot\boldsymbol{\omega}-\omega}=\delta_{\rm D}(\mathbf{I}-\mathbf{I}')\delta_{\rm D}(\mathbf{w}-\mathbf{w}'-\boldsymbol{\omega}[t-t'])\,,$$

while the second term in Eq. (A4) corresponds to the self-gravitating polarization of the halo induced by the perturbation. Note that since the field dynamical equation is solved with a right-hand side (*i.e.* a source breaking the mass conservation in phase space), Liouville's theorem is not obeyed anymore: a new fluid is injected into the halo. We may now assume that in Eq. (A2), $f(\mathbf{r}',\mathbf{v}',t')=f(\mathbf{w}',\mathbf{I}',t')$ is split in two: one contribution from dark matter particles exiting R_{200} or beyond R_{200}; another contribution describing particles on R_{200} with negative radial velocity. The former component may then be resumed over the corresponding region of phase space with a $1/|\mathbf{r}-\mathbf{r}'|$ weight, and yields ψ^e. The latter corresponds to $s^e(t')$.

APPENDIX B: IMPLEMENTATION

Let us describe in this appendix in greater details how Section 2 are implemented in practice, while focusing here on a simple isotropic halo (*i.e.* $F(\mathbf{I})=F(E)$, where $E=v^2/2+\Psi(r)$ is the energy, and $\Psi(r)$ the unperturbed potential). We will show here how to compute the operator, $\mathbf{K}$, (defined by Eq. (16)) and elements of $\mathbf{Q}$ (defined by Eq. (17)), for the corresponding basis, following e.g. Tremaine & Weinberg (1984), Murali (1999), Seguin & Dupraz (1994). We will then implement in practice the average induced correlation triggered by some ad hoc colored radial perturbation. Similarly, one could compute the non-linear coefficients, $[\![\ ]\!]$ entering Eq. (39), but the implementation of the non linear formalism of Section 3 and Section 4 are beyond the scope of this paper.

B1 Detailed angle-action linear response for isotropic spheres

The three-dimensional nature of galactic halo makes the implementation slightly more complicated than one would think at first sight. The assumption that the halo is spherical allow us to assume that the equilibrium is integrable. Hence the action space is effectively at most two-dimensional, but configuration space remains three-dimensional (though one angle is mute). In practice, this implies that integration over action space, occurring in *e.g.* Eq. (41) is effectively two-dimensional. On the other hand, the sum over $\mathbf{k}$ involves three indices, each corresponding to a degree of freedom.

Let us define I_1 as the radial action, $I_2\triangleq L$ as the total angular momentum and $I_3\triangleq L_z$ as the z-component of the angular momentum, so that

$$I_1=\frac{1}{\pi}\int_{r_p}^{r_a}\mathrm{d}r\sqrt{2[E-\Psi(r)]-I_2^2/r^2}\,.$$

Here r_a and r_p are respectively the apoapses and periapses of dark matter particles. This defines $\mathbf{I} \triangleq (I_1, I_2, I_3)$ introduced in Section 2.1. Similarly, Let us define the corresponding angles, $\mathbf{w} \triangleq (w_1, w_2, w_3)$ (see Fig. (1)) given by:

$$w_1 = \omega_1 \int_{r_p(\mathbf{I})}^{r} \frac{\mathrm{d}r}{\sqrt{2[E-\Psi(r)] - I^2/r^2}}\,, \quad w_2(\mathbf{I}, w_1) = \chi - \int_{r_p(\mathbf{I})}^{r(\mathbf{I},w_1)} \frac{\mathrm{d}r(\omega_2 - I_2/r^2)}{\sqrt{2[E-\Psi(r)] - I_2^2/r^2}}\,, \quad w_3 = \phi - \mathrm{asin}(\cot(\beta)\,\cot(\theta))\,, \tag{B1}$$

where $\cos\beta = L_z/L$.

B2 Computing the linear response operator

Following *very* closely the notation of Murali (1999), let us introduce a bi-orthogonal basis constructed around spherical harmonics:

$$\rho(\mathbf{r},t) = \sum_{\ell mn} a_{\ell mn}(t) d_n^{\ell m}(r) Y_{\ell m}(\mathbf{\Omega})\,, \quad \text{and} \quad \psi(\mathbf{r},t) = \sum_{\ell mn} a_{\ell mn}(t) u_n^{\ell m}(r) Y_{\ell m}(\mathbf{\Omega})\,, \tag{B2}$$

for respectively the density and the potential. Weinberg (1989) suggests the following potential-density pair

$$u_n^{\ell m}(r) = -\frac{4\pi G\sqrt{2}}{\alpha_{\mathbf{n}}|j_\ell(\alpha_{\mathbf{n}})|} R^{-1/2} j_\ell(\alpha_{\mathbf{n}} r/R), \quad \text{and} \quad d_n^{\ell m}(r) = -\frac{\alpha_{\mathbf{n}}\sqrt{2}}{|j_\ell(\alpha_{\mathbf{n}})|} R^{-5/2} j_\ell(\alpha_{\mathbf{n}} r/R), \tag{B3}$$

where j_ℓ stands for the spherical Bessel function and where $\alpha_{\mathbf{n}}$ obeys the relation $\alpha_{\mathbf{n}} j_{\ell-1/2}(\alpha_{\mathbf{n}}) = 0$. Here R is the truncation radius of the basis. Hernquist & Ostriker (1992) suggest another set of (non-normalised) biorthogonal functions defined by :

$$u_n^{\ell m}(r) = -\frac{-r^\ell}{(1+r)^{2\ell+1}} \sqrt{4\pi} C_n^{2\ell+3/2}(\xi), \quad \text{and} \quad d_n^{\ell m}(r) = \frac{K_{n\ell}}{2\pi} \frac{r^{\ell-1}}{(1+r)^{2\ell+3}} \sqrt{4\pi} C_n^{2\ell+3/2}(\xi), \tag{B4}$$

where $K_{n\ell} = n/2(n+4\ell+3) + (\ell+1)(2\ell+1)$, $\xi = (r-1)/(r+1)$ and $C_n^\ell(x)$ stand for ultraspherical polynomials.

The action angle transform of the potential basis is given by :

$$W_{\mathbf{k}}^{\ell n}(\mathbf{I}) \triangleq \psi_{\mathbf{k}}^{\mathbf{n}}(\mathbf{I}) = \frac{1}{2\pi} \int_{-\pi}^{\pi} \mathrm{d}w_1 \exp(-\imath k_1 w_1) u_n^{\ell k_3}(r) \exp[\imath k_2(\chi - w_2)], \tag{B5}$$

We may now rewrite Eq. (16) as

$$K_{\mathbf{n}}^{\mathbf{n}'}(\tau - t) = -\delta_{\ell'}^{\ell}\delta_{m'}^{m} \frac{(2\pi)^3}{4\pi G} \iint \mathrm{d}E \frac{L\mathrm{d}L}{\omega_1} \frac{\mathrm{d}F}{\mathrm{d}E} \sum_{\mathbf{k}} C_{\ell k_2} \imath \mathbf{k}\cdot\boldsymbol{\omega} \exp[\imath \mathbf{k}\cdot\boldsymbol{\omega}(\tau - t)] W_{\mathbf{k}}^{*\ell n'}(\mathbf{I}) \left[W_{\mathbf{k}}^{\ell n}(\mathbf{I}) + \frac{4\pi}{3} \delta_\ell^1 p_n^{\ell m} X_{\mathbf{k}}(\mathbf{I}) \right], \tag{B6}$$

where

$$p_n^{1m} = \int \mathrm{d}r r^2 d_n^{1m}(r) \frac{\partial \Psi}{\partial r}, \tag{B7}$$

and where

$$C_{\ell k_2} = \frac{2^{2k_2-1}}{\pi^2} \frac{(\ell - k_2)!}{(\ell + k_2)!} \frac{\Gamma^2[1/2(\ell + k_2 + 1)]}{\Gamma^2[1/2(\ell - k_2) + 1]}\,, \quad \text{if} \quad \ell + k_2 \quad \text{even, else} \quad 0\ . \tag{B8}$$

Here Γ is the standard Gamma function. Note that $X_{\mathbf{k}}(\mathbf{I})$ accounts for the fact that the response is computed in a non inertial referential frame. To take into account the barycentric drift of the halo, the perturbed Hamiltonian should include the induced inertial potential $\mathbf{a}_b \cdot \mathbf{r}$, where $\mathbf{a}_b$ is the acceleration of the barycenter in the frame of the unperturbed halo. Its action-angle transform is given by :

$$X_{\mathbf{k}}(\mathbf{I}) = \frac{1}{2\pi} \int_{-\pi}^{\pi} \mathrm{d}w_1 \exp(-ik_1 w_1) r \exp[ik_2(\psi - w_2)]. \tag{B9}$$

As can be seen from Eq. (B6), this inertial contribution is limited to the dipole component ($\ell = 1$) of the response : as expected, it is equivalent to a spatially homogeneous field force.[9]

[9] Technically speaking, the $\delta_{\ell 1}$ dependence arise from the fact that $\mathbf{r}$ is expressed as a function of $Y_{1m}(\mathbf{\Omega})$ spherical harmonics.

B3 Implementation and validation

The actual computation of the linear response of the halo to a tidal field is a two-steps procedure. First the kernel $\mathbf{K}$ must be computed via Eq. (B6). It involves an integration over the orbits' space and requires to Fourier transforms the the biorthogonal basis (W and X quantities) along orbits. It can be done by "throwing orbits" in the equilibrium potential and finding the associated sets of $(\mathbf{I}, \boldsymbol{\omega})$ in the halo's model: such a procedure provides the angle dependance of the basis' functions for a given action. Knowing $W(\mathbf{I}), X(\mathbf{I}), \boldsymbol{\omega}(\mathbf{I})$ over a given sampling of the $\mathbf{I}$ space, Eq. (B6) can be computed. In order to achieve high computing efficiency and accurate responses, we implemented the calculation of Eq. (B6) in a parallel fashion, where the integrals in each-subspace of the action space are computed by a different processor.

Second, the expansion $\mathbf{a}(t)$ of the halo's response is computed either by iteration or by means of a Volterra's Equation solver (e.g. Press et al. (1992)). We found that both methods give very similar results and differ only by their time consumption. The iterative method can be very fast if a proper initial guess is available but if it is not the case it may take a significant amount of time to achieve convergence. Conversely, the Volterra solver's time consumption is fixed for a given time resolution.

In order to validate our implementation, we set up two tests. The first one is suggested by Weinberg (1989). A Plummer's halo is embedded in an homogeneous force field and should experience a global drift decribed by the potential's response:

$$\psi(\mathbf{r}, t) = -\mathbf{r}_b(t) \cdot \nabla\Phi(\mathbf{r}), \tag{B10}$$

where $\mathbf{r}_b$ stands for the barycenter position and Φ stands for the equilibrium potential. We chose the force field to have a $a_0 \sin(\nu t)$ time dependance with $a_0 = 0.01$ and $\nu = 0.01$. The Plummer model has a unit mass M and caracteristic radius b. The response was computed using a 60×60 sampling in (E, L) and 20 radial terms of the basis given by Eq. (B3). We switched off the drift compensation modelised by the X term in Eq. (B6). Fig. (B1) shows the response computed at $t = 10$ (in units of $\sqrt{b^3/GM}$) along with the prediction given by Eq. (B10). Clearly the two responses coincide, providing a first validation of our implementation.

A second test involves reproducing the contraction of a Hernquist's halo induced by a central spherical mass (which would model the presence of a galaxy for example). This central mass is assumed to follow a Hernquist's profile, whose potential is given by:

$$\Phi(r) = -\frac{GM}{r+a}. \tag{B11}$$

The halo has a unit mass M and caracteristic radius a, while the central object has a final mass of $m_p = 0.001$ and $a_p = 0.25$ as a constant caracteristic radius. The perturber is turned on at $t = 0$ and follows a $m_p(t) = m_p(t_f)(3(t/t_f)^2 - 2(t/t_f)^3)$ temporal evolution, where t_f is the final time step. We compare the linear response at $t = t_f$ with the simulation of the same test-case using a perturbative particle code (Magorrian, private communication). The response was computed using a 60×60 sampling in 13 subregions of the whole (E, L) space and 21 radial terms of the basis given by Eq. (B4).

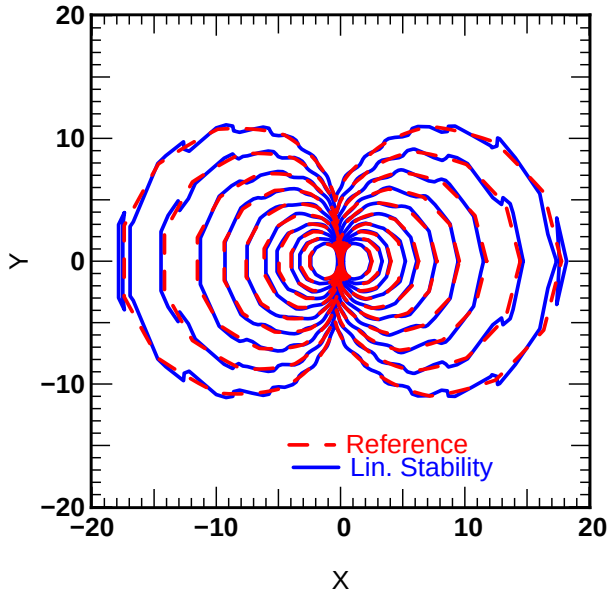

Figure B1. Isocontours in the X-Y plane of the potential's response of a Plummer Sphere embedded in a homogeneous force field (see text for details). The force field is aligned along the X axis. The dashed line stand for the prediction and the solid line stands for the linear calculation presented in this paper.

Self gravity of the response is *not* taken in account in both methods. Fig. (B2) shows the comparisons between the two type of calculations, made for two different growing time t_f. Clearly the two methods are in good agreement. One can see that matter is dragged toward the center and the longer it takes to grow the perturber, the further from the center are the affected regions.

B4 Statistical propagation: a test case

In this section, we compute the two-point statistics of a halo responding to a simple type of tidal perturbation as an illustration of statistical propagation. Without any assumption on the type of perturbation, we recall that the two-point statistics of the halo's response is given by Eq. (29) and can be derived directly from the perturbations' statistics. Let us simplify the correlation's computation by assuming that the halo is only tidally perturbed, so that Eq. (29) reduces to :

$$\left\langle \hat{\mathbf{a}} \cdot \hat{\mathbf{a}}^{*\top} \right\rangle = \left\langle \left[\hat{\mathbf{K}} \cdot \hat{\mathbf{b}}\right] \cdot (\mathbf{1} - \hat{\mathbf{K}})^{-1} \cdot (\mathbf{1} - \hat{\mathbf{K}})^{-1*\top} \cdot \left[\hat{\mathbf{K}} \cdot \hat{\mathbf{b}}\right]^{\top *} \right\rangle. \tag{B12}$$

Furthermore, let us also (rather crudely) assume that the tidal field is monopolar, and has a radial dependence equals to the Nth element of the radial basis which diagonalize the Poisson equation. Then, the tidal perturber's coefficient can be written as :

$$b^n_{\ell m}(t) = b(t)\delta_{nN}\delta_{\ell 0}\delta_{m0}, \tag{B13}$$

where the perturbing tidal field is described by :

$$\psi^e(r, \boldsymbol{\Omega}, t) = b(t) u^{\mathrm{N}}_{00}(r). \tag{B14}$$

Since no radial coupling occurs, the halo's response can be simply written as :

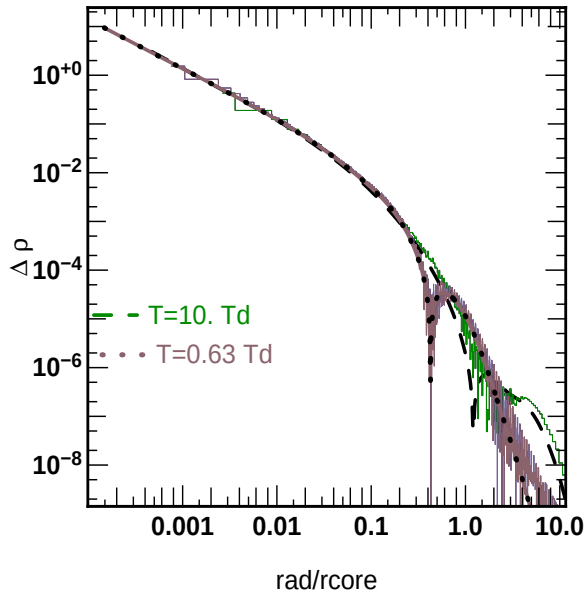

Figure B2. The radial profile of the density response of a Hernquist's halo due to a central pertuber. Lines stand for the linear response of the halo as the central pertubrer grows over a $t = 0.63t_{\rm d}$ (dotted line) and $t = 10t_{\rm d}$ timescale (dashed line). $t_{\rm d}$ is the dynamical time of the main halo within its core radius. Radii are given in units of the main halo's core radius. Density units are in code units. Superimposed are the calculations of the same response using a perturbative particle simulation (Magorrian, private communication). No scaling has been applied and the two methods agree quantitatively.

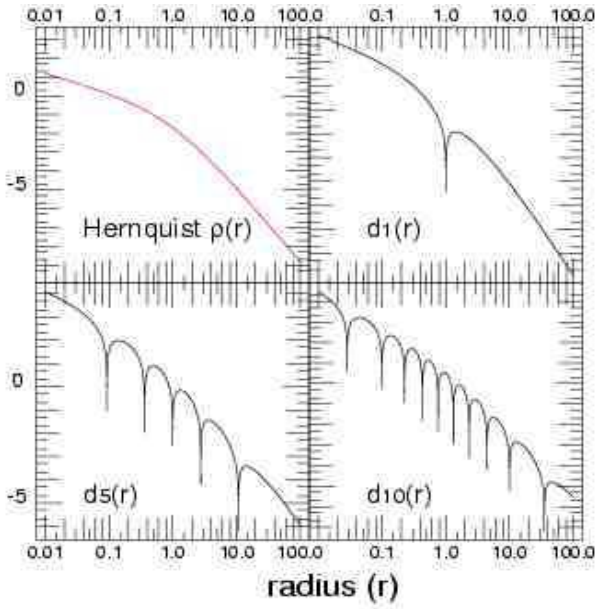

Figure B3. The halo's density profile chosen for the statistical propagation's example follows a hernquist model (top-left panel). We apply a monopolar tidal field $\psi^e(r)$ with a radial structure given by the $d^N(r)$ function of the Hernquist and Ostriker biorthogonal basis. Here are shown the corresponding density profiles $\rho^e(r) = \Delta\psi^e/4\pi G$ for $N = 1, 5, 10$.

$$\psi(r, \mathbf{\Omega}, t) = a(t) u_{00}^N(r). \tag{B15}$$

Consequently, the only remaining degree of freedom is the temporal variation of the tidal field. If we consider an *ensemble* of tidal environments and if we assume stationarity and gaussianity of the induced perturbations, it will be described by the temporal two-point correlation function of $b(t)$ coefficients, or equivalently by their temporal power spectrum $P_b(\nu)$:

$$P_b(\nu) = \langle \hat{b}(\nu)\hat{b}^*(\nu) \rangle, \tag{B16}$$

where ν stands for the frequency. If the temporal power spectrum of the response is given by $P_a(\nu)$ then Eq. (B12) reduces to:

$$P_a(\nu) = \langle \hat{a}(\nu)\hat{a}^*(\nu) \rangle = \frac{|\hat{K}^{00}_{NN}(\nu)|^2}{|1 - \hat{K}^{00}_{NN}(\nu)|^2} P_b(\nu). \tag{B17}$$

Eq. (B17) simply states that the frequency structure of the 'tidal noise' is transmitted to haloes via a (scalar) transfer function given by the response kernel.

Let us further describe our test halo again by a Hernquist's model (Hernquist (1990)). The corresponding kernel is computed following the procedure described by Section B2 using the Hernquist & Ostriker (1992) potential-density pair (see Fig. (B3)). Further details can be found in Murali (1999), Seguin & Dupraz (1994). The radial dependence of the tidal perturber is given by the N-th potential function $u_N(r) = u_N^{00}(r)$ of the basis described by Hernquist & Ostriker (1992). The associated density function is given by $d_N(r) = d_N(r)^{00} = \Delta u_N(r)/4\pi G$ and examples of such profiles are given in Fig. (B5) along with the halo's profile. For simplicity, the tidal frequency distribution has been chosen to follow a power law:

$$P_b(\nu) \sim \nu^{-2}. \tag{B18}$$

This power law describes the *ensemble* frequency behavior and therefore a single realisation of the tidal noise may deviate from this relation as long as statistical convergence is achieved. Fig. (B4) shows both an example of the time dependence of such a perturber and the time dependence of the induced response. One can see that the halo acts a low pass frequency filter and do not recover all the high frequency features present in the tidal field. Also, the halo response appears as delayed in time, reflecting the effect of the halo's own inertia.

The same computation was performed for an ensemble of 1000 different tidal perturbations. Fig. (B3) shows the power spectrum $P_b(\nu)$ averaged over all the realisations along with $P_a(\nu)$ averaged over the 1000 haloes' responses (shown as symbols with error bars). $P_b(\nu)$ departs from a power law at low frequencies ($\nu < 50$ in code units) because of the finite time range over which the tidal field is applied (not shown here). At higher frequencies, the perturbers' frequency distribution follows exactly Eq. (B18). Independantly, $P_a(\nu)$ is directly predicted from $P_b(\nu)$ using Eq. (B17), without relying on the computations of individual responses, and shown on the same plot as solid lines. Clearly the predicted power spectrum of the response matches the statistically averaged one and even reproduces 'bumpy' features seen at various frequencies. The filtering effect of the halo response can still be seen in the predicted spectra : $P_a(\nu)$ follows the ν^{-2} law at low frequencies but exhibits a steeper slope at higher frequencies. This cut-off effect is more important for large scale perturbations (low N) and reflects the fact that

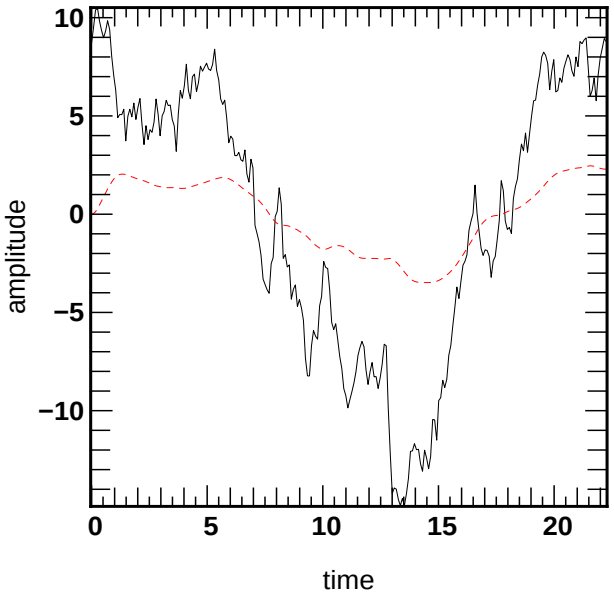

Figure B4. An example of time evolution of the tidal field's amplitude $b(t)$ (plain line). Its power spectrum $P_b(\nu)$ follows a ν^{-2} law. Assuming an N=2 radial dependance, the amplitude $a(t)$ of the induced halo's response can be computed (dashed line). The halo does not respond to high frequency features and globally its response is slightly delayed, reflecting its own inertia.

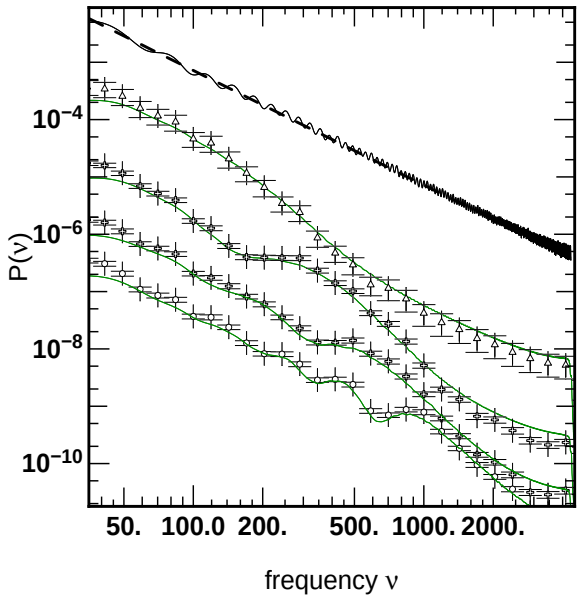

Figure B5. An example of statistical propagation. The average power spectrum of the 1000 tidal perturbations applied to the Hernquist halo (top curve) follows a ν^{-2} law (dashed thick curve). Symbols stand for power spectrum of the halo's response averaged over the 1000 realisations of $\psi^e(r,t)$ with four different radial dependences (with $N = 1, 3, 5, 10$, from top to bottom). The superimposed curves show the direct predictions on the power spectra, following Eq. (B17). For clarity these curves have been divided respectively by 1, 20, 40 and 70. Frequencies are in code units.

perturbations at high frequencies are unable to 'resonnate' efficiently with the halo's large scale modes. Conversely, tidal perturbations with features on small spatial scales (large N) are more likely to induce large frequencies and preserve the frequency structure of the perturbation. Moreover, the 'bumps' seen in the $P_a(\nu)$ curves reflect the eigen frequencies of the halo. The pertuber's scale-free spectrum hits resonances which react in a stronger fashion than any other frequency. Again, these resonances occur at larger frequencies as the radial order N increases : smaller radial scale perturbations relate to shorter caracteristic time scales.

The illustration presented in this section is admittedly simplistic but hints at the possibilities which can be foreseen for statistical propagation : for a given set of constrained environment, predictions on the statistics of the induced response can be made without relying on the computation of individual realisations. Predictions on spatial or spatio-temporal correlations of the halo's response can be made following the same procedure. It will possibly allow us to study the impact of the different scales of accretion or potential, the influence of the rate of change of these pertubrations and their relative relevance on the statistical properties of matter within the halo as discussed in Section 5.

APPENDIX C: SECULAR EVOLUTION WITH INFALL

Let us derive in this appendix the secular equation for the evolution of the ensemble average halo embedded in a typical cosmic environment (with infall and tidal field). This follows the pioneering work of Weinberg (2001a) and Ma & Bertschinger (2004). The settings in which they derive their coefficients differ: their starting point is the kinetic closure relation given by Klimontovich (1967), Ichimaru (1973), Gilbert (1970) who note that the Bogoliubov-Born-Green-Kirkwood-Yvon (BBGKY) hierarchy may be closed while assuming that the two-point correlation function will relax on a shorter dynamical time scale, whereas the one point distribution function evolves on a longer secular time scale[10]. Hence if one assumes that the distribution function F entering the linearized equation, Eq. (6), can be considered to be constant, then the second-order equation in the BBGKY hierarchy is automatically satisfied while the r.h.s. of the first equation is proportional to the propagated (via Eq. (A3)) excess correlation induced by the dressed clumps. This kinetic theory has been successfully applied in plasma physics, leading to the so called Lenard-Balescu (Lenard (1961), Balescu (1963)) collision term, and was also transposed by Weinberg (1993) for a multi-periodic "stellar" system.

Note that the BBGKY hierarchy is a $1/N$ expansion, where N is the number of particles in the system. Formally it would make sense here to identify N as a measure of the clumpiness of the medium, but this definition is qualitative only. We rely here on the *same* time ordering hierarchy, but the degree of clumpiness in the system is explicitly imposed by the boundary condition. In this appendix, the derivation is carried from first principles, while relying on an explicit infall and tidal field.

C1 Quasi linear equations in angle action variables

The collisionless Boltzmann equation of an open system may be written as:

$$\frac{\partial \mathrm{F}}{\partial t} + \{H, \mathrm{F}\} = S^e + s^e, \quad \text{with} \quad H = \frac{v^2}{2} + \Psi(\mathbf{I}, \mathbf{w}, t, T)\,, \tag{C1}$$

where F is defined by

$$\mathrm{F}(\mathbf{I}, \mathbf{w}, t, T) = F(\mathbf{I}, T) + f(\mathbf{I}, \mathbf{w}, t), \quad \text{and} \quad \Psi(\mathbf{I}, \mathbf{w}, t, T) = \Psi_0(\mathbf{I}, \mathbf{w}, T) + \psi(\mathbf{I}, \mathbf{w}, t) + \psi^e(\mathbf{I}, \mathbf{w}, t)\,, \tag{C2}$$

with F describing the secular evolution of the DF and f describing the fluctuations of the DF over this secular evolution. In Eq. (C1), the r.h.s. stands for the incoming infall, both fluctuating ($s^e[\mathbf{I}, \mathbf{w}, t]$) and secular ($S^e(\mathbf{I}, T)$). Since this system evolves secularly because of its environment, these actions are not conserved. The last two term on the r.h.s. of Eq. (C2) represents the fluctuating component tracing the motions of clumps within the environment of the halo[11]. Note that since $F(\mathbf{I}, T)$ is assumed to depend here only on the action, it represents a coarse-grained distribution function (averaged over the angles) for which we make no attempt to specify where each star is along its orbit nor how oriented the orbit is. Note also that the canonical variables $\mathbf{I}$ and $\mathbf{w}$ are the actions and the angles of the *initial* system. Developing the collisionless Boltzmann equation, Eq. (C1), over the secular and the fluctuating expansion leads to:

$$\frac{\partial F}{\partial t} + \frac{\partial f}{\partial t} + \boldsymbol{\omega} \cdot \frac{\partial f}{\partial \mathbf{w}} - \frac{\partial \psi}{\partial \mathbf{w}} \cdot \left(\frac{\partial F}{\partial \mathbf{I}} + \frac{\partial f}{\partial \mathbf{I}}\right) - \frac{\partial \psi^{\,e}}{\partial \mathbf{w}} \cdot \left(\frac{\partial F}{\partial \mathbf{I}} + \frac{\partial f}{\partial \mathbf{I}}\right) + \left[\frac{\partial \psi}{\partial \mathbf{I}} + \frac{\partial \psi^e}{\partial \mathbf{I}}\right] \cdot \frac{\partial f}{\partial \mathbf{w}} = S^e + s^e. \tag{C3}$$

This equation involves two time scales, t and T. On the fluctuation time scale, t, secular quantities can be described as static, leaving only the linearised open collisionless Boltzmann equation (Eq. (6)):

$$\frac{\partial f}{\partial t} + \boldsymbol{\omega} \cdot \frac{\partial f}{\partial \mathbf{w}} - \left(\frac{\partial \psi}{\partial \mathbf{w}} + \frac{\partial \psi^{\,e}}{\partial \mathbf{w}}\right) \cdot \frac{\partial F}{\partial \mathbf{I}} = s^e\,, \tag{C4}$$

where the amplitude of f is of first-order compared to F and involves only the fluctuating part of the external forcing, $s^e(\mathbf{I}, \mathbf{w}, t)$. On a longer time scale, T, the Boltzmann equation, Eq. (C3) can be T-averaged, considering that the average of fluctuations are zero on such time scales. This leads to a second equation:

$$\frac{\partial \langle F \rangle}{\partial T} = \left\langle \left[\frac{\partial \psi}{\partial \mathbf{w}} + \frac{\partial \psi^e}{\partial \mathbf{w}}\right] \cdot \frac{\partial f}{\partial \mathbf{I}} \right\rangle_T - \left\langle \left[\frac{\partial \psi}{\partial \mathbf{I}} + \frac{\partial \psi^e}{\partial \mathbf{I}}\right] \cdot \frac{\partial f}{\partial \mathbf{w}} \right\rangle_T + \langle S^e \rangle_T\,. \tag{C5}$$

The brackets denotes averaging over a time longer than the typical time scale of fluctuations:

$$\langle Y \rangle_T \triangleq 1/\Delta T \int_{T-\Delta T/2}^{T+\Delta T/2} \mathrm{d}t Y(t)\,.$$

The time interval, ΔT, should be chosen so that a given dark matter particle describing its orbit will encounter a few times the incoming clump at various phases along its orbit. Because the incoming clump is subject to dynamical friction, the resonance will only last so long, and induce a finite but small kick, $\Delta\mathbf{I}$ during ΔT. Because the infall displays some degree of temporal and spatial coherence, we may not assume that the successive kicks are uncorrelated, in contrast to the situation presented by Weinberg (2001a), Ma & Bertschinger (2004) or the classical image described in Brownian motion. In other words, when we

[10] This time ordering is originally due to Bogolyubov & Gurov (1947)

[11] We neglect here the secular drift of the external potential which should slowly shift the frequencies, $\boldsymbol{\omega}$ in Eq. (C3)

write an effective microscopic Langevin counterpart to the corresponding Fokker Planck equation, it will involve a coloured 3D random variable (see Eq. (60)).

Derivative and averaging may be exchanged considering that F and Ψ evolve slowly with respect to time. Terms involving the product of two first-order quantities survive to the time averaging because we cannot presume that the response in distribution function and potential within R_{200} are uncorrelated. In order to evaluate those quadratic terms, we may integrate Eq. (C4), while assuming that $F(\mathbf{I},T)$ is effectively constant w.r.t. time t. The solution, Eq. (7), may then be reinjected into the quadratic terms in Eq. (C5) so that they involves terms such as

$$\frac{\partial f}{\partial \mathbf{I}}\cdot\frac{\partial \psi}{\partial \mathbf{w}} = -\left(\sum_{\mathbf{k}_1,\mathbf{k}_2} \mathrm{e}^{\imath(\mathbf{k}_1+\mathbf{k}_2)\cdot\mathbf{w}}\psi_{\mathbf{k}_2}(\mathbf{I},t)\int_{-\infty}^{t}\mathrm{d}\tau \mathrm{e}^{\imath\mathbf{k}_1\cdot\boldsymbol{\omega}(\tau-t)}\psi_{\mathbf{k}_1}(\mathbf{I},\tau)\mathbf{k}_1\otimes\mathbf{k}_2\right):\frac{\partial^2 F}{\partial \mathbf{I}^2} - \left(\sum_{\mathbf{k}_1,\mathbf{k}_2} \mathrm{e}^{\imath(\mathbf{k}_1+\mathbf{k}_2)\cdot\mathbf{w}}\mathbf{k}_1\psi_{\mathbf{k}_2}(\mathbf{I},t)\mathbf{k}_2\cdot\frac{\partial}{\partial \mathbf{I}}\int_{-\infty}^{t}\mathrm{d}\tau \mathrm{e}^{\imath\mathbf{k}_1\cdot\boldsymbol{\omega}(\tau-t)}\psi_{\mathbf{k}_1}(\mathbf{I},\tau)\right)\cdot\frac{\partial F}{\partial \mathbf{I}}\,. \tag{C6}$$

where we may factor the action derivative of $F(\mathbf{I},T)$ out of the τ-time integral because the secular distribution is assumed to be constant over a few dynamical times. Since the l.h.s. of Eq. (C5) does not depend on $\mathbf{w}$, we may average its r.h.s. over $\mathrm{d}\mathbf{w}$. This implies that in Eq. (C6), only the $\mathbf{k}_1=-\mathbf{k}_2$ terms remain. We rely effectively on the averaging theorem (Binney & Tremaine (1987)) to convert orbit averages into angle average. The corresponding evolution equation hence depends on the actions only, as expected. Note that in doing so, we assume that no other resonances matter. The secular equation, Eq. (C5), becomes finally after some similar algebra for the other contributions:[12]

$$\frac{\partial F}{\partial t} = \langle \mathrm{D}_0(\mathbf{I})\rangle - \langle \mathbf{D}_1(\mathbf{I})\rangle\cdot\frac{\partial F}{\partial \mathbf{I}} - \langle \mathbf{D}_2(\mathbf{I})\rangle:\frac{\partial^2 F}{\partial \mathbf{I}^2}, \tag{C7}$$

where

$$\langle D_0(\mathbf{I})\rangle = \frac{1}{(2\pi)^3}\int\langle S_e\rangle_T\mathrm{d}\mathbf{w} + \left\langle\sum_{\mathbf{k}}\imath\mathbf{k}\cdot\frac{\partial}{\partial \mathbf{I}}\left([\psi^*_{\mathbf{k}}(\mathbf{I},t)+\psi^{e*}_{\mathbf{k}}(\mathbf{I},t)]\int_{-\infty}^{t}\mathrm{e}^{\imath\mathbf{k}_1\cdot\boldsymbol{\omega}(\tau-t)}s_e(\mathbf{k},\mathbf{I},\tau)\mathrm{d}\tau\right)\right\rangle_T, \tag{C8}$$

while the drift coefficient, $\mathbf{D}_1$, obeys

$$\langle \mathbf{D}_1(\mathbf{I})\rangle = \left\langle\sum_{\mathbf{k}}\mathbf{k}\ \mathbf{k}\cdot\frac{\partial}{\partial \mathbf{I}}\left([\psi^*_{\mathbf{k}}(\mathbf{I},t)+\psi^{e*}_{\mathbf{k}}(\mathbf{I},t)]\int_{-\infty}^{t}\mathrm{e}^{\imath\mathbf{k}\cdot\mathbf{!}(\tau-t)}[\psi_{\mathbf{k}}(\mathbf{I},\tau)+\psi^{e}_{\mathbf{k}}(\mathbf{I},\tau)]\mathrm{d}\tau\right)\right\rangle_T, \tag{C9}$$

and the diffusion coefficient, $\mathbf{D}_2$, is given by

$$\langle \mathbf{D}_2(\mathbf{I})\rangle = \left\langle\sum_{\mathbf{k}}\mathbf{k}\otimes\mathbf{k}[\psi^*_{\mathbf{k}}(\mathbf{I},t)+\psi^{e*}_{\mathbf{k}}(\mathbf{I},t)]\int_{-\infty}^{t}\mathrm{e}^{\imath\mathbf{k}\cdot\mathbf{!}(\tau-t)}[\psi_{\mathbf{k}}(\mathbf{I},\tau)+\psi^{e}_{\mathbf{k}}(\mathbf{I},\tau)]\mathrm{d}\tau\right\rangle_T. \tag{C10}$$

Note that the infall coefficient, D_0, includes both the secular infall, and a contribution arising from the possible correlation between the fluctuating tidal field and the fluctuating infall. It may be an explicit function of time, T, reflecting the fact that, as more mass is accreted, the profile of dark matter changes with time. The coefficients D_0, $\mathbf{D}_1$ and $\mathbf{D}_2$ are also an implicit function of time because of the time average, $\langle\ \rangle_T$ and via the secular distribution function, $F(\mathbf{I},T)$ which occurs in $\psi_{\mathbf{k}}(\mathbf{I},t)$ through Eq. (18). Clearly, if the potential, and/or the source term are completely decorelated in time, so that $\langle\psi^*_{\mathbf{k}}(\mathbf{I},t)\psi^*_{\mathbf{k}}(\mathbf{I},\tau)\rangle_T\propto\delta_{\mathrm{D}}(t-\tau)$ and $\langle\psi^*_{\mathbf{k}}(\mathbf{I},t)s^{e*}_{\mathbf{k}}(\mathbf{I},\tau)\rangle_T\propto\delta_{\mathrm{D}}(t-\tau)$, Eq. (C10) or (C9) would vanish. Provided ΔT is long compared to the typical correlation time of the potential (and/or the source term), we may take the limit $t\to\infty$ in the integrals entering Eqs. (C8)-(C10). Note finally that Eq. (C7) does not derive from a kinetic theory in the classical sense, in that it does not rely on a diffusion process in velocity space induced by the discrete number of particles in the system.

C2 Linking the infall, drift and diffusion to the cosmic two-point correlations

Up to this point we investigated the secular evolution of a *given* (phase averaged) halo, undergoing a given inflow and tidal field accretion history. Let us now invoke ergodicity so as to replace temporal averages by ensemble averages in Eqs. (C8)-(C10). In doing so, we now try and describe a *mean* galactic halo embedded in the typical environment presenting the most likely correlations. This involves replacing $\langle\ \rangle_T$ with $\langle\ \rangle\triangleq E\{\ \}$. Let us use Eq. (10) to expand Eq. (C10). This yields:

$$\langle \mathbf{D}_2(\mathbf{I},T)\rangle = \sum_{\mathbf{k}}\mathbf{k}\otimes\mathbf{k}\sum_{\mathbf{n},\mathbf{n}'}\left(\int_{-\infty}^{\infty}\langle \mathrm{a}^*_{\mathbf{n}'}(t)\mathrm{a}_{\mathbf{n}}(\tau)\rangle\mathrm{e}^{\imath\mathbf{k}\cdot\boldsymbol{\omega}(\tau-t)}\mathrm{d}\tau\right)\psi^{[\mathbf{n}']*}_{\mathbf{k}}(\mathbf{I})\psi^{[\mathbf{n}]}_{\mathbf{k}}(\mathbf{I}), \tag{C11}$$

where $\mathrm{a}_{\mathbf{n}}(t)\triangleq a_{\mathbf{n}}(t)+b_{\mathbf{n}}(t)$ corresponds to the coefficient of the total (self-consistent plus external) potential. If the first-order perturbations are stationary, let us write the two-point cross-correlation of the temporal fields, $\langle \mathrm{a}_{\mathbf{n}}(t),\mathrm{a}_{\mathbf{n}'}(\tau)\rangle$ as $\mathrm{C}[\mathrm{a}_{\mathbf{n}},\mathrm{a}_{\mathbf{n}'}](t-\tau)$ so that the integral in Eq. (C11) may be carried as (assuming parity for the correlation function):

[12] note that when $S^e=s^e=0$ this equation is conservative by construction.

$$\int_0^\infty \mathrm{C}[\mathrm{a}_{\mathbf{n}},\mathrm{a}_{\mathbf{n}'}](\Delta\tau)\mathrm{e}^{\imath\mathbf{k}\cdot\boldsymbol{\omega}\Delta\tau}\mathrm{d}\Delta\tau = P_{\mathrm{a}}^{\mathbf{n},\mathbf{n}'}[\mathbf{k}\cdot\boldsymbol{\omega}], \tag{C12}$$

giving the temporal power spectrum evaluated at the temporal frequency, $\mathbf{k}\cdot\boldsymbol{\omega}$. Consequently, the diffusion coefficient becomes:

$$\langle \mathbf{D}_2(\mathbf{I})\rangle = \sum_{\mathbf{k}} \mathbf{k}\otimes\mathbf{k} \sum_{\mathbf{n},\mathbf{n}'} \psi_{\mathbf{k}}^{[\mathbf{n}']*}(\mathbf{I})\psi_{\mathbf{k}}^{[\mathbf{n}]}(\mathbf{I}) P_{\mathrm{a}}^{\mathbf{n},\mathbf{n}'}[\mathbf{k}\cdot\boldsymbol{\omega}]. \tag{C13}$$

The same procedure may be applied to the other coefficient:

$$\langle \mathbf{D}_1(\mathbf{I})\rangle = \sum_{\mathbf{k}} \mathbf{k} \sum_{\mathbf{n},\mathbf{n}'} \mathbf{k}\cdot\frac{\partial}{\partial\mathbf{I}} \left(\psi_{\mathbf{k}}^{[\mathbf{n}']*}(\mathbf{I})\psi_{\mathbf{k}}^{[\mathbf{n}]}(\mathbf{I}) P_{\mathrm{a}}^{\mathbf{n},\mathbf{n}'}[\mathbf{k}\cdot\boldsymbol{\omega}]\right), \tag{C14}$$

while, for the secular correlation, Eq. (C8):

$$\langle D_0(\mathbf{I})\rangle = \frac{1}{(2\pi)^3}\int \langle S_e\rangle_T \mathrm{d}\mathbf{w} + \sum_{\mathbf{k}} \mathbf{k} \sum_{\mathbf{n},\mathbf{n}'} \mathbf{k}\cdot\frac{\partial}{\partial\mathbf{I}} \left(\psi_{\mathbf{k}}^{[\mathbf{n}']*}(\mathbf{I})\sigma_{\mathbf{k}}^{[\mathbf{n}],e}(\mathbf{I}) P_{\mathrm{ac}}^{\mathbf{n},\mathbf{n}'}[\mathbf{k}\cdot\boldsymbol{\omega}]\right), \tag{C15}$$

where $P_{\mathrm{ac}}^{\mathbf{n},\mathbf{n}'}[\omega]$ is the mixed power spectrum given by $\langle \hat{\mathrm{a}}_{\mathbf{n}}^* \hat{c}_{\mathbf{n}}\rangle = \langle [\hat{a}_{\mathbf{n}}^* + \hat{b}_{\mathbf{n}}^*]\hat{c}_{\mathbf{n}}\rangle$. Hence

$$P_{\mathrm{ac}}^{\mathbf{n},\mathbf{n}'}[\mathbf{k}\cdot\boldsymbol{\omega}] = \left((\hat{A}_b+1)\times(1)\cdot\langle\hat{\mathbf{b}}^*\otimes\hat{\mathbf{c}}\rangle + \hat{A}_c\times(1)\cdot\langle\hat{\mathbf{c}}^*\otimes\hat{\mathbf{c}}\rangle\right)[\mathbf{k}\cdot\boldsymbol{\omega}]\,. \tag{C16}$$

Recall also that (given Eq. (19) and Eq. (49))

$$P_{\mathrm{a}}^{\mathbf{n},\mathbf{n}'}[\mathbf{k}\cdot\boldsymbol{\omega}] = \left((\hat{A}_b+1)\times(\hat{A}_b^*+1)\cdot\langle\hat{\mathbf{b}}\otimes\hat{\mathbf{b}}^*\rangle + \hat{A}_c\times\hat{A}_c^*\cdot\langle\hat{\mathbf{c}}\otimes\hat{\mathbf{c}}^*\rangle + (\hat{A}_b+1)\times\hat{A}_c^*\cdot\langle\hat{\mathbf{b}}\otimes\hat{\mathbf{c}}^*\rangle + \hat{A}_c\times(\hat{A}_b^*+1)\cdot\langle\hat{\mathbf{c}}\otimes\hat{\mathbf{b}}^*\rangle\right)[\mathbf{k}\cdot\boldsymbol{\omega}]. \tag{C17}$$

where A_b and A_c involve $\mathbf{K}$ and therefore the secular distribution function, F, via Eq. (16). Recall that A_b and A_c involve $(1-\hat{\mathbf{K}})^{-1}$, which reflects the fact that the perturbation is dressed by the self-gravity of the halo. Eq. (C7), together with Eqs. (C13)-(C14) and Eq. (C17) provides a consistent framework in which to evolve secularly the mean distribution of a galactic halo within its cosmic environment. Note that it is possible via Eq. (51) to apply non-linear corrections to the induced correlation within R_{200}.

APPENDIX D: PERTURBATION THEORY TO HIGHER ORDER

D1 Perturbative dynamical equations

In this section, we 'solve' the dynamical equation to order n, which will allow us in the next section to present the N-point correlation to order n.

D1.1 Perturbation theory to all orders

Recall that for $n \geqslant 2$, $f_{\mathbf{k}}^{(\mathrm{n})}(\mathbf{I},t)$obeys Eq. (34). Given Eq. (15) it follows that

$$\begin{aligned} a_{\mathbf{p}}^{(\mathrm{n})}(t) \;=\; & \sum_{\mathbf{q},\mathbf{k}} \int \mathrm{d}\tau \exp(\imath\mathbf{k}\cdot\boldsymbol{\omega}[\tau-t])\,[a_{\mathbf{q}}^{(n)}(\tau)+\delta_1^n\, b_{\mathbf{q}}(\tau)]\left((2\pi)^3\int \mathrm{d}\mathbf{I}\psi_{\mathbf{k}}^{[\mathbf{n}]}(\mathbf{I})\psi_{\mathbf{k}}^{[\mathbf{p}]*}(\mathbf{I})\,\frac{\partial F}{\partial\mathbf{I}}\cdot\imath\mathbf{k}\right) - \\ & \sum_{k=1}^{n-1}\sum_{\mathbf{q},\mathbf{k}} \int \mathrm{d}\tau \exp(\imath\mathbf{k}\cdot\boldsymbol{\omega}[\tau-t])[a_{\mathbf{q}}^{(k)}(\tau)+\delta_1^k\, b_{\mathbf{q}}(\tau)]\left((2\pi)^3\int \mathrm{d}\mathbf{I}\left\{\psi^{[\mathbf{q}]}(\mathbf{w},\mathbf{I}),f^{(n-k)}(\mathbf{w},\mathbf{I},t)\right\}_{\mathbf{k}}\psi_{\mathbf{k}}^{[\mathbf{p}]*}(\mathbf{I})\right), \end{aligned} \tag{D1}$$

where the first term in Eq. (D1) corresponds to the usual self-gravity coupling at order n, and the sum corresponds to the feed of lower order potential coupling into the n$^{\mathrm{th}}$ order equation. Here $f_{\mathbf{k}}^{(\mathrm{n})}(\mathbf{I},t)$ obeys

$$\begin{aligned} f_{\mathbf{k}}^{(\mathrm{n})}(\mathbf{I},t) \;=\; & \sum_{\mathbf{q}}\int \mathrm{d}\tau\exp(\imath\mathbf{k}\cdot\boldsymbol{\omega}[\tau-t])\times\left[\frac{\partial F}{\partial\mathbf{I}}\cdot\imath\mathbf{k}\,\psi_{\mathbf{k}}^{[\mathbf{q}]}[a_{\mathbf{q}}^{(\mathrm{n})}(\tau)+\delta_1^{\mathrm{n}}\,b_{\mathbf{q}}(\tau)]+\sum_{k=1}^{\mathrm{n}-1}[a_{\mathbf{q}}^{(k)}(\tau)+\delta_1^k\,b_{\mathbf{q}}(\tau)]\{f^{(n-k)},\psi_{\mathbf{k}}^{[\mathbf{q}]}\}_{\mathbf{k}}\right] + \\ & \sum_{\mathbf{q}}\int \mathrm{d}\tau\exp(\imath\mathbf{k}\cdot\boldsymbol{\omega}[\tau-t])c_{\mathbf{q}}(\tau)\delta_{\mathbf{n}}^1\sigma_{\mathbf{k}}^{e,[\mathbf{q}]}. \end{aligned} \tag{D2}$$

Note that the response in Eq. (D2) is, as expected, out of phase with respect to the potential excitation, $a_{\mathbf{n}}(\tau)$ because of inertia (hence the modulation in $\exp(\imath\mathbf{k}\cdot\boldsymbol{\omega}(\tau-t))$). Now, to nth order Eq. (D1), (D2) may be rewritten formally as (using the contraction rule Eq. (46)):

$$\begin{aligned} \mathbf{a}^{(\mathrm{n})} = \mathbf{K}_1\cdot\mathbf{a}^{(\mathrm{n})} + \mathbf{K}_2\cdot\left(\sum_{i_1+i_2=\mathrm{n}}[\mathbf{a}^{(i_1)}+\delta_{i_1}^1 b]\otimes[\mathbf{a}^{(i_2)}+\delta_{i_2}^1\mathbf{b}]\right) + \cdots + \mathbf{K}_j\cdot\left(\sum_{i_1+\cdots+i_j=\mathrm{n}}\bigotimes_j[\mathbf{a}^{(i_1)}+\delta_{i_1}^1\mathbf{b}]\right)\cdots + \mathbf{K}_{\mathrm{n}}\cdot\bigotimes_{\mathrm{n}}[\mathbf{a}^{(1)}+\mathbf{b}] + \\ \mathbf{Q}_2\cdot\left(\mathbf{a}^{(\mathrm{n}-1)}\otimes\mathbf{c}\right) + \cdots + \mathbf{Q}_j\cdot\left(\sum_{i_1+\cdots+i_j=\mathrm{n}-1}\left[\bigotimes[\mathbf{a}^{(i_1)}+\delta_{i_1}^1\mathbf{b}]\right]\otimes\mathbf{c}\right) + \cdots + \mathbf{Q}_{\mathrm{n}}\cdot\left[\bigotimes_{\mathrm{n}-1}[\mathbf{a}^{(1)}+\mathbf{b}]\right]\otimes\mathbf{c}\,, \end{aligned} \tag{D3}$$

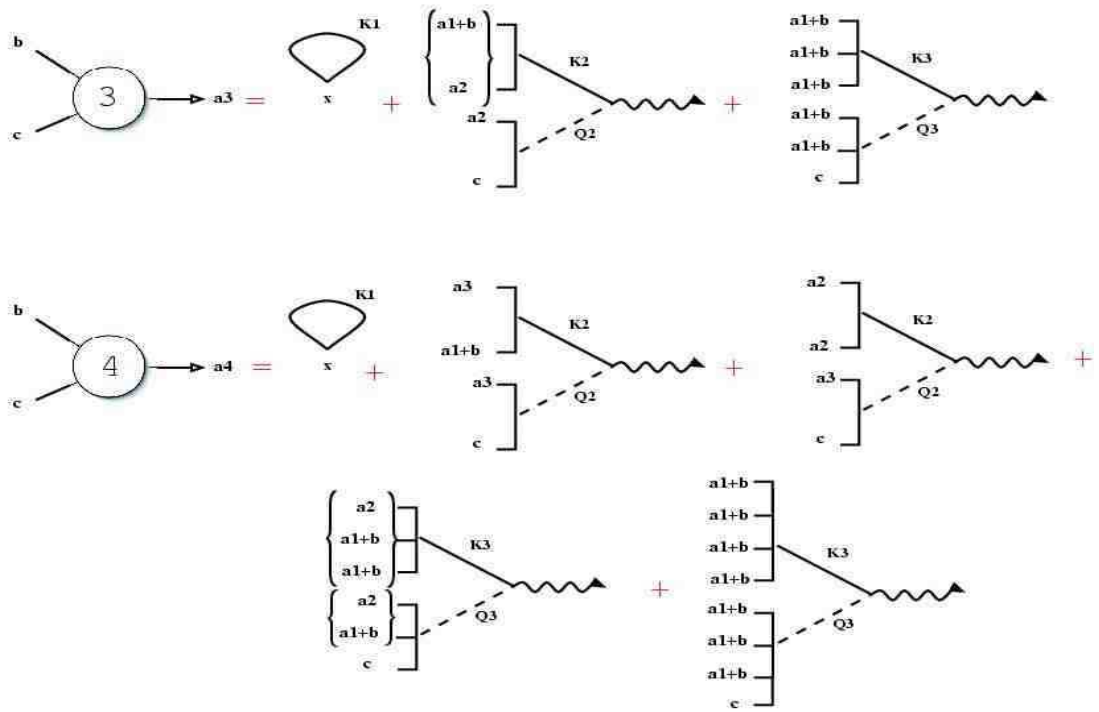

Figure D1. diagrammatic representation of the expansion to third (*top diagram*, corresponding to Eq. (D5)) and fourth (*bottom diagram*, given Eq. (D6)) order; again (see Fig. (5) for details) the coupling of the tidal interaction (through the $b_{\rm n}$ coefficients) and the incoming infall (expanded over the $c_{\rm n}$ coefficients) yields the coefficient of the response inside R_{200}. The coupling is achieved via the operator $\mathbf{K}_i$ and $\mathbf{Q}_i$ as explained in Fig. (D2); the curly brace in front of the diagrams account for the number of such diagrams entering the expansion, corresponding to the permutation of the input (recalling that the order matters). Note also for each branch the sum of the order of the sub branch correspond to the order of the expansion.

where the kernels $\mathbf{K}_1$ and $\mathbf{K}_2$ are given by Eqs. (41)-(42), while $\mathbf{K}_{\rm n}, {\rm n}\geqslant 2$ obey formally:

$$(\mathbf{K}_{\rm n})_{\mathbf{p},\mathbf{q}_1,\mathbf{q}_2\cdots,q_{\rm n}}[\tau_1-t,\tau_2-\tau_1,\cdots,\tau_{\rm n}-\tau_{\rm n-1}] = [2\pi]^3\sum_{\mathbf{k}}\int {\rm d}\mathbf{I}\exp(\imath\mathbf{k}\cdot\boldsymbol{\omega}[\tau_1-t])\sum_{\mathbf{k}_1+\mathbf{k}_2=\mathbf{k}}[\![\exp(\imath\mathbf{k}_1\cdot\boldsymbol{\omega}[\tau_2-\tau_1])\cdots\times$$
$$\sum_{\mathbf{k}_{2{\rm n}-1}+\mathbf{k}_{2{\rm n}}=\mathbf{k}_{\rm n}}\left[\!\!\left[\exp(\imath\mathbf{k}_{2{\rm n}-3}\cdot\boldsymbol{\omega}[\tau_{\rm n}-\tau_{\rm n-1}])\frac{\partial F}{\partial\mathbf{I}}\cdot\imath\mathbf{k}_{2{\rm n}-3}\psi^{[\mathbf{q}_{\rm n}]}_{\mathbf{k}_{2{\rm n}-3}},\psi^{[\mathbf{q}_{\rm n-1}]}_{\mathbf{k}_{2{\rm n}-2}}\right]\!\!\right]\cdots,\psi^{[\mathbf{q}_2]}_{\mathbf{k}_4}\left]\!\!\right],\psi^{[\mathbf{q}_1]}_{\mathbf{k}_2}\right]\!\!\right]\psi^{[\mathbf{p}]*}_{\mathbf{k}}\,. \tag{D4}$$

Note that the ${\rm n}^{\rm th}$ order Kernel involves "only" one integral over action space, but n coupling in configuration space and ${\rm n}+1$ time ordered instants $(t,\tau_1,\cdots\tau_{\rm n})$. Note also that Eq. (D1) implies that secular perturbation theory accounts for both the rate of change in frequency of the system, via $\partial^n\boldsymbol{\omega}/\partial\mathbf{I}^{\rm n}$, the rate of change in equilibrium via $\partial^{\rm n}F/\partial\mathbf{I}^{\rm n}$ but also the rate of change in the incoming flow via $\partial^{\rm n}\sigma^{[\mathbf{p}],e}/\partial\mathbf{I}^{\rm n}$. Note finally that the relative phases (causality) are accounted for via the ordered time integrals. For instance Eq. (D3) reads to third order:

$$\begin{aligned}\mathbf{a}^{(3)} \;=\;& \mathbf{K}_1\cdot\mathbf{a}^{(3)}+\mathbf{K}_2\cdot\left([\mathbf{a}_1^{(1)}+\mathbf{b}]\otimes\mathbf{a}^{(2)}+\mathbf{a}^{(2)}\otimes[\mathbf{a}^{(1)}+\mathbf{b}]\right)+\\ &\mathbf{K}_3\cdot\left([\mathbf{a}^{(1)}+\mathbf{b}]\otimes[\mathbf{a}^{(1)}+\mathbf{b}]\otimes[\mathbf{a}^{(1)}+\mathbf{b}]\right)+\mathbf{Q}_3\cdot\left([\mathbf{a}_1^{(1)}+\mathbf{b}]\otimes[\mathbf{a}_1^{(1)}+\mathbf{b}]\otimes\mathbf{c}\right)+\mathbf{Q}_2\cdot\mathbf{a}^{(2)}\otimes\mathbf{c}\,,\end{aligned} \tag{D5}$$

and is illustrated in Fig. (D1) together with $\mathbf{a}^{(4)}$:

$$\begin{aligned}\mathbf{a}^{(4)} \;=\;& \mathbf{K}_1\cdot\mathbf{a}^{(4)}+\mathbf{K}_2\cdot\left(\mathbf{a}^{(3)}\otimes[\mathbf{a}^{(1)}+\mathbf{b}]+[\mathbf{a}^{(1)}+\mathbf{b}]\otimes\mathbf{a}^{(3)}+\mathbf{a}^{(2)}\otimes\mathbf{a}^{(2)}\right)+\\ &\mathbf{K}_3\cdot\left(\mathbf{a}^{(2)}\otimes[\mathbf{a}^{(1)}+\mathbf{b}]\otimes[\mathbf{a}^{(1)}+\mathbf{b}]+[\mathbf{a}^{(1)}+\mathbf{b}]\otimes\mathbf{a}^{(2)}\otimes[\mathbf{a}^{(1)}+\mathbf{b}]+[\mathbf{a}^{(1)}+\mathbf{b}]\otimes[\mathbf{a}^{(1)}+\mathbf{b}]\otimes\mathbf{a}^{(2)}\right)+\\ &\mathbf{K}_4\cdot[\mathbf{a}^{(1)}+\mathbf{b}]\otimes[\mathbf{a}^{(1)}+\mathbf{b}]\otimes[\mathbf{a}^{(1)}+\mathbf{b}]\otimes[\mathbf{a}^{(1)}+\mathbf{b}]+\\ &\mathbf{Q}_2\cdot\left(\mathbf{a}^{(3)}\otimes\mathbf{c}\right)+\mathbf{Q}_3\cdot\left(\mathbf{a}^{(2)}\otimes[\mathbf{a}^{(1)}+\mathbf{b}]\otimes\mathbf{c}+[\mathbf{a}^{(1)}+\mathbf{b}]\otimes\mathbf{a}^{(2)}\otimes\mathbf{c}\right)+\mathbf{Q}_4\cdot[\mathbf{a}^{(1)}+\mathbf{b}]\otimes[\mathbf{a}^{(1)}+\mathbf{b}]\otimes[\mathbf{a}^{(1)}+\mathbf{b}]\otimes\mathbf{c}\,.\end{aligned} \tag{D6}$$

Note that Eq. (D6) depends recursively on Eq. (D5) and both depends recursively on Eq. (44) and (43). When the recursion is carried through, (see Fig. (D2)) the expected relative complexity of the non-linear evolution appears clearly.

D1.2 Reordering to higher order

In the main text, we give in Eq. (53) and above the first- and second-order reshuffling of the perturbation in $\mathbf{b}$ and $\mathbf{c}$. Similarly, the third-order term reads in terms of products of $\mathbf{b}$ and $\mathbf{c}$ as

$$\begin{aligned}\mathbf{a}^{(3)}=&A_{bbb}\cdot\mathbf{b}\otimes\mathbf{b}\otimes\mathbf{b}+A_{ccc}\cdot\mathbf{c}\otimes\mathbf{c}\otimes\mathbf{c}+A_{bbc}\cdot\mathbf{b}\otimes\mathbf{b}\otimes\mathbf{c}+A_{ccb}\cdot\mathbf{c}\otimes\mathbf{c}\otimes\mathbf{b}+\\&A_{bcb}\cdot\mathbf{b}\otimes\mathbf{c}\otimes\mathbf{b}+A_{cbb}\cdot\mathbf{c}\otimes\mathbf{b}\otimes\mathbf{b}+A_{bcc}\cdot\mathbf{b}\otimes\mathbf{c}\otimes\mathbf{c}+A_{cbc}\cdot\mathbf{c}\otimes\mathbf{b}\otimes\mathbf{c}\,,\end{aligned}$$

where (following the same convention as in the main text for the brackets)

$$\begin{aligned}
A_{bbb} &= \mathbf{K}_3'\circ\mathbf{K}_1''+\mathbf{K}_2'\circ[\mathbf{K}_1'',\mathbf{K}_2'\circ\mathbf{K}_1'']+\mathbf{K}_2'\circ[\mathbf{K}_2'\circ\mathbf{K}_1'',\mathbf{K}_1'']\,,\\
A_{ccc} &= \mathbf{K}_3'\circ\mathbf{Q}_1'+\mathbf{K}_2'\circ\left\{[\mathbf{Q}_1',\mathbf{K}_2'\circ\mathbf{Q}_1'+\mathbf{Q}_2'\circ[\mathbf{Q}_1',\mathbf{1}]]+[\mathbf{K}_2'\circ\mathbf{Q}_1'+\mathbf{Q}_2'\circ[\mathbf{Q}_1',\mathbf{1}],\mathbf{Q}_1']\right\}+\mathbf{Q}_3'\circ[\mathbf{Q}_1',\mathbf{Q}_1',\mathbf{1}]+\\
&\quad\mathbf{Q}_2'\circ[\mathbf{K}_2'\circ\mathbf{Q}_1'+\mathbf{Q}_2'\circ\mathbf{Q}_1',\mathbf{1}],\mathbf{1}]\,,\\
A_{bbc} &= \mathbf{K}_3'\circ[\mathbf{K}_1'',\mathbf{K}_1'',\mathbf{Q}_1']+\mathbf{Q}_3'\circ[\mathbf{K}_1'',\mathbf{K}_1'',\mathbf{1}]+\mathbf{K}_2'\circ[\mathbf{K}_1'',\mathbf{K}_2'\circ[\mathbf{K}_1'',\mathbf{Q}_1']+\mathbf{Q}_2'\circ[\mathbf{K}_1'',\mathbf{1}]]\,,\\
A_{bcb} &= \mathbf{K}_3'\circ[\mathbf{K}_1'',\mathbf{Q}_1',\mathbf{K}_1'']+\mathbf{K}_2'\circ[\mathbf{K}_2'\circ[\mathbf{K}_1'',\mathbf{Q}_1']+\mathbf{Q}_2'\circ[\mathbf{K}_1'',\mathbf{1}],\mathbf{K}_1'']\,,\\
A_{ccb} &= \mathbf{K}_3'\circ[\mathbf{Q}_1',\mathbf{Q}_1',\mathbf{K}_1'']+\mathbf{K}_2'\circ[\mathbf{Q}_1',\mathbf{K}_2'\circ[\mathbf{Q}_1',\mathbf{K}_1'']]\,,\\
A_{cbb} &= \mathbf{K}_3'\circ[\mathbf{Q}_1'',\mathbf{K}_1'',\mathbf{K}_1'']+\mathbf{K}_2'\circ[\mathbf{Q}_1',\mathbf{K}_2'\circ\mathbf{K}_1'']\,,\\
A_{bcc} &= \mathbf{K}_3'\circ[\mathbf{K}_1'',\mathbf{Q}_1',\mathbf{Q}_1']+\mathbf{Q}_3'\circ[\mathbf{K}_1'',\mathbf{Q}_1',\mathbf{1}]+\mathbf{K}_2'\circ[\mathbf{K}_1'',\mathbf{K}_2'\circ\mathbf{Q}_1'+\mathbf{Q}_2'\circ[\mathbf{Q}_1',\mathbf{1}]]+\mathbf{K}_2'\circ[\mathbf{K}_1'',\mathbf{K}_2'\circ\mathbf{Q}_1'+\mathbf{Q}_2'\circ[\mathbf{Q}_1',\mathbf{1}]]+\\
&\quad\mathbf{Q}_2'\circ[\mathbf{K}_2'\circ[\mathbf{K}_1'',\mathbf{Q}_1']+\mathbf{Q}_2'\circ[\mathbf{K}_1'',\mathbf{1}],\mathbf{1}]\,,\\
A_{cbc} &= \mathbf{K}_3'\circ[\mathbf{Q}_1',\mathbf{K}_1'',\mathbf{Q}_1']+\mathbf{Q}_3'\circ[\mathbf{Q}_1'',\mathbf{K}_1',\mathbf{1}]+\mathbf{K}_2'\circ[\mathbf{K}_2'\circ[\mathbf{Q}_1',\mathbf{K}_1''],\mathbf{K}_1'']+\mathbf{K}_2'\circ[\mathbf{Q}_1',\mathbf{K}_2'\circ[\mathbf{K}_1'',\mathbf{Q}_1']+\mathbf{Q}_2'\circ[\mathbf{K}_1'',\mathbf{1}]]+\\
&\quad\mathbf{Q}_2'\circ[\mathbf{K}_2'\circ[\mathbf{Q}_1',\mathbf{K}_1''],\mathbf{1}]\,.
\end{aligned}\tag{D7}$$

Generically, after reordering, Eq. (53) becomes

$$\begin{aligned}
a_{\mathbf{p}}^{(\mathrm{n})}(t) &= \left(\sum_{\mathbf{i}_1,\cdots\mathbf{i}_\mathrm{n}\in[\mathbf{b},\mathbf{c}]}A_{\mathbf{i}_1\cdots\mathbf{i}_\mathrm{n}}\cdot(\mathbf{i}_1\otimes\cdots\otimes\mathbf{i}_\mathrm{n})\right)_{\mathbf{p}}(t)\,,\\
&= \sum_{\mathbf{i}_1,\cdots\mathbf{i}_\mathrm{n}\in[\mathbf{b},\mathbf{c}]}\int_{-\infty}^{t}\mathrm{d}\tau_1\cdots\int_{-\infty}^{\tau_n-1}\mathrm{d}\tau_\mathrm{n}\sum_{\mathbf{q}_1\cdots\mathbf{q}_\mathrm{n}}\left[A_{\mathbf{i}_1\cdots\mathbf{i}_\mathrm{n}}\right]_{\mathbf{p},\mathbf{q}_1\cdots\mathbf{q}_\mathrm{n}}(t-\tau_1,\cdots\tau_\mathrm{n}-\tau_{\mathrm{n}-1})[\mathbf{i}_1]_{\mathbf{q}_1}(\tau_1)\cdots[\mathbf{i}_\mathrm{n}]_{\mathbf{q}_\mathrm{n}}(\tau_\mathrm{n})\,,
\end{aligned}\tag{D8}$$

which involves 2^n terms. Here $\left[A_{\mathbf{i}_1\cdots\mathbf{i}_\mathrm{n}}\right]_{\mathbf{p},\mathbf{q}_1\cdots\mathbf{q}_n}(\theta_1,\cdots\theta_\mathrm{n})$ is some linear tensor of order $\mathrm{n}+1$ which returns the n^{th} order response to the excitation $b_i(\theta),c_j(\theta)$ at various times $\theta_1,\theta_2\cdots\theta_p$. Note that it involve the equilibrium distribution function, F_0 and its derivatives with respect to the actions, $\mathbf{I}$, together with the properties of the basis function.

D2 The N-point correlation function

In the main text, we presented the calculation of the two-point correlation of the fields within the R_{200} sphere. More generally we are interested in the N-point correlation of, say, the density (at various times):

$$\begin{aligned}
C_\mathrm{N} &\triangleq \langle\rho(x_1)\rho(x_2)\cdots\rho(x_\mathrm{N})\rangle=\sum_{\mathrm{n}=\mathrm{N}}^{\infty}\varepsilon^\mathrm{n}\sum_{p_1+p_2+\cdots p_\mathrm{N}=\mathrm{n}}\langle\rho^{(p_1)}(x_1)\rho^{(p_2)}(x_2)\cdots\rho^{(p_\mathrm{N})}(x_\mathrm{N})\rangle\,,\\
&= \sum_{\mathrm{n}=\mathrm{N}}\varepsilon^\mathrm{n}\sum_{p_1+p_2+\cdots p_\mathrm{N}=\mathrm{n}}\sum_{\mathbf{q}_1,\cdots,\mathbf{q}_\mathrm{N}}\rho^{[\mathbf{q}_1]}(\mathbf{r}_1)\cdots\rho^{[\mathbf{q}_\mathrm{N}]}(\mathbf{r}_\mathrm{N})\langle a_{\mathbf{q}_1}^{(p_1)}(\tau_1)\cdots a_{\mathbf{q}_\mathrm{N}}^{(p_\mathrm{N})}(\tau_\mathrm{N})\rangle\,.
\end{aligned}\tag{D9}$$

Now, solutions to the n^{th} order perturbation theory are given by Eq. (D8). It follows that

$$\begin{aligned}
\langle a_{\mathbf{q}_1}^{(p_1)}(\tau_1)\cdots a_{\mathbf{q}_\mathrm{N}}^{(p_\mathrm{N})}(\tau_\mathrm{N})\rangle &= \sum_{\mathbf{i}_1,\cdots\mathbf{i}_{p_1}\in[\mathbf{b},\mathbf{c}]}\cdots\sum_{\mathbf{i}_1,\cdots\mathbf{i}_{p_\mathrm{N}}\in[\mathbf{b},\mathbf{c}]}\sum_{\mathbf{q}_{1,1}\cdots\mathbf{q}_{p_\mathrm{N},p_\mathrm{N}}}\int\mathrm{d}^{p_1}\theta\left[A_{\mathbf{i}_1\cdots\mathbf{i}_{p_1}}\right]_{\mathbf{q}_1,\mathbf{q}_{1,1}\cdots\mathbf{q}_{1,p_1}}(\tau_1,\theta_{1,1},\cdots,\theta_{1,p_1})\cdots\times\\
&\quad\int\mathrm{d}^{p_\mathrm{N}}\theta\left[A_{\mathbf{i}_1\cdots\mathbf{i}_{p_\mathrm{N}}}\right]_{\mathbf{q}_\mathrm{N},\mathbf{q}_{p_\mathrm{N},1}\cdots\mathbf{q}_{p_\mathrm{N},p_\mathrm{N}}}(\tau_\mathrm{N},\theta_{1,p_1}\cdots,\theta_{p_\mathrm{N},p_\mathrm{N}})\times\\
&\quad\langle[\mathbf{i}_1]_{\mathbf{q}_{1,1}}(\theta_{1,1})\cdots[\mathbf{i}_{p_1}]_{\mathbf{q}_{1,p_1}}(\theta_{p_\mathrm{N},1})\cdots[\mathbf{i}_{p_\mathrm{N}}]_{\mathbf{q}_{1,p_\mathrm{N}}}(\theta_{1,p_\mathrm{N}})\cdots[\mathbf{i}_{p_\mathrm{N}}]_{\mathbf{q}_{p_\mathrm{N}p_\mathrm{N}}}(\theta_{p_\mathrm{N},p_\mathrm{N}})\rangle\,.
\end{aligned}\tag{D10}$$

If the perturbation is a centered Gaussian random field, Wick's theorem states that:

$$\begin{aligned}
&\langle[\mathbf{i}_1]_{\mathbf{q}_{1,1}}(\theta_{1,1})\cdots[\mathbf{i}_{p_1}]_{\mathbf{q}_{1,p_1}}(\theta_{p_\mathrm{N},1})\cdots[\mathbf{i}_{p_\mathrm{N}}]_{\mathbf{q}_{1,p_\mathrm{N}}}(\theta_{1,p_\mathrm{N}})\cdots[\mathbf{i}_{p_\mathrm{N}}]_{\mathbf{q}_{p_\mathrm{N}p_\mathrm{N}}}(\theta_{p_\mathrm{N},p_\mathrm{N}})\rangle=\\
&\qquad\sum_{\text{all permutations}}\prod\langle[\mathbf{i}_1]_{\mathbf{q}_{1,1}}(\theta_{1,1})[\mathbf{i}_{p_1}]_{\mathbf{q}_{1,p_1}}(\theta_{p_\mathrm{N},1})\rangle\cdots\langle[\mathbf{i}_{p_\mathrm{N}}]_{\mathbf{q}_{1,p_\mathrm{N}}}(\theta_{1,p_\mathrm{N}})[\mathbf{i}_{p_\mathrm{N}}]_{\mathbf{q}_{p_\mathrm{N}p_\mathrm{N}}}(\theta_{p_\mathrm{N},p_\mathrm{N}})\rangle\,.
\end{aligned}\tag{D11}$$

Putting Eqs. (D10)-(D11) into Eq. (D9) yields formally the N-point correlation function to arbitrary order. A special case in given in the main text corresponding to third order expansion of the two-point correlation, Eq. (54). The N-point correlation of other (possibly mixed) moments of the distribution function may be computed following the same route.

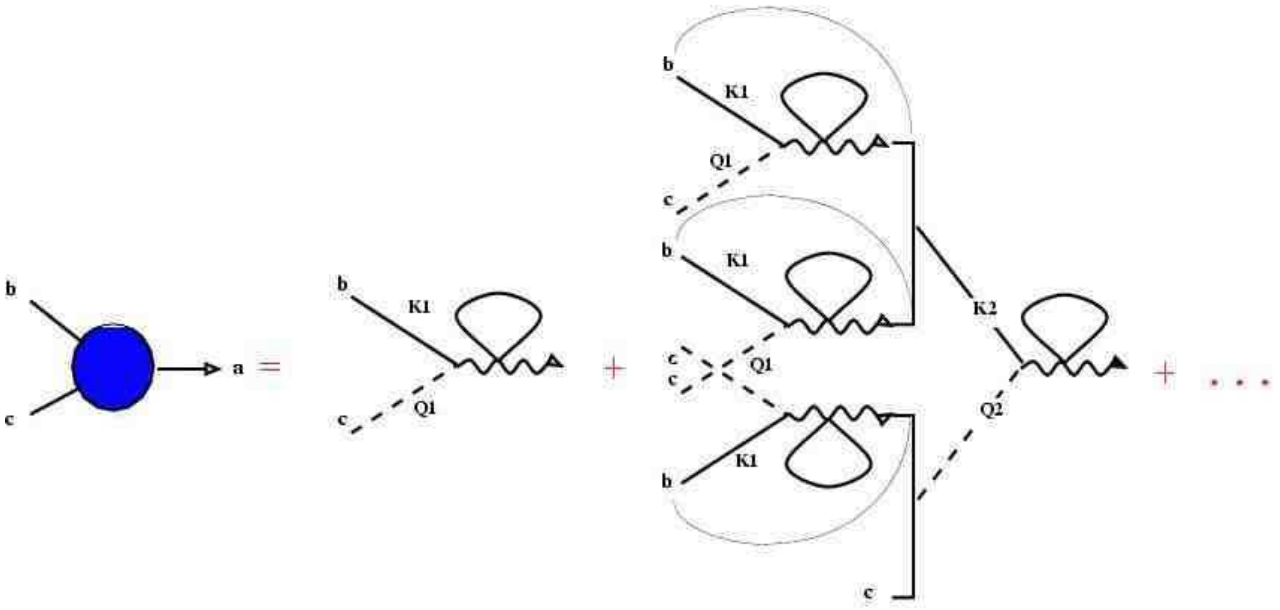

Figure D2. Reordered diagrammatic representation to second-order (first-order included) of the expansion given in Eqs. (43)-(44). This time only $b_{\rm n}$ and $c_{\rm n}$ are inputs. The closed loop accounts for the self-gravity and represents $(1-\hat{\mathbf{K}}_1)^{-1}$. The thin loop traces the fact that the perturbed potential contributes also directly to the second-order term via $\mathbf{a}_1+\mathbf{b}$ (see Eq. (44) for details). Note that in each diagram, each oblique line represents a sum over $\mathbf{k}$ and a time integral. The dashed line stands for infall coupling, while the thick line stands for the tidal coupling.

D2.1 Synthetic hierarchy

D3 Perturbation theory in the complex Fourier plane

Let us close this appendix by a presentation of the perturbative solutions in the complex Fourier plane. In frequency space, Eq. (39) reads:

$$\begin{aligned}\hat{a}^{(2)}_{\mathbf{p}}(\omega) \;=\; & \sum_{\mathbf{q}_1}\hat{a}^{(2)}_{\mathbf{q}_1}(\omega)\left([2\pi]^3\sum_{\mathbf{k}}\int \mathrm{d}\mathbf{I}\psi^{[\mathbf{q}_1]}_{\mathbf{k}}(\mathbf{I})\psi^{[\mathbf{p}]}_{\mathbf{k}}(\mathbf{I})\,\frac{\partial F}{\partial \mathbf{I}}\cdot\mathbf{k}\frac{1}{\mathbf{k}\cdot\boldsymbol{\omega}-\omega}\right)+\\ & [2\pi]^3\sum_{\mathbf{k}}\int \mathrm{d}\mathbf{I}\sum_{\mathbf{q}_1,\mathbf{q}_2}\int \mathrm{d}\omega'[\hat{a}^{(1)}_{\mathbf{q}_1}(\omega')+\hat{b}_{\mathbf{q}_1}(\omega')]\frac{\imath}{\mathbf{k}\cdot\boldsymbol{\omega}-\omega'}\times\\ & \sum_{\mathbf{k}_1+\mathbf{k}_2=\mathbf{k}}\left[\!\!\left[\frac{\imath}{\mathbf{k}_1\cdot\boldsymbol{\omega}-(\omega-\omega')}\left[\frac{\partial F}{\partial \mathbf{I}}\cdot\imath\mathbf{k}_1\psi^{[\mathbf{q}_2]}_{\mathbf{k}_1}(\mathbf{I})\,[\hat{a}^{(1)}_{\mathbf{q}_2}(\omega')+\,\hat{b}_{\mathbf{q}_2}(\omega')]+\sigma^{e,[\mathbf{q}_2]}_{\mathbf{k}_1}(\mathbf{I})\hat{c}_{\mathbf{q}_2}[\omega']\right],\psi^{[\mathbf{q}_1]}_{\mathbf{k}_2}\right]\!\!\right]\psi^{[\mathbf{p}]}_{\mathbf{k}}\,. \end{aligned}\tag{D12}$$

Following Eq. (45), let us also define in frequency space the contraction rule:

$$(\hat{\mathbf{K}}\cdot\hat{\mathbf{Z}})_{\mathbf{p}}(\omega)\triangleq\sum_{\mathbf{q}}\hat{K}_{\mathbf{p},\mathbf{q}}(\omega)\hat{Z}_{\mathbf{q}}(\omega)\,,\tag{D13}$$

(note that Eq. (D13) only involve a sum and no integral) and the higher order contraction rule (*cf.* Eq. (46)):

$$(\hat{\mathbf{K}}_{\rm n}\cdot\hat{\mathbf{Z}}^1\otimes\cdots\otimes\hat{\mathbf{Z}}^{\rm n})_{\mathbf{p}}(\omega)\triangleq\sum_{\mathbf{q}_1,\cdots\mathbf{q}_n}\int \mathrm{d}\omega_1\cdots\int \mathrm{d}\omega_{\rm n}\hat{K}_{\mathbf{p},\mathbf{q}_1,\cdots\mathbf{q}_n}(\omega_1,\cdots,\omega_{\rm n})\delta_D(\omega-\sum_{i=1}^{\rm n}\omega_i)\hat{Z}^1_{\mathbf{q}_1}(\omega_1)\cdots\hat{Z}^{\rm n}_{\mathbf{q}_{\rm n}}(\omega_{\rm n})\,.\tag{D14}$$

The operator, $\hat{\mathbf{K}}_{\rm n}[\omega_1,\omega_2,\cdots,\omega_{\rm n}]$, obeys

$$\begin{aligned}&(\hat{\mathbf{K}}_{\rm n})_{\mathbf{p},\mathbf{q}_1,\mathbf{q}_2\cdots,q_n}[\omega_1,\omega_2,\cdots,\omega_{\mathbf{n}}]=[2\pi]^3\sum_{\mathbf{k}}\int \mathrm{d}\mathbf{I}\frac{\imath}{\mathbf{k}\cdot\boldsymbol{\omega}-\omega_1}\times\\ &\sum_{\mathbf{k}_1+\mathbf{k}_2=\mathbf{k}}\left[\!\!\left[\frac{\imath}{\mathbf{k}_1\cdot\boldsymbol{\omega}-\omega_2}\cdots\sum_{\mathbf{k}_{2n-1}+\mathbf{k}_{2n}=\mathbf{k}_{\rm n}}\left[\!\!\left[\frac{\imath}{\mathbf{k}_{2{\rm n}-3}\cdot\boldsymbol{\omega}-\omega_{\rm n}}\frac{\partial F}{\partial \mathbf{I}}\cdot\imath\mathbf{k}_{2{\rm n}-3}\psi^{[\mathbf{q}_{\rm n}]}_{\mathbf{k}_{2{\rm n}-3}},\psi^{[\mathbf{q}_{\rm n-1}]}_{\mathbf{k}_{2{\rm n}-2}}\right]\!\!\right]\cdots,\psi^{[\mathbf{q}_2]}_{\mathbf{k}_4}\right]\!\!\right],\psi^{[\mathbf{q}_1]}_{\mathbf{k}_2}\right]\!\!\right]\psi^{[\mathbf{p}]}_{\mathbf{k}}\,.\end{aligned}\tag{D15}$$

APPENDIX E: OTHER COSMOLOGICAL PROBES

In this appendix, we discuss other non-linear statistical probes of the cosmic environment of haloes, expanding over Section 5.1.

E1 Dark matter disintegration

It has been claimed that dark matter could be made of neutralinos which can be traced indirectly via their disintegration signature, which scales like the square of the local dark matter density (Stoehr et al. (2003)). The total number of γ photons received during integration time, t_γ reads

$$N_{\rm a}(\mathbf{\Omega}, t_\gamma) = D_{\rm eff}\, t_\gamma\, \frac{N_{\rm cont}}{2}\, \frac{\langle\sigma v\rangle}{m_\chi^2}\, \frac{\Delta\Omega}{4\pi}\, \frac{1}{\Delta\Omega} \int {\rm d}\mathbf{\Omega} \int {\rm d}r \rho^2_{\rm DM}(r)\,, \\ \triangleq \quad W_\chi \int {\rm d}\mathbf{\Omega} \int {\rm d}r \rho^2_{\rm DM}(r)\,, \tag{E1}$$

where $D_{\rm eff}$ is the effective size of the telescope, $\Delta\Omega$ the angular resolution of the telescope, and $N_{\rm cont}(E_\gamma)$ is the number of continuum photons and $\langle\sigma v\rangle$ is the continuum cross-section of neutralinos of mass, m_χ. The integral accounts for measured flux of γ photons arising from neutralinos desintegrating in the direction, $\mathbf{\Omega}$. (See Stoehr et al. (2003) for details about the computation of $N_{\rm cont}$, $D_{\rm eff}$ and $\langle\sigma v\rangle$). Since the $N_{\rm a}(\mathbf{\Omega}, T)$ scales like the line integral of the square of the density along the line of sight, it is straightforward to propagate the statistical properties of the density fluctuations to that of $N_{\rm a}$. For instance, the cosmic mean will scale like

$$\langle N_{\rm annih}(\mathbf{\Omega})\rangle = W_\chi \int {\rm d}r \langle\rho_{\rm DM}(\mathbf{r})\rangle^2 + W_\chi \int {\rm d}r \langle\delta\rho^2_{\rm DM}(\mathbf{r})\rangle\,, \tag{E2}$$

where

$$\langle\delta\rho^2_{\rm DM}(\mathbf{r})\rangle = \sum_{\mathbf{n},\mathbf{n}'} \langle a_{\mathbf{n}} a_{\mathbf{n}'}\rangle \rho^{[\mathbf{n}]}(\mathbf{r})\rho^{[\mathbf{n}']}(\mathbf{r})\,. \tag{E3}$$

Hence we expect an excess of annihilation because of the polarized clumps within the halo. Similarly, we may predict the angular correlation function, or the related variance as a function of smoothed angular scale as

$$\langle\delta N_{\rm a}(\mathbf{\Omega})\delta N_{\rm a}(\mathbf{\Omega}')\rangle \quad = W_\chi^2 \iint {\rm d}r{\rm d}r' \langle\delta\rho^2_{\rm DM}(\mathbf{\Omega}, r)\delta\rho^2_{\rm DM}(\mathbf{\Omega}', r')\rangle \\ = W_\chi^2 \sum_{\mathbf{n}_1,\mathbf{n}_2,\mathbf{n}_3,\mathbf{n}_4} \langle a_{\mathbf{n}_1} a_{\mathbf{n}_2} a_{\mathbf{n}_3} a_{\mathbf{n}_4}\rangle \iint {\rm d}r{\rm d}r' \times \\ \rho^{[\mathbf{n}_1]}(r, \mathbf{\Omega})\rho^{[\mathbf{n}_2]}(r, \mathbf{\Omega})\rho^{[\mathbf{n}_3]}(r', \mathbf{\Omega}')\rho^{[\mathbf{n}_4]}(r', \mathbf{\Omega}')\,, \tag{E4}$$

where $\delta N_{\rm annih}(\mathbf{\Omega}) \triangleq N_{\rm annih}(\mathbf{\Omega}) - \langle N_{\rm annih}(\mathbf{\Omega})\rangle$. Note that we assumed here that the resolution of the telescope was effectively infinite (*i.e.* $\Delta\Omega \to 0$ in Eq. (E1)). Now we may rely on Wick theorem to express the four-point correlation entering Eq. (E4) as products of two-point correlations. Calling $\delta a \triangleq a - \langle a\rangle$, we have $\langle\delta a_{\mathbf{n}_1}\delta a_{\mathbf{n}_2}\delta a_{\mathbf{n}_3}\rangle = 0$, and

$$\langle\delta a_{\mathbf{n}_1}\delta a_{\mathbf{n}_2}\delta a_{\mathbf{n}_3}\delta a_{\mathbf{n}_4}\rangle \;=\; \langle\delta a_{\mathbf{n}_1}\delta a_{\mathbf{n}_2}\rangle\langle\delta a_{\mathbf{n}_3}\delta a_{\mathbf{n}_4}\rangle + \\ \langle\delta a_{\mathbf{n}_1}\delta a_{\mathbf{n}_3}\rangle\langle\delta a_{\mathbf{n}_2}\delta a_{\mathbf{n}_4}\rangle + \langle\delta a_{\mathbf{n}_2}\delta a_{\mathbf{n}_3}\rangle\langle\delta a_{\mathbf{n}_1}\delta a_{\mathbf{n}_4}\rangle\,. \tag{E5}$$

If the infall is statistically isotropic, Eq. (E4) may be averaged over the direction, $\mathbf{\Omega}$ and reads:

$$\langle\delta N_{\rm annih}(\mathbf{\Omega})\delta N_{\rm annih}(\mathbf{\Omega}')\rangle_\Omega = \sum_\ell C_\ell^{\rm annih} P_\ell[\mathbf{\Omega}\cdot\mathbf{\Omega}']\,, \tag{E6}$$

where

$$C_\ell^{\rm annih} = W_\chi^2 \sum_\ell C_{\ell_1}^{\rm DM} C_{\ell_2}^{\rm DM} U^\ell_{\ell_1,\ell_2}\,. \tag{E7}$$

Note that the geometric factor, $U^\ell_{\ell_1,\ell_2}$, only depends on the basis function, $\rho^{[\mathbf{n}]}(\mathbf{r})$ and possibly the resolution of the telescope if it is not assumed to be infinite:

$$U^\ell_{\ell_1,\ell_2} = \sum_{\mathbf{n}_1,\mathbf{n}_2,\mathbf{n}_3,\mathbf{n}_4} \int {\rm d}\mathbf{\Omega} Y_\ell^{m*}(\mathbf{\Omega}') \int {\rm d}\mathbf{\Omega}' Y_\ell^{m*}(\mathbf{\Omega}') \times \\ \iint {\rm d}r{\rm d}r' \rho^{[\mathbf{n}_1]}(r, \mathbf{\Omega})\rho^{[\mathbf{n}_2]}(r, \mathbf{\Omega})\rho^{[\mathbf{n}_3]}(\mathbf{\Omega}', r')\rho^{[\mathbf{n}_4]}(\mathbf{\Omega}', r')\,, \tag{E8}$$

given that $\rho^{[\mathbf{n}]}(\mathbf{r}) = u^n_{\ell m}(r) Y_\ell^m(\mathbf{\Omega})$ and given the properties of spherical harmonics, the integral $\int {\rm d}\mathbf{\Omega} Y^{m_1}_{\ell_1}(\mathbf{\Omega}) Y^{m_2}_{\ell_2}(\mathbf{\Omega}) Y^{m_3}_{\ell_3}(\mathbf{\Omega}') Y^{m_4}_{\ell_4}(\mathbf{\Omega}') {\rm d}\mathbf{\Omega}$ can be re expressed iteratively in terms of Clebsch-Jordan coefficients. Ensemble average and comparison with the observation is possible at the high ℓ limit corresponding to the small-scale structure of the dark matter halo, for which we may expect independent angular regions of the Galactic halo to be representative of an ensemble average.

E2 Bremsstrahlung X-ray emission of stacked haloes

Assuming that the gas traces the dark matter, we may reproduce the thought experiment of Section E1, though the ensemble average is constructed while staking projections of haloes on the sky rather than in a galactocentric framework.

The emissivity per unit volume at frequency ν, $\varepsilon_\nu(\mathbf{r})$, for a hydrogen plasma is given by (Peacock (1999))

$$\varepsilon_\nu(\mathbf{r}){\rm d}\mathbf{r}{\rm d}\nu \quad = \quad \frac{\epsilon_{\rm X} n_{\rm e}^2(\mathbf{r})}{\sqrt{T_e(\mathbf{r})}} \left(1 + \log_{10}\left[\frac{k_B T_e(\mathbf{r})}{h\nu}\right]\right) \times \\ \exp\left(-\frac{h\nu}{k_B T_e(\mathbf{r})}\right) {\rm d}\mathbf{r}{\rm d}\nu\,, \tag{E9}$$

where T_e is the temperature in Kelvin, ν the frequency in Hz, k_B the Boltzmann constant, h the Planck constant, and $\epsilon_{\rm X} \triangleq 6.810^{-32}$ for an emissivity in ${\rm Wm^{-3}Hz^{-1}}$. Let us assume here that the cluster is isothermal, hence the variation of T_e with z are neglected compared to that of n_e squared.[13]. Let us also assume that L/M is the mass to light ratio of the cluster is constant. Hence the emissivity per unit surface, σ_ν, is given by

$$\sigma_\nu(\mathbf{R}) = \int {\rm d}z\, ({\rm L/M})^2\, \varepsilon_\nu(\mathbf{R}, z) \triangleq W_X \int {\rm d}z \rho^2_{\rm DM}(\mathbf{R}, z)\,. \tag{E10}$$

Hence, taking an ensemble average yields:

$$\langle\sigma_\nu(\mathbf{R})\rangle = W_X \int {\rm d}z \langle\rho_{\rm DM}\rangle^2(\mathbf{R}, z) + W_X \int {\rm d}z \langle\delta\rho^2_{\rm DM}\rangle(\mathbf{R}, z)\,, \tag{E11}$$

where

$$\langle\rho^2_{\rm DM}\rangle(\mathbf{R}, z) = \sum_{\mathbf{n},\mathbf{n}'} \langle a_{\mathbf{n}} a_{\mathbf{n}'}\rangle \rho^{[\mathbf{n}]}(\mathbf{r})\rho^{[\mathbf{n}']}(\mathbf{r})\,. \tag{E12}$$

The two-point correlation of the cosmic fluctuation of the emissivity is given by

[13] this is a better approximation than for the SZ effect

$$\frac{\langle\delta\sigma_v(\mathbf{R})\delta\sigma_v(\mathbf{R}')\rangle}{\langle\sigma_v(R)\rangle^2}=\frac{\iint \mathrm{d}z\mathrm{d}z'\langle\delta\rho^2_{\rm DM}(\mathbf{R},z)\delta\rho^2_{\rm DM}(\mathbf{R}',z')\rangle}{\langle\sigma_v(R)\rangle^2},$$

where

$$\langle\delta\rho^2_{\rm DM}(\mathbf{R},z)\delta\rho^2_{\rm DM}(\mathbf{R}',z')\rangle = \sum_{\mathbf{n}_1,\mathbf{n}_2,\mathbf{n}_3,\mathbf{n}_4}\langle a_{\mathbf{n}_1}a_{\mathbf{n}_2}a_{\mathbf{n}_3}a_{\mathbf{n}_4}\rangle\times \rho^{[\mathbf{n}_1]}(\mathbf{R},z)\rho^{[\mathbf{n}_2]}(\mathbf{R},z)\rho^{[\mathbf{n}_3]}(\mathbf{R}',z')\rho^{[\mathbf{n}_4]}(\mathbf{R}',z')\,. \quad \text{(E13)}$$

Note the cancellation of the dependence on W_X (hence T or M/L) in Eq. (E13). Relying again on Wick's theorem, Eq. (E5), we may express the four-point correlations as a products of known (*cf.* Eq. (E5)) two-point correlations.

E3 Galactic halo's ellipticity

More generally, let us consider a problem which depends non trivially on the perturbed distribution function, *e.g.* the ellipticity, $e_{\rm H}$, of the departure from sphericity of the substructures induced by the environment around a given halo. The ellipticity is defined as

$$e_{\rm H}=\frac{3\lambda_1}{\sum_i\lambda_i}-1\triangleq\mathcal{G}(\delta\rho(\mathbf{r}))\,,\quad\text{with}\quad\{\lambda_i\}=\mathrm{Eigenval}(\mathbf{I}_{\rm H})\,, \quad \text{(E14)}$$

and

$$\mathbf{I}_{{\rm H},i,j}=\int_{\leqslant R_{200}}\mathrm{d}\mathbf{r}\delta\rho(\mathbf{r})x_ix_j\Big/\int_{\leqslant R_{200}}\mathrm{d}\mathbf{r}\rho_{\rm NFW}(\mathbf{r})\,, \quad \text{(E15)}$$

(so that λ_1 is the largest eigenvalue of $\mathbf{I}_{\rm H}$ and $e_{\rm H}=0$ if the halo' s perturbation is spherical). Since we know the statistical properties of $\delta\rho(\mathbf{r})$, we may predict the statistical properties of $e_{\rm H}$. In practice, assuming $\mathcal{G}$ is a well-behaved function of its arguments, we may Taylor-expand $e_{\rm H}$ with respect to $\delta\rho$ as :

$$e_{\rm H}=\sum_n\left(\frac{\partial^n\mathcal{G}}{\partial\delta\rho^n}\right)\cdot[\delta\rho(\mathbf{r}_1)-\langle\delta\rho(\mathbf{r}_1)\rangle]\cdots[\delta\rho(\mathbf{r}_n)-\langle\delta\rho(\mathbf{r}_n)\rangle] \quad \text{(E16)}$$

Note that the derivative in Eq. (E16) is a Frechet functional derivative, so that the dot involves an integration over $\mathbf{r}$. Hence the ensemble average, $\langle e_{\rm H}\rangle$ will involve N-point correlations, and reads

$$\langle e_{\rm H}\rangle=\sum_n\sum_{\mathbf{i}_1\cdots\mathbf{i}_n}\langle a_{\mathbf{i}_1}\cdots a_{\mathbf{i}_n}\rangle\left(\frac{\partial^n\mathcal{G}}{\partial\delta\rho^n}\right)\cdot\rho^{[\mathbf{i}_1]}(\mathbf{r})\cdots\rho^{[\mathbf{i}_n]}(\mathbf{r}_n)\,, \quad \text{(E17)}$$

where, once again, we may rely on Wick's theorem to reexpress $\langle a_{i_1}\cdots a_{i_n}\rangle$ as products of two-point correlations. Since the relationship between the density perturbation and the ellipticity is not linear, we expect a non zero ellipticity on average.

Note that in principle, we may reconstruct the full PDF of e. Formally, calling $z\triangleq(e,a_2,\cdots a_{\mathbf{n}})$ (so that $z=(\mathcal{G}(a_1,\cdots,a_{\mathbf{n}}),a_2\cdots,a_{\mathbf{n}})=g(a_1,\cdots,a_{\mathbf{n}})$), inverting for z as a function of $\{a_i\}$ (provided the ellipticity is not degenerate in a_1), and marginalizing over the other coefficients yields:

$$\mathrm{PDF}(e)=\int\mathrm{d}a_2\cdots\mathrm{d}a_{\mathbf{n}}\mathrm{PDF}\left(g^{-1}(z)\right)/\left|\frac{\partial z}{\partial a_{\mathbf{n}}}\right|\,.$$

Now in practice, Eq. (E17) might not be the simplest procedure to compute $\langle e_{\rm H}\rangle$, and monte carlo resimulation may turn out to be more practical.

E4 Metal lines in QSO DLA systems

Let us finally consider a more convolved observable, which will depend on both the clump distribution within the haloes, but also on their velocities.

In the red part of a high resolution spectrum of quasars, groups of absorption features are found, corresponding to the physical situation where the light emitted by the quasar is partially absorbed by the metal-rich[14] clumps which the line of sight happens to intercept. Formally, the normalized flux in a QSO is proportional to minus the log of the optical depth along the line of sight. The optical depth in the metal transition is (Pichon et al. (2001)):

$$\tau(w,\mathbf{R}) = \frac{c\,\sigma_0}{H(\overline{z})\sqrt{\pi}}\int_{-\infty}^{+\infty}\frac{n_Z(v,\mathbf{R})}{b(v,\mathbf{R})}\times \exp\left(-\frac{(w-v-v_z(v,\mathbf{R}))^2}{b(v,\mathbf{R})^2}\right)\mathrm{d}v\,, \quad \text{(E18)}$$

where c is the velocity of light, σ_0 is the metal absorption cross-section, $H(\bar{z})$ is the Hubble constant at redshift $\overline{z}$, $n_Z(v,\mathbf{R})$ the ionized metal number density field, $b(v,\mathbf{R})$ the Doppler parameter (accounting for the thermal broadening of the line), and $v_p(v,\mathbf{R})$ is the peculiar velocity, at impact parameter, $\mathbf{R}$ from the centre of the cluster. The observed normalized flux, F, is simply $F=\exp(-\tau)$. If we assume here again constant biasing, so that $n_Z\propto\rho_{\rm DM}$. This assumption may be lifted once the identification of virialized substructure described in Section 3.3.1 is carried through. The two-point correlation of the optical depth fluctuation will involve statistical properties of both the density and the velocity field in a non trivial manner.

$$\frac{1}{\langle\tau\rangle^2(w,R)}\langle\delta\tau(w,\mathbf{R})\delta\tau(w',\mathbf{R})\rangle\,, \quad \text{(E19)}$$

with

$$\delta\tau(w,\mathbf{R})=\tau(w,\mathbf{R})-\langle\tau\rangle(w,R)\,. \quad \text{(E20)}$$

Note that the distance to the halo center, $\mathbf{R}\triangleq b(\cos[\vartheta_b],\sin[\vartheta_b])$ still occurs in Eq. (E20). Since we do not know in general the impact parameter of the line of sight with respect to the halo center, let us marginalize over its *a priori* probability distribution, which we may infer from *e.g.* the PT model (which at these scales corresponds essentially to the autocorrelation of the unperturbed universal halo profile). Given that we consider systems at the redshift of a damped Lyman-α, we may assume that we fall close to a galactic structure. Calling $p_b(b,\bar{z},M)\mathrm{d}b\mathrm{d}\bar{z}$ the probability of a given point in space to be at a distance, b within $\mathrm{d}b$ of an object of mass larger than M, which is at redshift $\bar{z}$ within $\mathrm{d}\bar{z}$, we may construct the weighted sum :

$$C_\tau(\Delta w) = \int_0^\infty\mathrm{d}b\int_0^\infty\mathrm{d}\bar{z}\int_0^{2\pi}\mathrm{d}\vartheta_b p_b(b,z,M)\times \quad \text{(E21)}$$
$$\langle\delta\tau(w,b\cos[\vartheta_b],b\sin[\vartheta_b])\delta\tau(w+\Delta w,b\cos[\vartheta_b],b\sin[\vartheta_b])\rangle_w\,.$$

This quantity may now be compared to the observable. Let us assume some equation of state for the metal phase, so that

[14] Since we make predictions at lower redshift we need to concentrate on metals such as $\mathrm{Mg_{II}}$, or $\mathrm{Fe_{II}}$ which are found typically at redshift $z\leqslant 1.5$ in the visible

$b(\mathbf{R}, z) = b_0 \left(\rho(\mathbf{R}, z)/\,\bar{\rho}\right)^{\gamma}$. Eq. (E18) may then be written formally as $\delta\tau(w, \mathbf{R}) = \mathcal{T}\left[\delta\rho(v, \mathbf{R}), v_z(v, \mathbf{R})\right]$. Let us Taylor expand this expression in the neighborhood of the mean density fluctuation as:

$$\delta\tau(w, \mathbf{R}) = \sum_n \left(\frac{\partial^n \mathcal{T}}{\partial\delta\rho \cdots \partial\delta v_z}\right) \cdot [\delta\rho(\mathbf{r}_1) - \langle\delta\rho(\mathbf{r}_1)\rangle] \cdots [\delta v_z(\mathbf{r}_n) - \langle\delta v_z(\mathbf{r}_n)\rangle] \,. \quad \text{(E22)}$$

Again the derivative in Eq. (E22) is a functional derivative (*cf.* Section E3). Eqs. (E21)-(E22) together with Eq. (29) yield the expected correlation as a function of the statistical environment.